PARAMETRIC STUDY ON WATER-COOLING PLATES TO IMPROVE COOLING PERFORMANCE ON 18650 LI-ION BATTERY

RAKSIT NANTHATANTI

A THESIS REPORT SUBMITTED IN PARTIAL FULFILLMENT

OF THE REQUIREMENTS FOR THE DEGREE OF

MASTER OF ENGINEERING IN AUTOMOTIVE AND ADVANCED TRANSPORTATION ENGINEERING

(INTERNATIONAL PROGRAM)

SCHOOL OF ENGINEERING

KING MONGKUT'S INSTITUTE OF TECHNOLOGY LADKRABANG

YEAR 2024

KMITL-2024-EN-M-277-287

THESIS TITLE	Parametric Study on Water-Cooling Plates to Improve Cooling Performance on 18650 Li-ion Battery
STUDENT NAME	Mr. Raksit Nanthatanti
STUDENT ID	64601182
DEGREE	Master of Engineering
PROGRAM	Automotive and Advanced Transportation Engineering (International Program)
YEAR	2024
ADVISOR	Prof.Dr.Jarruwat Charoensuk

ABSTRACT

In this study, the performance of a liquid cooling plate for lithium-ion battery modules was investigated.

The major factors tested in steady-state conditions were inlet temperature, water velocity, number of cooling channels, and cooling barrier length. The number of cooling channels and the inlet velocity of cooling water were found to have a significant impact on water flow distribution inside the cooling channel. Changing the cooling barrier length had less influence on water flow. The average velocity of the fluid flowing over the bounding surfaces can be affected by the channel count, and the inlet temperature of the liquid also affects the maximum temperature of the battery pack.

The maximum temperature at the outlet section was typically shown in the 3-channel arrangement when the lowest water velocity was used. The heat removal rate from the battery pack was consistent, conforming to the basic theory of the steady flow energy equation, and it needed to be equal to the heat generation rate inside the battery. The study achieved velocity consistency and water dispersion. The average velocity of the fluid flowing over bounding surfaces was affected by the channel count, and the inlet temperature of the liquid also influenced the maximum temperature of the battery pack. If the inlet velocity increased, the water distribution in the channel would become worse and the channel velocity would become more different in each block. The four-channel design produces the best velocity uniformity since the standard deviation was observed to be the lowest.

The maximum amount of pressure drop appeared to be in the 2-channel configuration compared to the 3-channel and 4-channel designs. The standard deviation was also greater in 2 channel design, reflecting uneven flow velocity.

In addition, the 6-channel had the least flow cross-sectional area due to the space limitation and causing the gap width of only 12 mm whereas the 2, 3 and 4-channels had 41, 32.5, and 20.5 mm.

In general, the 6 channel had more friction resistance among other configurations when flow passes through the channel. With the highest SD , It had the least uniformity among all configurations which brings the pressure drop to be the highest.

The second accomplishment was a three-dimensional thermal model to simulate a battery cooling system. Under typical working circumstances, the temperature distribution of the entire battery pack was exhibited. The results showed that deploying a 30 °C water inlet temperature helped keep the battery cell temperature within permissible limits. At a charging rate of 0.75 C and a maximum heating value of 0.307 W, the highest average temperature of the 9th cell was within acceptable limits, resulting in the highest percentage of battery performance (120%). Transient simulation results indicated that the highest average temperature at the 9^{th} cell occurred within a specific time range, demonstrating the importance of considering transient conditions in the cooling system design. The simulation results were expected to aid in the design of a battery cooling system based on a mini-channel in a liquid-cooling configuration.

The statement also emphasizes that the inlet temperature of the cooling liquid has an impact on the maximum temperature of the battery pack. This implies that the temperature of the cooling fluid entering the system plays a crucial role in determining how effectively heat is transferred away from the battery pack. Maintaining a specific inlet temperature may be a critical factor in ensuring optimal cooling performance and preventing the battery from reaching excessively high temperatures.

Overall, the study provides insights into the factors influencing the performance of the liquid cooling system for lithium-ion battery modules and offers valuable information for the design of efficient cooling systems. The results of the simulation would help to design a battery cooling system based on a mini-channel in a liquid-cooling configuration. The average velocity of the fluid flowing over bounding surfaces is influenced by the channel

count. This suggests that the number of cooling channels in the system has a notable effect on the flow dynamics and how efficiently the cooling fluid moves through the system. The design with a specific channel count may contribute to achieving a more consistent and controlled flow.

Keywords: cooling efficiency, channel count, lithium-ion battery, flow dynamics

ACKNOWLEDGEMENT

First, I would like to express my deep appreciation to my NSTDA advisor, Dr.-Ing Manop Masomtob. He always helps and encourages me by making time in his busy schedule for me. I am grateful for his insightful advice, direction, and support from the beginning to the end of our project. In the research sector, I have learned and assimilated fresh information. Furthermore, he has not only offered research ideas for my research. but he has also clarified the conceptual foundation and boosted my understanding of battery management and design techniques for liquid cooling in battery systems by providing me with my full modules of the liquid-cooled plate. I couldn't have finished my master's thesis on time without his assistance. Second, I want to express my heartfelt gratitude to Prof. Dr.Jarruwat Charoensuk for his input and remarks on both my thesis and paper. Throughout my research, he was always motivating and encouraging.

Next, I want to thank NSTDA and TAIST-Tokyo Tech for supplying me with a scholarship. I'm also grateful to the National Energy Technology Center (ENTEC) and King Mongkut's Institute of Technology Ladkrabang (KMITL) for providing support.

Finally, I would like to express deep appreciation for my parents, who have consistently provided me with sound guidance, inspiration, and unrestricted affection since the moment I was born. I would not have achieved this without their perpetual emotional and financial encouragement during my research route over the two years.

Raksit Nanthatanti

Author

TABLE OF CONTENTS

Chapter **Page**

LIST OF TABLES

Table **Page**

LIST OF FIGURES

Figure **Page**

LIST OF FIGURES(Cont'd)

Figure **Page**

LIST OF FIGURES(Cont'd)

Figure **Page**

LIST OF SYMBOLS

q_{cond}	Heat conduction (W)
R_{int}	Internal Resistance of Battery (Ω)
I	Battery current (A)
T_{max}	Maximum Surface temperature(C)
T_{avg}	Average temperature (C)
T_i	Inlet temperature of cooling water [°C]
T_o	Outlet temperature of cooling water [°C]
Δs	Entropy change [J/°C]
ΔT	Temperature difference [°C]
SOC	State of Charge
P_{fluid}	Pressure of fluid in cooling channel(Pa)
V_{avg}	Average Velocity (m/s)
d V_{oc} /dT	The differential of open circuit voltage
C_p	Specific heat capacity of cooling water (J/kg·°C)
k	Thermal conductivity (W/m·°C)
Q	Heat Removal rate (KW)
$\dot{m}_w$	The mass flowrate of Inlet water [kg/s]
$\dot{v}_w$	The volumetric flowrate of Inlet water [m^3/s]
ρ_ω	Density of cooling water [Kg/m^3]
A	cross-sectional area of Inlet cooling Tap[m^2]
D	Diameter of Inlet cooling Tap(m)
ρ_{al}	Density of Aluminum Plate[Kg/m^3]
μ	kinematic viscosity (Pa·s)

LIST OF DEFINITIONS

BTMS	battery thermal management system
C	discharging rate
CC	constant current
CV	constant voltage
CFD	computational fluid dynamics
DOD	depth of discharge
EVs	electric vehicles
FEA	finite elements analysis
FEM	finite element method
PCM	phase change material
3D	three-dimensional
DRS	Direct refrigerant system
Li-ion	Lithium ion
NCA	Lithium nickel cobalt aluminum oxide
NMC	Lithium nickel manganese cobalt oxide

CHAPTER 1

INTRODUCTION

1.1 Research Background

At the present, Electric vehicles (EVs) tend the solution for modern vehicles. EVs require less number necessary parts compared to Internal combustion engine vehicles (ICEVs) and can use electricity from alternative energy resources such as wind turbines, photovoltaic, water dam powers, etc. However, battery pack cost, driving range, and thermal management system are the challenge of EVs. To reduce the battery cost, the number of battery cells must be decreased; consequently, the driving range is shortened, and the battery temperature is raised. Therefore, the thermal management system needs to be developed to prolong the life of the battery pack

1.1.1The effect of heat on Battery performance

The battery is one of the most important parts of electric vehicles (EVs). The modern development of EVs requires higher capacity and power densities from battery packs. It is always expected that the number of battery cells can be packed as much as possible to maximize the output capacity and power density. However, high power load usage leads to a serious thermal issue due to heat generation. The temperature is sensitive to the battery performance and lifetime of battery cells. If the battery temperature is higher, the battery performance is higher because the higher temperature can accelerate the chemical reaction over the rated limit as shown in Fig.1.1 and Fig1.21.1.2Battery cooling system

There are different forms of thermal management for battery packs. They are primarily divided into three categories: liquid cooling [8–10], cooling using phase change materials (PCMs), and cooling using air [2-4]. These techniques have benefits and drawbacks. According to D. Chen et al. [11], air cooling is simple to build but has poor cooling effectiveness and is insufficient to sustain temperature under adverse circumstances. The PCM cooling system based can efficiently lower temperatures and eliminate temperature differences, but its use is limited by phase changes in volume and encapsulation. It is a strong system to use liquid cooling. Its ability to remove heat is, however, limited. Due to the addition of several techniques, it is now better suited

for battery heat management systems and some techniques added such as channel design, flow rate, and coolant inlet temperature control are applied to enhance the performance of the cooling system.

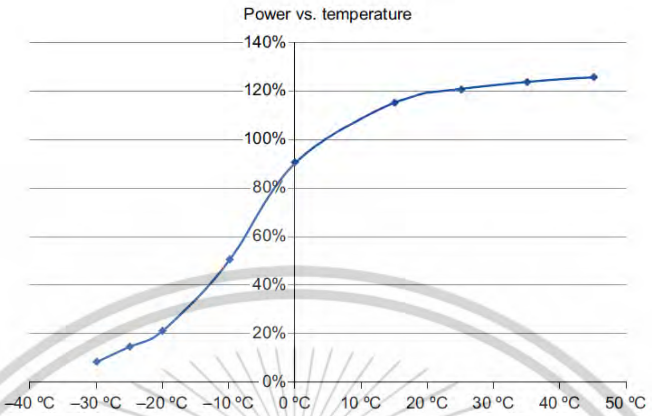

Fig. 1.1 The power as a function of the lithium-ion battery temperature

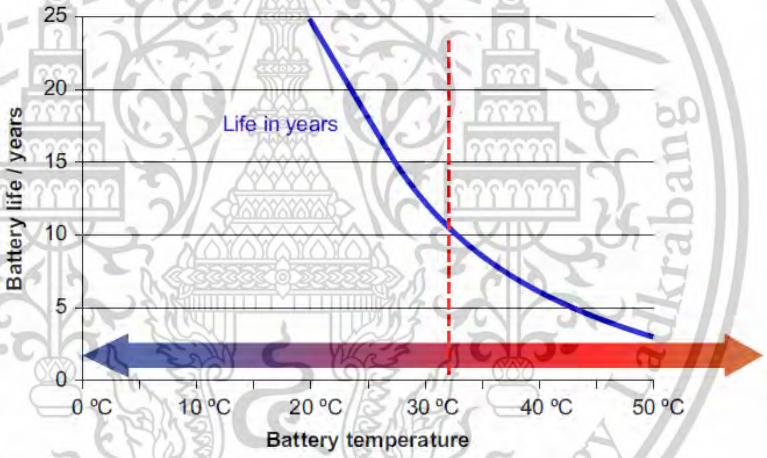

Fig.1.2 The battery life as the function of lithium-ion battery temperature

On the other hand, battery life is lower when the battery temperature is higher. Therefore, a suitable battery temperature needs to be considered. A. Greco, X. et al. [1] have reported that the battery temperature should be maintained in the range of 20–40°C and that the maximum temperature difference for entire packs should be less than 5°C. The battery life will reduce at higher temperatures, which is the most important factor that influences battery aging and causes premature battery failure. Higher temperatures mean a faster chemical reaction inside the battery, which increases water loss and corrosion as well, so the Temperature of the battery should be no more than 33 °C, as A. Greco, X. et al. [1] explained, to maintain the battery life

to be more than 10 years, as the current prediction is that an electric car battery will last from 10 to 20 years before they need to be replaced

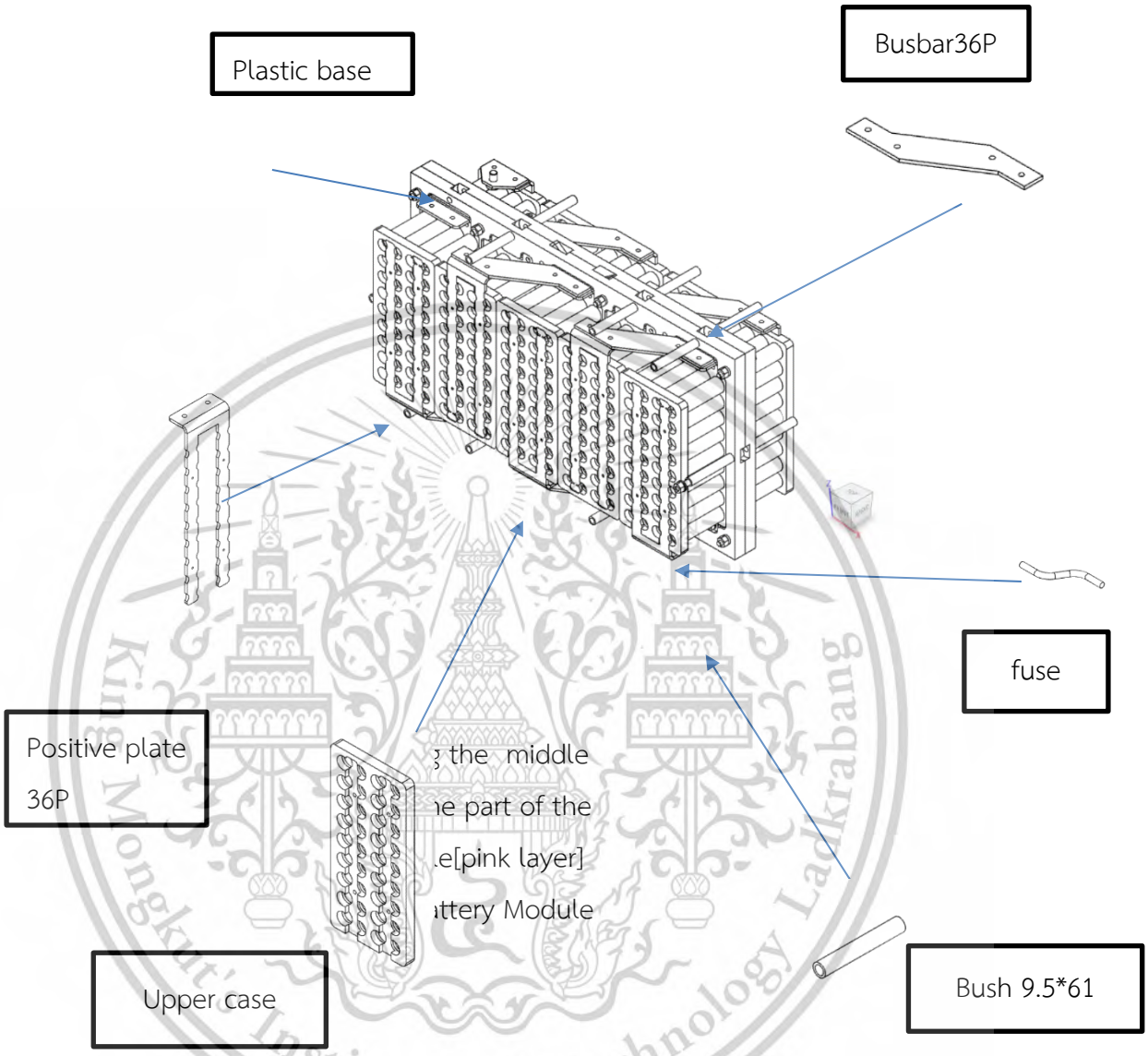

Fig. 1.3 10S36P Battery Module Model

1.1.3The 10S36P Battery Module

1st Remove the upper case and positive plate because they are not considered for cooling in the positive terminal.

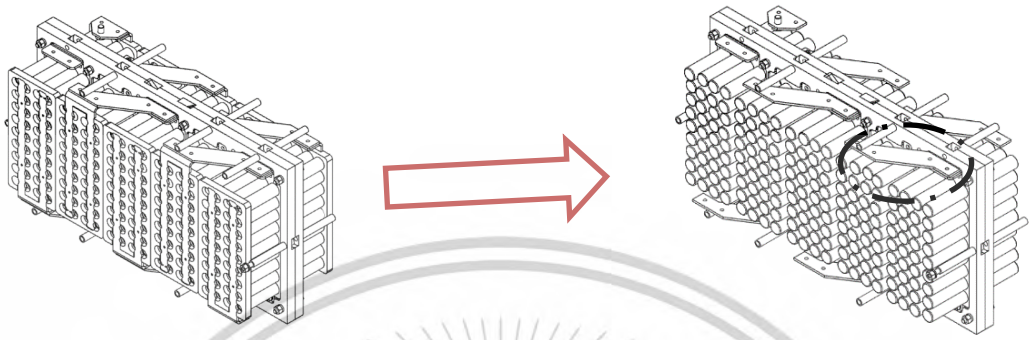

2nd Neglect the ohmic heating on the busbar that conducts the heat to the positive terminal. So, the busbar will be removed.

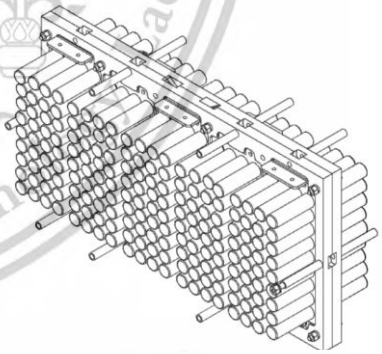

3rd Remove all of the insulation parts [the bushes and all connectors] that can fasten the battery module.

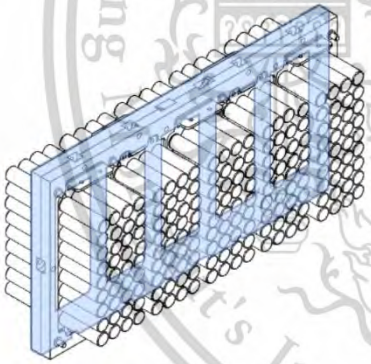

5th Cutting the xz plane to show half the cooling module because the cooling system is symmetric

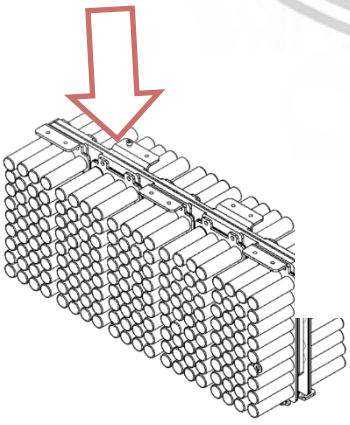

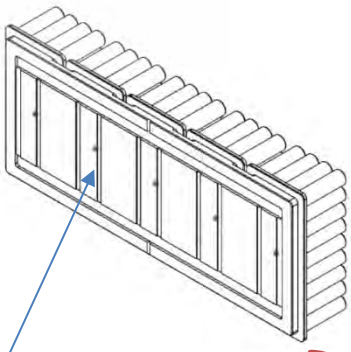

Liquid Cooling Plate

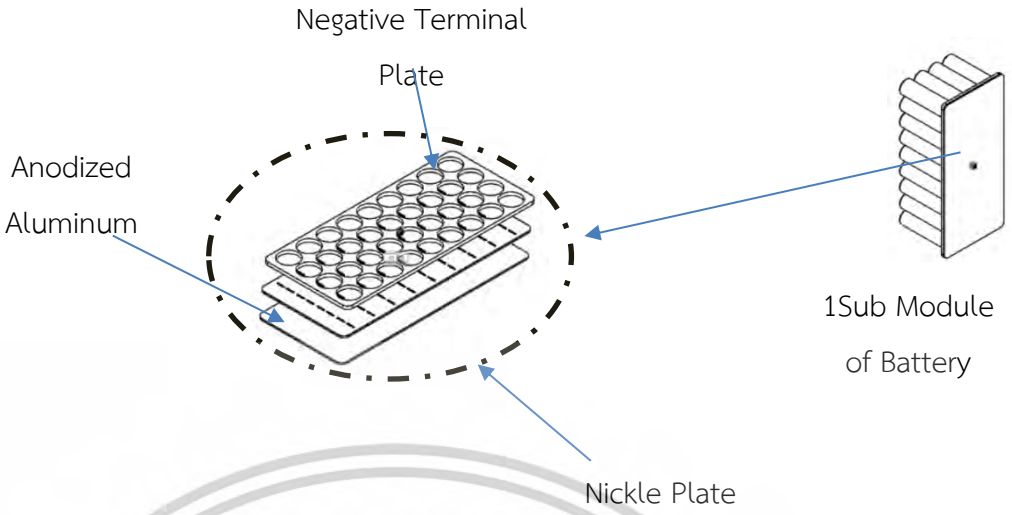

Fig 1.4 18650 Li-ion Battery Module with cooling channel configuration

Fig.1.4 displays the Battery module, which has one hundred and eighty 18650 Li-ion battery cells in the battery pack. Each battery module contains 36 cells and is enclosed within aluminum cooling plates. This module is made up of several parts. The first is Busbar, which is a copper strip with connectors for connecting to the battery's negative terminal and is intended to restrict potential negative differences and reduce multiple connections to specific terminals. Then there's the plastic base, which acts as insulation between the battery pack on both sides. When only each battery module is considered, it has three parts: the nickel coating, which contributes to higher energy density; a larger storage capacity and enhanced electrical conductivity. Anodized aluminum plate can create a stable aluminum oxide layer that is completely integrated. This one is used as a cooling liquid plate because it can protect the dielectric substrates from being damaged during heat transfer through the battery module.

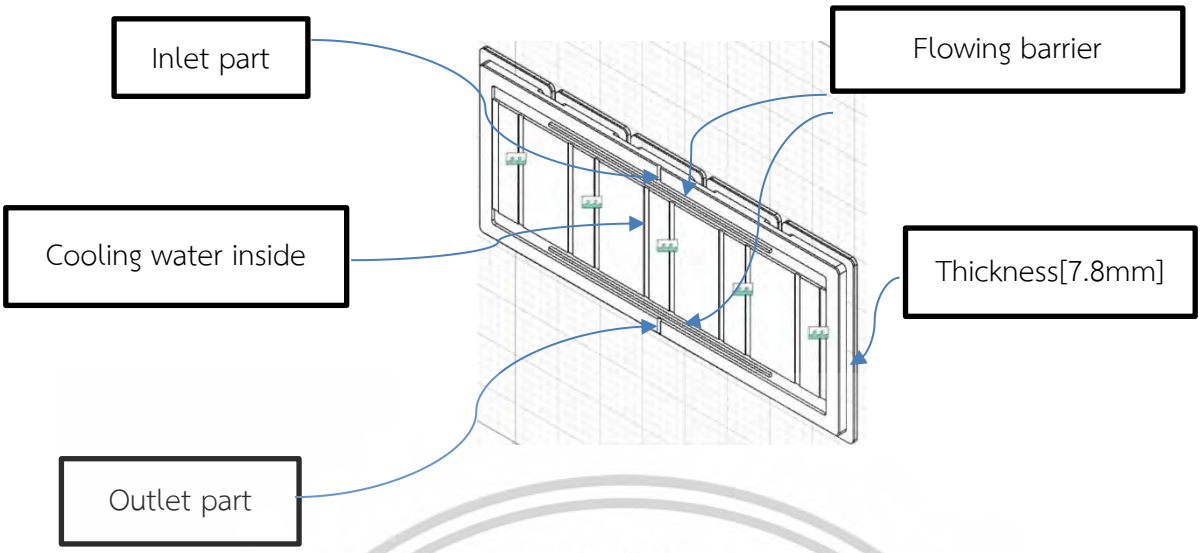

Fig.1.5 Previous design of liquid cooling plates with two flow channel per base for the water-cooling system

1.2Research Objectives

This study will look into two aspects to determine how much heat is removed from a battery and find the cooling performance, as explained below in the three main sections.

Firstly, consider the external factors that significantly influence heat conduction on the battery surface. The design idea is to vary the number of cooling channels on the aluminum cooling plate with barriers at the inlet and outlet sections, then adjust the cooling channel configuration by making the cooling channel space equal, which is different from the previous design and can affect the cooling performance.

Secondly, the key elements influencing the display of a velocity plot are the flow parameters, which are the main variables in the cooling module, such as the mass flow rate and the intake temperature of the water. The domain and working fluid are specified by geometry, followed by a steady-state simulation to determine the amount of pressure drop at the inlet-outlet section. the temperature differences and maximum temperature of the water at the output slots in every configuration, and the last one is to compare the results to find the cooling performance at each type.

Finally, the heat-removed value from the battery module to the aluminum cooling liquid plate will be calculated, and the plot data will be compared later with numerous designs.

1.3Scopes of Work

Focusing only on the NSTDA patent design of the liquid cooling plate and use the steady-state model to simulate the heat generation of the battery and the outlet temperature of water when the number of channels inside the cooling plate is designed and investigated. The fully developed model was applied to this asymmetric model.

The simplified battery module in simulation [9 cells in one row] will be used to reduce the time consumption of parametric studies by considering only flow simulation and the distribution of temperature inside the battery from the 1^{st} cell to the 9^{th} cell. Therefore, the commercial 18650 lithium-ion battery cells from the Toriyama brand with a Li-Ni-Mn-Co (NMC) cathode were used in this investigation. At C-rate 0.75 C, the proposed current, the maximum heat generation rate to be used in the simplified battery is at 80% charged, or SOC = 0.8, and gains the maximum charging current [2A], so the simulation is set at 0.75 C during the charging event [a nearly ideal value at the charging process].

1.4Expected Results

1. Difference Temperature of cooling water (ΔT) plot with Inlet velocity of cooling water [m/s] in steady state condition
2. Maximum Temperature of water through the cooling path from the inlet to outlet sections for each configuration [2, 3, 4, 6 channels] and heat removal value from the battery module that compared with a different design with the cooling plate
3. Velocity map of the flow visualization running at a constant heat source and displaying a three-dimensional transient issue on one roll of battery pack

4. The temperature distribution of the 9th cell will be shown, and the average velocity within the water channel at the center flow will be compared to various cooling channel designs [2, 3, 4, 6 channels per base].

1.5 Thesis Outline

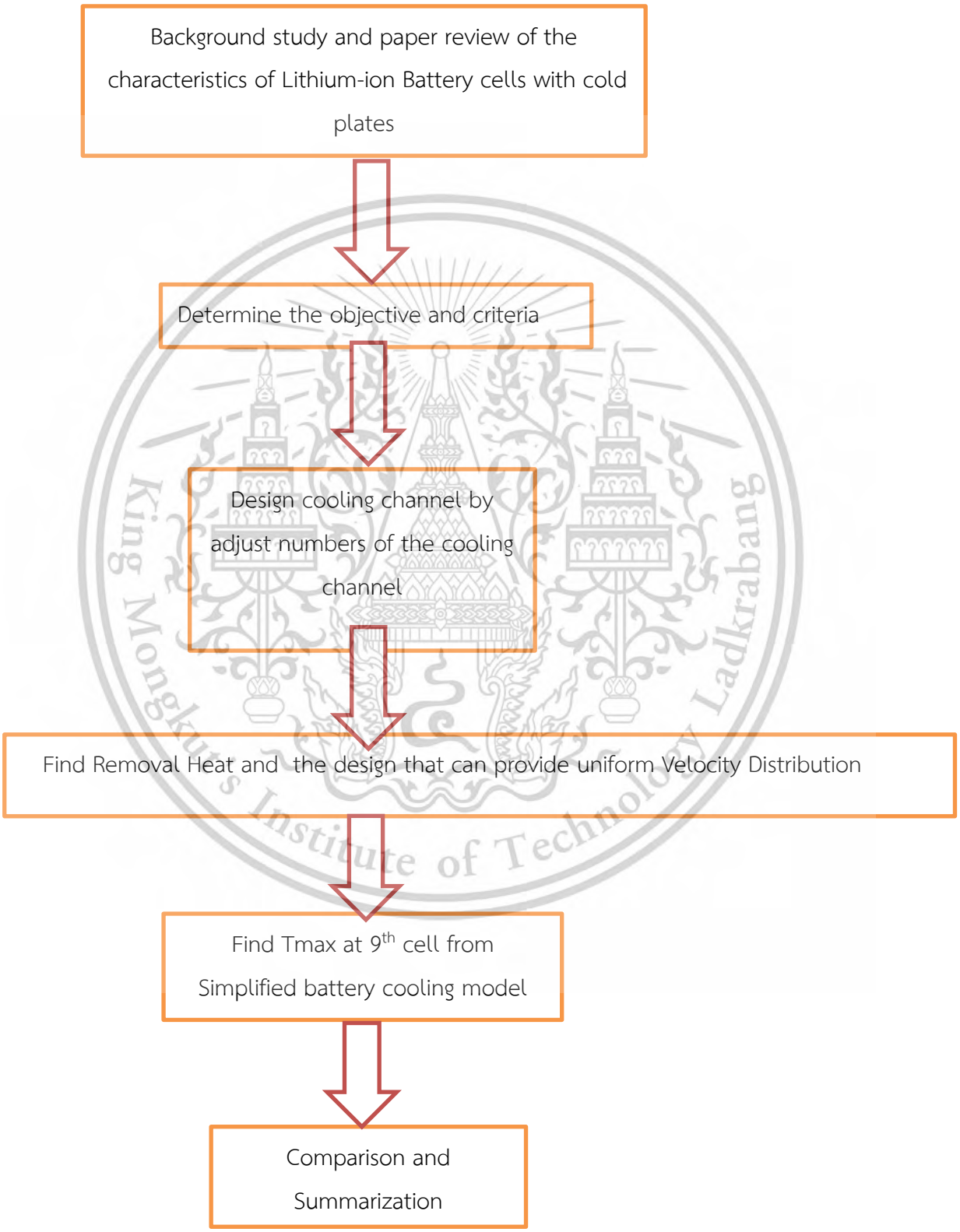

CHAPTER 2

LITERATURE REVIEW

2.1 Li-ion Batteries

Lithium batteries are available in three different shapes and sizes: cylindrical, prismatic, and pouch cell. The layers in cylindrical cells are rolled and placed in a cylinder, as shown in Fig. 2.1. The mechanical stability and simplicity of manufacture of this cell structure are advantages. For thinner design criteria, the prismatic cell shown in Fig. 2.2 was wrapped in packages. Pouch cells offer the most efficient packing since they do not have a metal container and may be stacked.

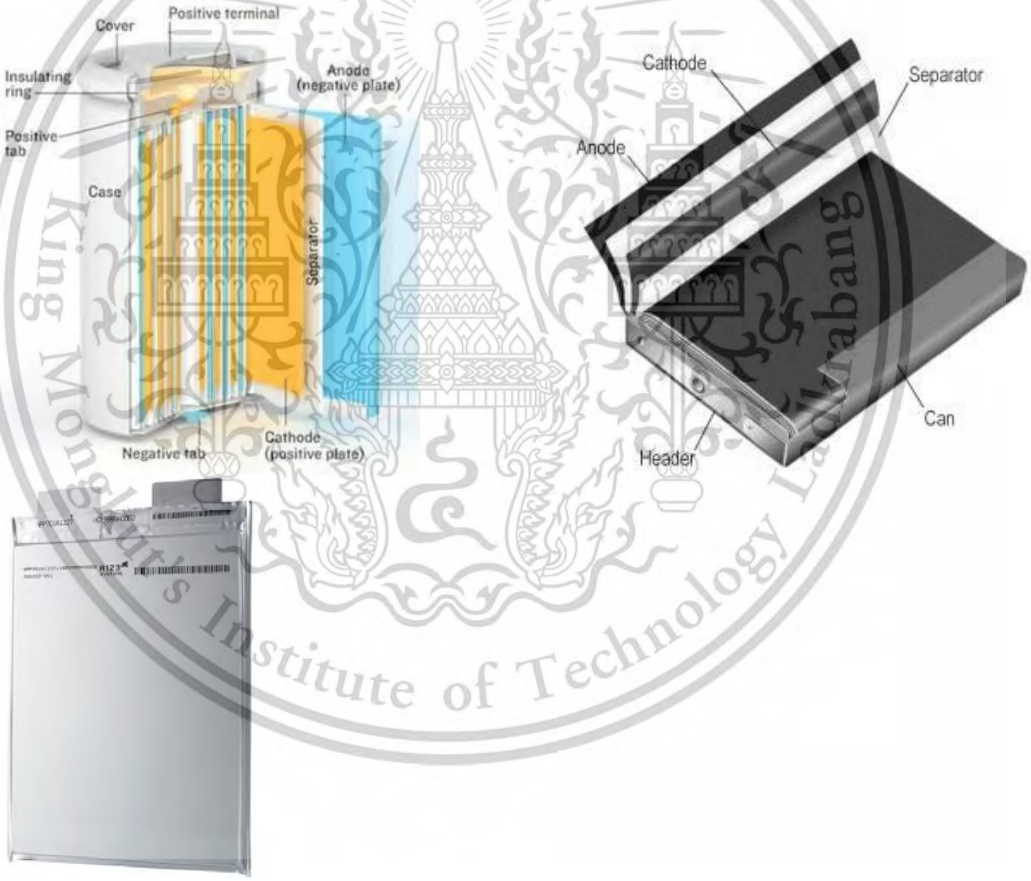

Fig.2.1 Lithium-ion cylindrical cell composition [2] Fig.2.2 Lithium-ion prismatic cell composition [3] Fig.2.3Lithium-ion pouch cell composition [3]

To investigate the challenges of lithium battery heat management, several previous scholarly publications have been reported, and this review focuses on recent publications to provide better knowledge of lithium-ion thermal management.

2.1.1Heat generated inside the batteries

Since the battery's cooling is inversely proportional to the heat generated within it, it is critical to understand where the heat comes from Bernardi et al[13]. The heat generated within a battery was calculated using a thermodynamic energy balance. He analyzes four factors that influence this equilibrium. The first is the electrical energy generated within the battery. Secondly, reversible reactions and entropic heating inside. The third process is the heat produced when the concentration of the battery temperature changes while the reaction progresses.

The heat dissipated by the material phase transitions is the final process in the energy balance.

The heat of mixing and phase shift are disregarded in the preceding phrase. The first term represents the overpotentials during charge transfer at the interface and ohmic losses. The second term is the reversible entropic heat from the reaction [24].

2.1.2Thermal management impact on battery performance

The operational efficiency of lithium-ion batteries is highly reliant on cell temperature. The optimal operating temperature for lithium batteries is 15-35 ^{o}C [20]. Operating outside of this range will have an negative impact on the battery's performance and long lifespan.

2.1.3Degrading performance

High cell temperatures raise the internal resistance of the cell, reducing output power. Furthermore, higher temperatures will result in a greater loss of cycle performance. Lifecycle decline is the reduction of the cell's capacity whenever it is charged and then discharged. Cells that operate at greater temperatures acquire a greater amount of capacity after each cycle than cells that operate at lower temperatures [25].

2.1.4Temperature distribution

More heat will be created in battery packs as their size and charge/discharge rates rise. If this heat is not effectively dispersed, it will build up inside the battery packs. Furthermore, convective heat transmission is greater on the pack's exterior surfaces. As a result, the temperature distribution inside the battery packs will be uneven. As previously established, the performance of a cell is greatly dependent on its temperature. This indicates that temperature inequity will result in capacity variability between cells. This results in an impermeable cycle in which the cells with the right temperature must give more power to compensate for the low-performing cells, which leads to a rise in cell temperature [26].

In addition, lithium cells have a low tolerance to overcharging, so the overall charging capacity of a battery pack is limited to its lowest-performing cell [27]2.1.5Thermal Runaway

When the temperature of the cell reaches a particular threshold, a sequence of undesirable exothermic reactions will occur that can raise the temperature. This chain reaction will continue and result in an event known as a thermal runaway. Feng et al. [28] conducted an experiment using prismatic 25 Ah Li-ion batteries and measured interior cell temperatures of up to 870 °C. If a thermal runaway is not adequately handled, the outstanding amount of heat and gas produced might result in a fire or explosion. Thermal runaway can occur for a variety of reasons, including excessive temperature, overload, and short-circuiting.

When the SEI (solid electrolyte interface) decomposes, thermal runaway occurs. The SEI was utilized as the barrier between the negative electrode and the liquid electrolyte. When the SEI is destroyed, the electrolyte and electrode begin to react at roughly 100 °C. The reaction in this stage has become more exothermic, and the temperature of the battery will be raised. The separator between the anode and cathode melts around 130 °C, resulting in an internal short circuit. A chain reaction may begin at 200 °C that occurs in the lithium metal oxide, and then the electrolyte reacts with oxygen and disintegrates [20].

2.2 Thermal management system for batteries (BTMS)

When the cell's temperature exceeds a certain point, a series of unwanted exothermic processes occur. As previously stated, inappropriate battery temperature has a negative impact on battery performance, durability, and safety. As a result, each battery system requires a BTMS. The primary task of a BTMS is to retain the batteries at the proper temperature range while also ensuring uniform temperature distribution across the battery pack. Following that, depending on the use of the battery packs, several characteristics such as weight, size, reliability, and cost must be evaluated.

2.2.1 Air cooling

Air is the most common method of cooling and has been widely employed in a variety of sectors. Air may appear to be a poor cooling medium due to its low heat capacity and thermal conductivity.

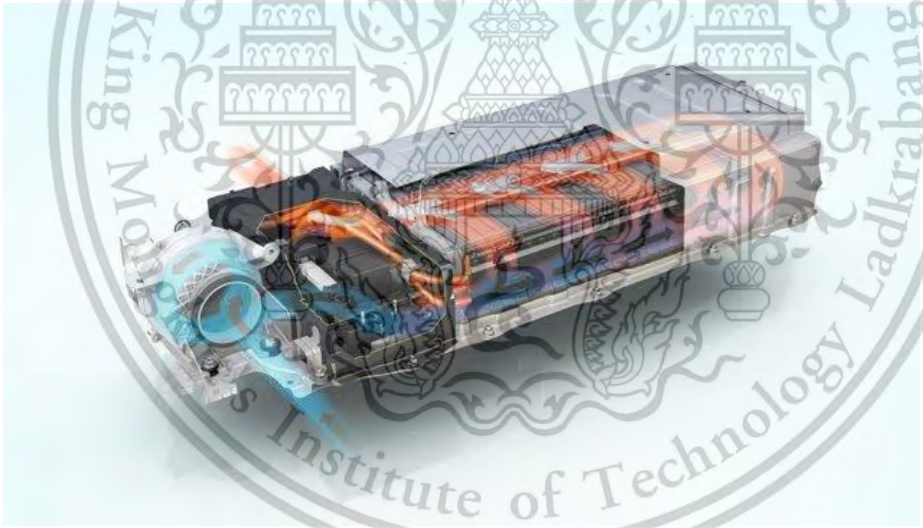

Fig.2.4 Toyota Prius Battery Pack with air cooling [33]

However, because of its simplicity and low cost, it remains an appealing cooling option [20]. The Toyota Prius and Nissan Leaf are two well-known examples. Natural convection (Passive cooling) and forced convection (Active cooling) can be used to cool. Natural convection is only appropriate for low-density batteries. Furthermore, blowers and fans are often employed to increase the convection coefficient [26]. Due

to its poor heat capacity, when air is utilized to cool a sequence of batteries, the temperature rises rapidly. As a result, cell temperatures at the pack outlet rise, resulting in an uneven temperature distribution. As a result, further precautions must be taken to ensure homogeneity, such as increasing the coolant medium speed, introducing turbulence in the flow, and modifying the positioning of each cell.

Wang et al. [30] investigated several cylindrical cell arrangements and fan locations. The optimum cooling performance was discovered when the fan was positioned on top of the module, and the most desirable layout in terms of cooling effect and cost was discovered when the cells were organized side by side in a square pattern. In a CFD simulation, Mahamoud et al. [31] have shown that employing reciprocating air flow may considerably enhance thermal performance of a battery module. Changing the direction of the airflow every 120 seconds can minimize the temperature differential between cells by 72% and the maximum temperature by 27%.

2.2.2Liquid cooling

When compared to air, liquid coolants offer various advantages. Liquid coolants have a higher convective heat removal rate than air due to their larger density and heat capacity without negatively impacting cooling capacity. Because of their larger density and heat capacity, liquid coolants can be 3500 times more effective in removing heat from battery packs than air cooling. When compared to air cooling, they can save up to 40% of battery power. Furthermore, liquid cooling can minimize noise levels. However, there are drawbacks to liquids as well, such as expense, complexity, and the possibility of leakage [26].

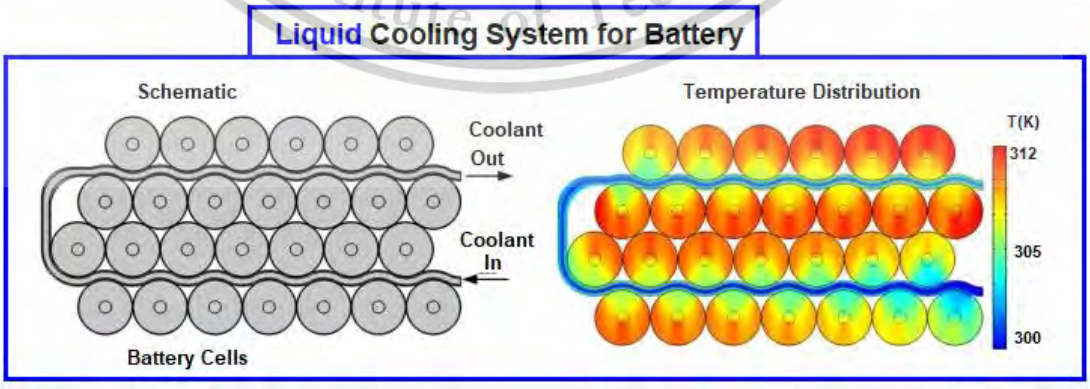

Fig.2.5 Liquid cooling system for Battery

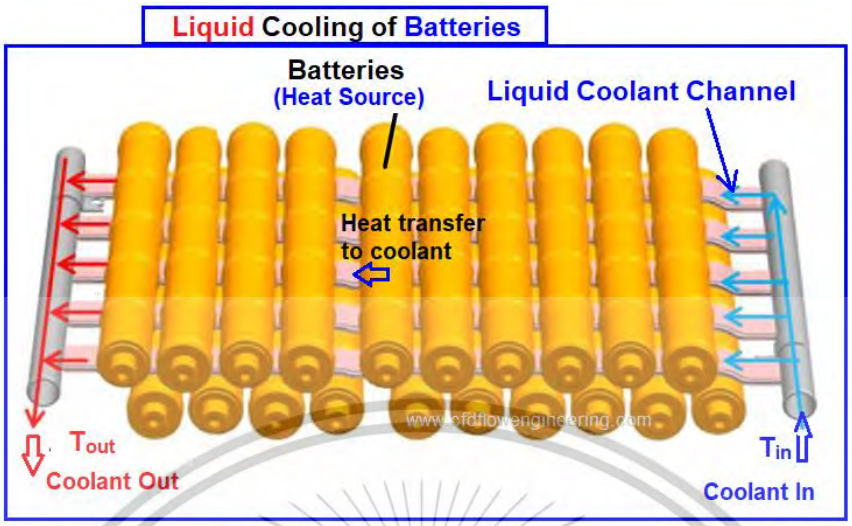

Fig.2.6 Liquid cooling of Batteries and heat transfer takes place from the cells to cooling channels

2.2.3Indirect liquid cooling

Water is employed as one of the most efficient coolants in a variety of industrial applications. The biggest issue with directly cooling batteries with water is the possibility of short-circuiting. In order to prevent electrical conduction with the cells while retaining high thermal conductivities,

indirect approaches are utilized. In their vehicles, EV manufacturers such as GM and Tesla use indirect cooling. Between each prismatic cell, GM employs cold plates. The cold plates are narrow and have several microchannels running through them. Tesla uses wavy tubes that pass between cylindrical cells. To fill the gap between the cells and cooling channels, a thermally conducting yet electrically isolating substance was employed.

Although the wavy tubes appear less efficient due to the tiny heat transfer contact surfaces, they are mechanically and electrically safer. All coolant connections are made outside of the battery shell, removing potential leak zones.

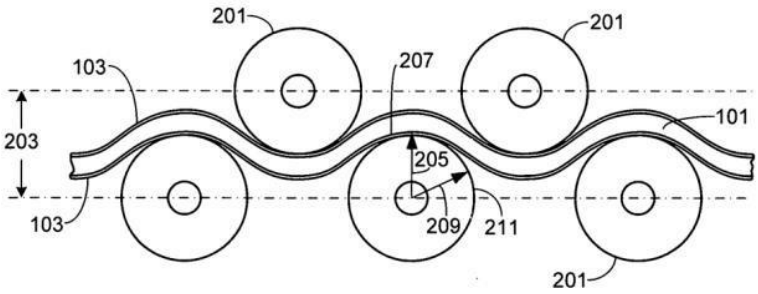

Fig.2.7 Tesla cooling system schematic [32]

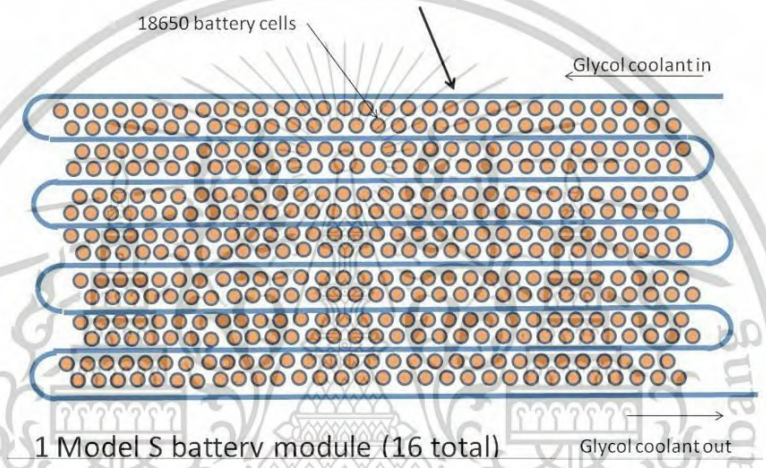

Fig.2.8 Tesla cooling system configuration [33]

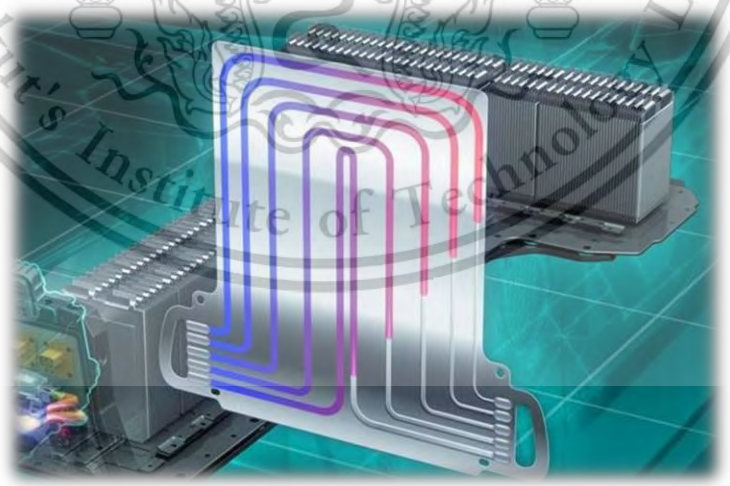

Fig.2.9 Chevrolet Volt Cooling system [33]

2.2.4Direct liquid cooling (Immersion)

Direct cooling, also known as immersion cooling, cools the cell equally across its whole surface. This reduces hot and cold areas in the cell and boosts its performance. A dielectric coolant with low viscosity and high thermal conductivity and thermal capacity should be used for direct cooling.

Immersion cooling is becoming more common in data center servers and power electronics. Immersion for BTMS is currently uncommon in the mass-produced EV market. This is most likely due to financial and safety concerns. As of today, immersion cooling for batteries has only been employed for prototype high-performance EVs and EV racing, according to the authors. 3M (Minnesota Mining and Manufacturing Company) manufactures dielectric liquids for cooling applications.

The 3M Novec 7200 Engineered Fluid [34] was utilized by Xing Mobility for electric racing [35]. The fluid has a boiling point of 76 °C, which keeps the cells from overheating and causing thermal runaway. For the cells, we utilize simple containers for computing, which will be submerged in liquid [36].

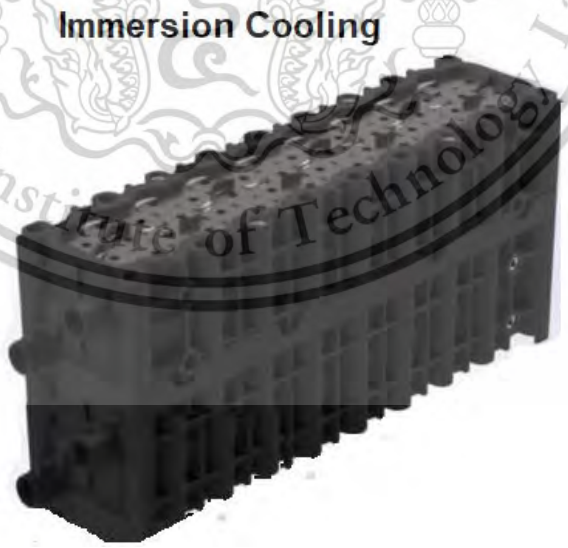

Fig.2.10 Xing battery module with immersion cooling [35]

2.2.5Phase change material (PCM)

Hallaj and Selman [39] were the first to employ PCMs for BTMS. Because of its high latent heat, the phase change material works as a heat sink during battery discharge. When the cells are in standby mode, the PCM emits heat into the cells and the surrounding environment. The melting point of the PCMs utilized for thermal control is within the optimum performance range of lithium batteries.

To improve heat conductivity, they combine paraffin (as PCM, with a melting range of 32–38 °C) with graphite flakes. The graphite flakes will also form a semi-matrix block containing paraffin. As a result, even when the paraffin is melted, it remains within the matrix, and the entire composition retains its solid structure. Another advantage of solid PCM is that it functions as a shield in the event that one cell experiences a thermal runaway

Fig.2.11 Battery module with PCM

However, there is a disadvantage to PCM. If the batteries are run for an extended period of time and the ambient temperature is too high, the PCM may fully melt and even behave as a thermal barrier due to its limited thermal conductivity. If the temperature was lower, the PCM would add thermal mass to the modules, making it more difficult for the cells to attain the proper temperature[20].

Overall, PCM might be the optimum passive option for low-operating-rate modules, or it can be supplemented with active cooling (e.g., indirect liquid cooling) for greater operating rates and harsh ambient temperatures.

2.2.6Heating

When comparing the battery's thermal control, it includes both cooling and heating. However, there have been few studies on heating. This might be due to the exothermic nature of battery operation, in which there is continual heating from cell activity. Furthermore, cooling techniques to prevent thermal runaway, which happens at high temperatures, have risen. Thermal runaway has devastating implications, but low operating temperatures only degrade battery performance.

Nonetheless, with the growth of the EV industry and the importance of their range in recent years, many BTMS technologies have been researched to enhance the performance of EVs in cold settings. The heating method's criteria are identical to those for cooling, and the time it takes to heat up the batteries is within the optimal range.

2.3 Characteristics of Geometry Model

CAD software makes the model for setting boundary conditions, meshing parts, and solver settings. After that, the steady-state model of the cooling channel will be used to find the temperature, pressure drop, and Reynolds number at the outlet section using various parameters such as inlet temperature and inlet velocity

2.3.1 Geometry and Materials

This work's 3D-model CAD file has both solid and fluid components. The solid components of the work are the 36 battery cells in the battery module, 1 nickel plate, 1 insulation layer, and 1 anodized aluminum plate. Some solid components, such as the battery module housing, the positive common plate, and the aluminum wire, are not considered in the model because of their poor heat transfer.

2.3.2 The calculation of heat generation

The cooling system assumed that the temperature of the entire battery was constant, so the term for the battery's internal conductivity was left out, as was the heat transfer from the battery cell to an electrical wire and the surrounding environment. The equation below can be used to estimate heat generation [12, 13] where the heat generated inside the battery was denoted by the symbol $Q_b(t)$, which is composed of two sources: Joule heating , $Q_J(t)$and entropy change-related heat generation, $Q_E(t)$

$$Q_J(t) + Q_E(t) = Q_b(t) \quad (1)$$

The two sources of heat generation are specified in Equations (2) and (3) as

$$Q_J(t) = I^2 R_{int} \quad (2)$$

Where $Q_J(t)$ stands for the heat of Ohmic losses, often known as Joule heating (W), I for battery current (A), and R_{int} for internal resistance, which is made up of three terms: diffusion resistance, Ion transport resistance, and Ohmic resistance [14]

$$Q_E(t) = -T\Delta S\frac{I}{nF} \quad (3)$$

Where $Q_E(t)$ is the heat generation due to entropy change (W), *T* is the absolute temperature of the battery (°C), ΔS is the entropy change (J/K), n is the number of electrons (mol) and *F* is Faraday's constant ($9.65{\cdot}10^5$ s·A/mol).and $Q_E(t)$ from (3) also equal to $-I\left(T\frac{dV_{OC}}{dT}\right)$ when the current I is negative for charging. The state-of-charge (soc) and temperature of the cell affect the open circuit potential (V_{OC}) and total internal resistance (R_{int}) of the battery.

$$-T\Delta S\frac{I}{nF} = -I\left(T\frac{dV_{OC}}{dT}\right) \quad (4)$$

While setting heat generation rate, This equation below explained how to calculate the internal heat generation

$$Q_b(t) = I(V_{OC} - V) - I\left(T\frac{dV_{OC}}{dT}\right) = I^2R_{int} - I\left(T\frac{dV_{OC}}{dT}\right) \quad (5)$$

The heating resulting from the Joule effect (irreversible heat generation) is represented by $I(V_{OC} - V)$ and $\frac{dV_{OC}}{dT}$ is represented the differential of open circuit voltage with respect to change in temperature of battery cells.

Finally , the battery state of charge (SOC)was estimated by ampere-hour integration

$$SOC = SOC_{t=0} - \frac{1}{C_N}\int I(t)dt \quad (6)$$

Where $SOC_{t=0}$=1 (when the battery is 100% charged)and $C_N$is the nominal capacity of the cell

2.3.3 Numerical of heat generation model

The heat generation model was performed using Finite Elements Analysis (FEA) with The Conjugate heat transfer equation in laminar flow will be shown as below

$$\rho(u * \nabla) * u = \nabla * \begin{bmatrix} -pI + \mu(\nabla u + (\nabla u)\mu(\nabla u + (\nabla u)^T) \\ -\frac{2}{3}\mu(\nabla * u)I \end{bmatrix} + F \quad (7)$$

$$\nabla * (\rho u) = 0 \quad (8)$$

$$\rho Cp * \text{u trans}\nabla\text{T} = \nabla * (k\nabla T) + Q_b(t) \quad (9)$$

Those equations [7-9] will be used in the mode based on the heat conjugate heat module. Moreover, the heat generation model was analyzed using a time-dependent study to analyze the temperature distribution within the battery cell. It is important to note that the heat source of the model in this work is the heat calculation from Kulranut J al [17]

2.3.4Numerical modeling of battery cell based on the proposed cooling strategy

The geometry of the battery module was simplified based on the chosen cooling method. This simplification involved omitting certain components that were considered less influential on heat transfer. Parts such as the insulator between battery cells, small aluminum conducting wires (fuses), positive and negative bus bars, and the plastic housing plate were excluded from the model. This decision assumed that these components contribute minimally to heat transfer.

The battery model was implemented using a transient model to study real-time surface temperature. Transient modeling allows for the analysis of temperature variations over time, providing insights into dynamic thermal behaviors during different operating conditions. The fluid flow within the system was modeled as laminar flow under non-isothermal conditions. Laminar flow refers to smooth, orderly fluid motion, and non-isothermal flow indicates that the fluid temperatures are not constant. This modeling choice considers both fluid flow characteristics and heat transfer dynamics.

The simplified geometry of the battery cell with a fluid domain was employed to investigate the thermal characteristics of the battery cell. This likely involved examining how heat was distributed and dissipated within the battery cell during different operational scenarios. To manage computational time due to the large number of mesh elements in the simulation, efforts were made to streamline the model. While simplifying the geometry can reduce computation time, it was acknowledged that running the simulation still requires a significant amount of time.

2.3.5 Governing Equation for Modeling of Battery

To solve the 2D steady flow in the cooling channels of battery Pack, the continuity equation, momentum equation, and energy equations are written as follows:

Continuity equation

$$\nabla(\vec{v}) = 0 \tag{10}$$

Momentum conservation equation

$$\nabla(\rho v\vec{v}) = -\frac{\nabla P}{\rho} + \frac{\mu}{\rho}\nabla^2\vec{v} \tag{11}$$

Energy conservation equation

$$\rho c_p\left(v_x\frac{\partial E}{\partial x} + v_y\frac{\partial E}{\partial y} + v_z\frac{\partial E}{\partial z}\right) = k_T\left(\frac{\partial^2 E}{\partial x^2} + \frac{\partial^2 E}{\partial y^2} + \frac{\partial^2 E}{\partial z^2}\right) \tag{12}$$

The steady flow energy equation

$$\dot{m}_w C_P(T_i - T_o) = -\dot{Q}_b(t) = q_b\forall \tag{13}$$

$$\dot{m}_w = \rho_\omega \dot{v}_w \tag{14}$$

$\dot{v}_w$=V*A (15)

$A = \pi(\frac{D}{2})^2$ (16)

$\dot{Q} = \dot{q}_b \forall$ (17)

When $\dot{Q}_b(t)$ = The heat removed rate of the liquid inside cooling channel [KW]

$\dot{q}_b$= The volumetric heat generation rate inside battery [W/m^3]

$\dot{v}_w$ = The volumetric flowrate of Inlet water [m^3/s]

ρ_ω = Density of cooling water [998 Kg/m^3]

C_P = Heat capacity of cooling water[4.187 KJ/kg·K]

T_i = Inlet temperature [℃]

T_o= Outlet temperature [℃]

$\forall$ = The entire volume of 18650 Li-ion Battery[m^3]

m = Fluid mass within the cooling channel [Kg]

$\dot{m}_w$=the mass flowrate of Inlet water [kg/s]

V = water velocity Inlet [m/s]

A= cross-sectional area[m^2]

D= Diameter of Inlet cooling Tap(m)

2.3.6 The standard deviation of the uniform flow

Standard deviation = $\sqrt{\frac{\sum(v_i - \bar{v})^2}{n}}$

Where

v_i = the channel velocity in each channel (m/s)

$\bar{v}$ = the average channel velocity at mid point (m/s)

n = the amount of channel

Uniform flow in a channel refers to a flow where the velocity is consistent across the cross-sectional area. The standard deviation is a measure of how much the velocity varies from the mean velocity. When the standard deviation is low, it indicates that the flow is more uniform. Conversely, a high standard deviation suggests more variability and thus less uniform flow [called non-uniform].

Furthermore, unequal speed between the middle of the pipe and the pipe surface causes shear force in the fluid. If the maximum speed of flow was close to the average speed, it would cause the low shear force compared to the case with deviating from an average speed. So, the SD value will be calculated to make sure that the uniform flow has the least amount by comparing the average velocity with the velocity at the midpoint of the cooling channel.

The pressure drop in a channel refers to the reduction in pressure as the fluid flows from the upstream to the downstream end.

This drop was influenced by the flow velocity and friction forces within the channel. When the flow velocity increases, the frictional forces (which are related to the shear force) also increase. This can lead to a greater pressure drop. If the flow is perfectly uniform, the pressure drop might be least under ideal conditions, meaning the channel velocity was evenly distributed across the channel. This implies that the flow velocity at the inlet and outlet would be nearly the same.

2.3.7 Heat generation inside Battery

For setting battery simulation, the generated heat of the battery cell can be estimated by $Q_J(t) + Q_E(t) = Q_b(t)$ and the function for $Q_E(t)$ can be approximated using this equation function f(t) = 0.0002t + 0.3817 as shown in Fig.2.13.

The reversible one is calculated by the change in entropy $Q_E(t) = Q_{rev} = -T\Delta S\frac{I}{nF}$ and the irreversible part may be calculated by the Ohmic heat $Q_J(t) = I^2R_{int}$ or $Q_{irrev} = \mathrm{I}(E_{rev} - V_c)$. The graph below shows the relationship between Internal resistance function change with time

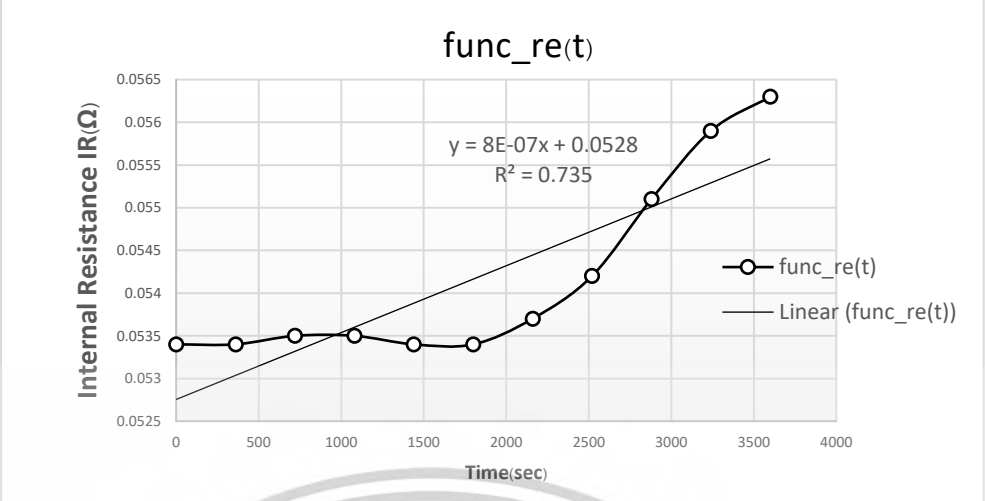

Fig.2.12 Internal resistance change as a function of time[0-3600s] and its linear fit function, func_re(t) when charging rate 0.75C

When using $Q_J(t)$ as heat source rate = 20*(2.6^2)*func_re(t) W and I = 2.75 A while independent time = 3600 s and The maximum internal resistance of the battery was 0.056 Ω when the current rate was in the discharge process, then insert func_re(t) from Fig. 2.12 and the entropy change equation at the heat source rate $Q_E(t)$ = 20*func_ent(t) W from Fig. 2.13.

Setting up a model using steady state simulation with maximum heat generation at 3600 s $Q_b(t = 3600s)$when charging rate of 0.75 C [0.307 W] from Kulranut et al. [17], and the result will display the maximum temperature of the battery in the steady and transient cases in Topics 4.2 and 4.3, respectively [simulated only 9 cells in 1 row].

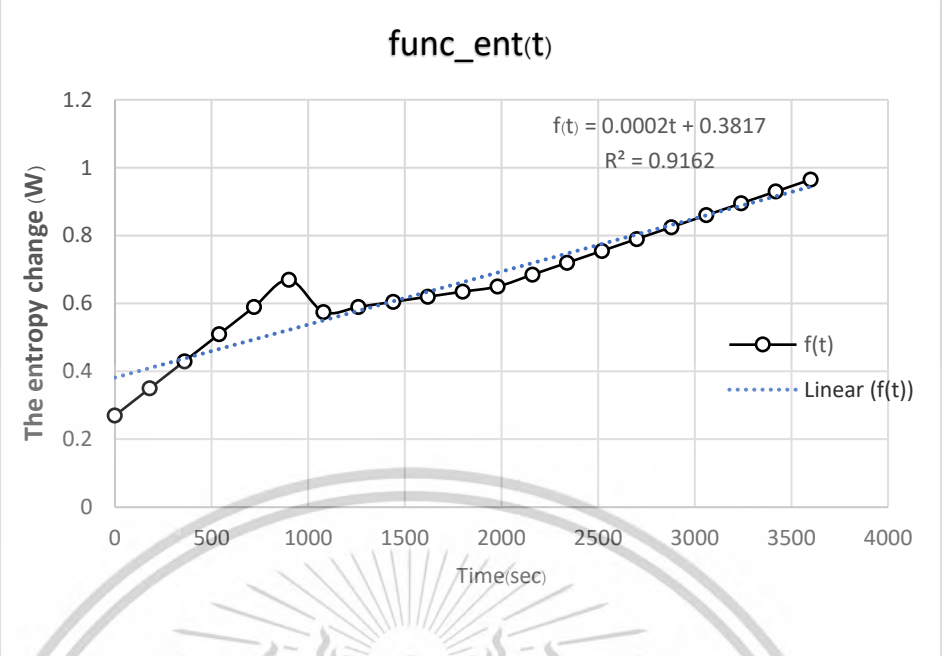

Fig.2.13 Entropy change as a function of time[0-3600s] and its linear fit function, f(t) when charging rate 0.75C

The conjugate heat transfer model for the laminar flow pattern was used in this work. Heat source as a function of time was used for each of the thirty-six battery cells calculated by ohmic heat loss function and Entropy change; it is transferred through the copper plate and the aluminum plate in the form of heat conduction before it is transferred from the aluminum plate by the coolant by heat conduction.

CHAPTER 3

RESEARCH METHODOLOGY

3.1 Design Strategy of cooling plate by varying the numbers of cooling channels configurations

The design concept involves varying the number of cooling channels on an aluminum cooling plate with barriers at the inlet and outlet sections, while also adjusting the cooling channel gap. The goal is to determine the primary factor affecting the cooling performance by examining different designs of the liquid cold plate and analyzing various flow parameters in the cooling channel section, such as mass flow rate and temperature differences.

The primary design variation involves changing the number of cooling channels on the aluminum cooling plate. This adjustment is made to understand how the cooling performance is influenced by the number of channels. Barriers are included at the inlet and outlet sections of the cooling channels. These barriers can impact the flow dynamics and the distribution of cooling within the channels. The cooling channel gap is adjusted to be equal to the previous design. This parameter variation is likely to be explored to assess its impact on cooling performance.

3.2 Cooling Channel Specifications

The liquid channel's outflow is located on the bottom plate's output side, connecting the cooling plate to the bottom plate. The cooling channel has dimensions of 167 mm in width, 410 mm in span, 7.8 mm in length, and 7.8 mm in thickness.The cooling barrier has a dimension of 260 mm in length and 2.5 mm in thickness.Inside the cooling channel, water flows through a channel that is 6 mm wide and 112 mm long.The liquid channel features circular inlets and outlets with sizes of 4 mm.

Several factors are identified as influencing the cooling performance:

Pressure in Cooling Channel: The pressure passing through the cooling channel influences velocity dispersion on the aluminum cooling block and the removal of heat from the battery module.

Water Velocity and Temperature: The velocity and temperature of the water flowing through the channel play a crucial role in determining how effectively heat is removed from the system.

Inlet-Outlet Location and Path: The location of the inlet and outlet, as well as the path taken by the cooling water, also affect how temperature is distributed on the aluminum cooling block.

In summary, the design concept focuses on systematically varying design parameters to understand their impact on cooling performance. The specifications provided for the cooling channel and associated components give insight into the physical dimensions and characteristics of the system being studied.

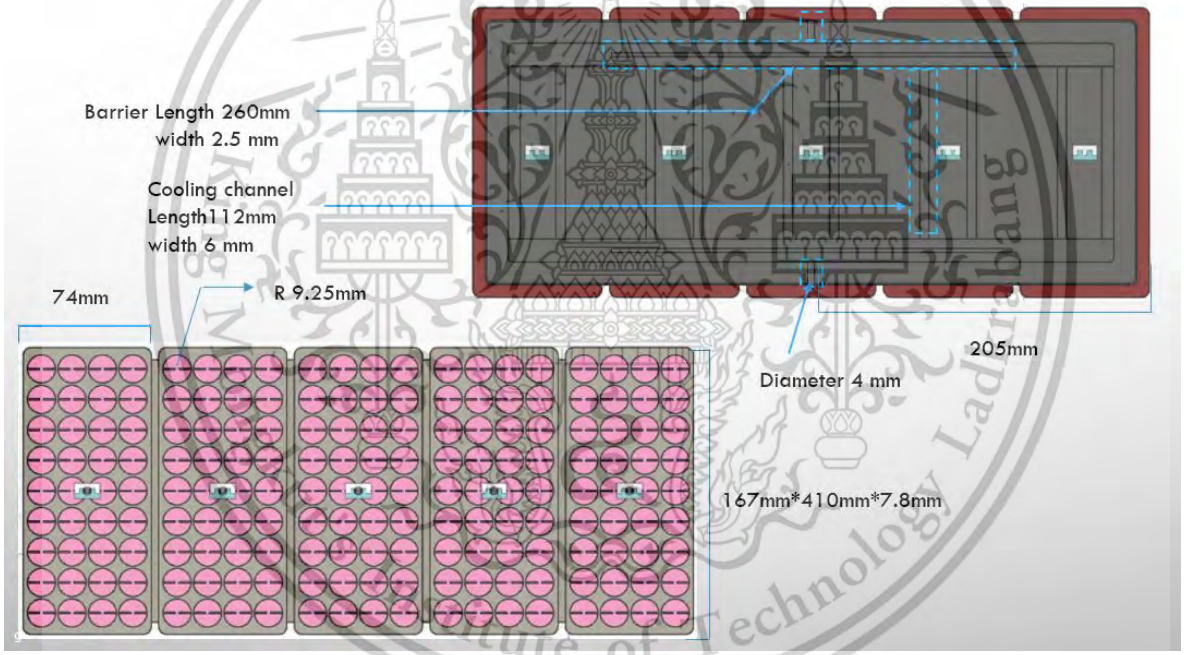

Fig.3.1 The Specification of the Previous Design Version of the Cooling Plate

The channel geometry impacts the average velocity (V_{avg})which later affects the boundary layers generated by the fluid flowing along the bounding surfaces. The inlet temperature of the liquid cooling plate also has a great impact on the temperature of the battery cells. Moreover, the heat removed from the 18650 Li-ion battery by the aluminum cooling plate is similarly influenced by all of these factors. The maximum

acceptable battery temperature is 33°C, even though the desirable differential temperature between battery packs should be less than 5°C, which can enhance the battery cell's cooling efficiency [16]. To keep the operating temperature of the battery pack within the appropriate range, an aluminum cooling plate with efficient cooling must be created.

The temperature, velocity, and fully developed flow all varied with the conditions. The main variables used in this model were inlet temperature, water velocity, and the number of channels. The number of cooling channels can affect the system's total cooling capacity.

3.3First Design of Cooling channel per base

Separate the half axisymmetric model to be 2.5 block of channel per base [length 96.25 mm].Then divide the one block of channel per base to be 2,3,4 and 6 parts respectively while fixing cooling channel gap at 6 mm

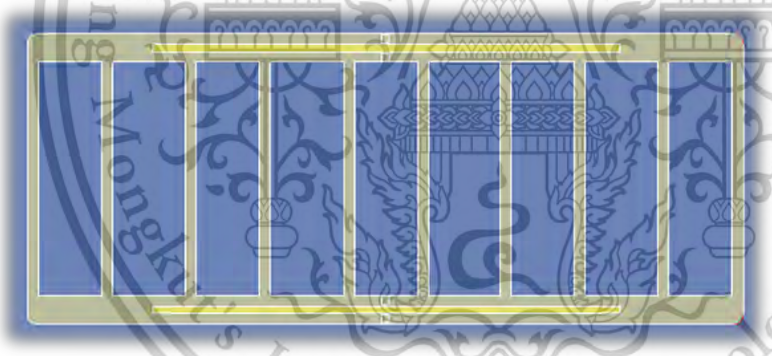

2 Cooling channel base design [length 48.125 mm]

Fig 3.2 First Design of 2 cooling channel per base

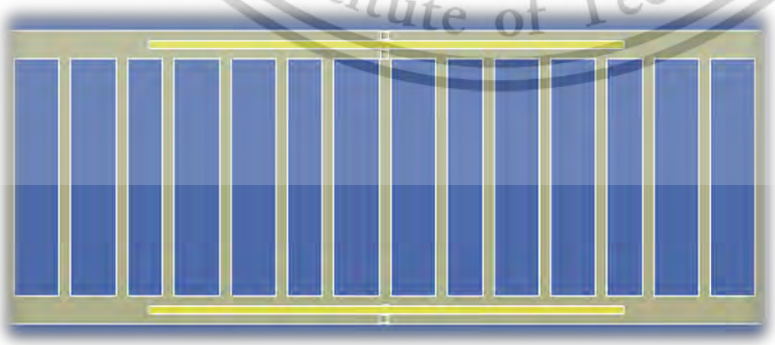

3 Cooling channel base design [length 32.08mm]

Fig.3.3 First Design of 3 cooling channel per base

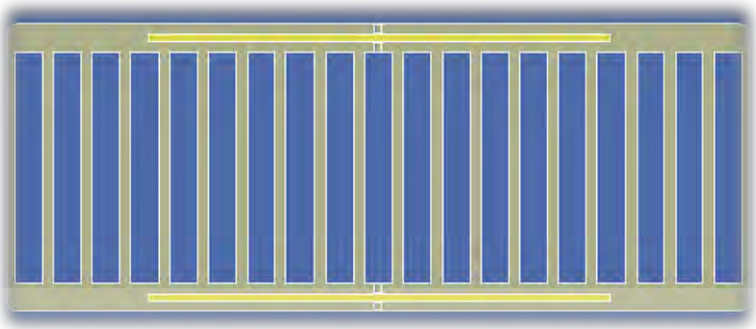

4 Cooling channel base design [length 24.0625 mm]

Fig.3.4 First Design of 4 cooling channel per base

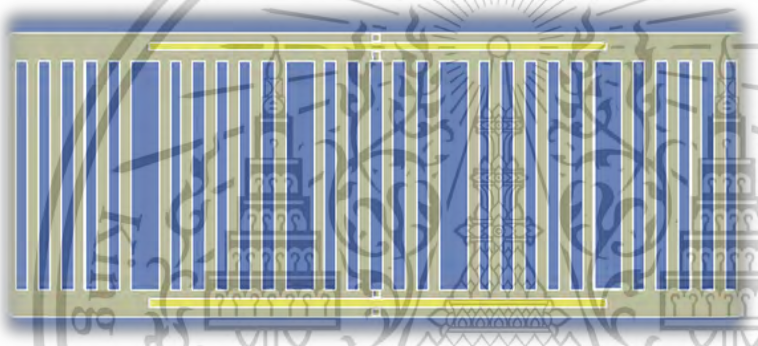

6Cooling channel base design [length 16.042mm]

Fig.3.5 First Design of 6 cooling channel per base

3.4 Cooling channel design modification

3.4.1)Decreasing the cooling barrier length from 260 mm to 160 mm to ensure more water flow distribution in the cooling channel configuration while the cooling gap length is fixed.

** 1 channel per base = 96.5 mm**

3.4.2)Modifying the water-cooling gap length to have equal space [41, 32.5, 20.5, and 12 mm from center to center] Firstly , separate the cooling channel length to have 10 number of channels for 2 channel base, 13 number of channels for 3 channel base and 20 number of channels for 4 channel base; to make the water velocity to be more uniformed distributed inside the liquid aluminum cooling plate design that can determine what was the factor affecting the water cooling dispersion by examining

various designs of the liquid cold plate .then finding which channel design can produce the best velocity uniformity by calculating the standard deviation value in the next chapter and making flow turbulence increase. If the maximum value of velocity inside appears on a cooling channel design with a low SD value. Then it can be predicted that this channel design has the best cooling performance among all types. but it's also necessary to find the amount of heat removed to make a comparison between numerous designs.

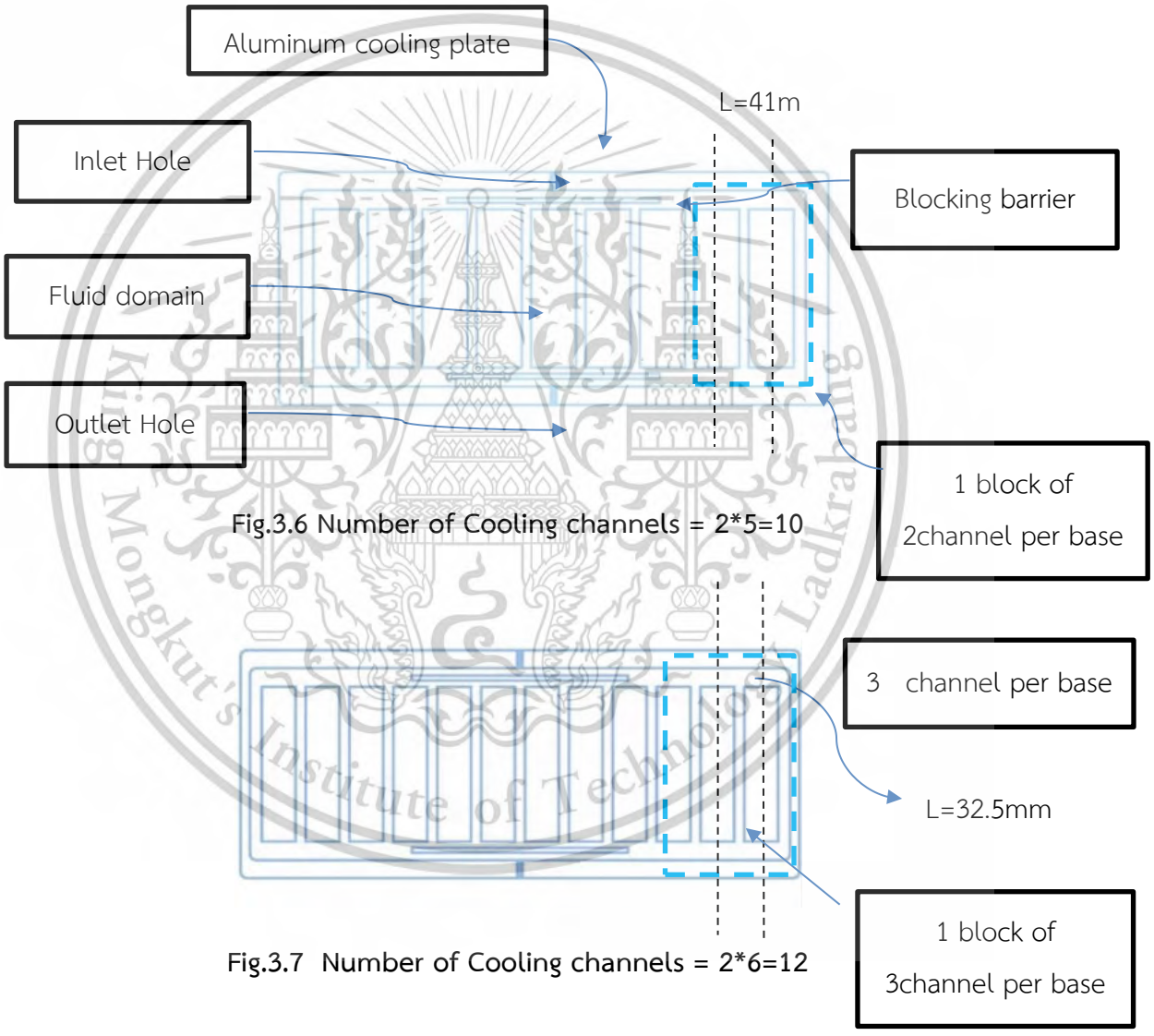

Fig.3.6 Number of Cooling channels = 2*5=10

Fig.3.7 Number of Cooling channels = 2*6=12

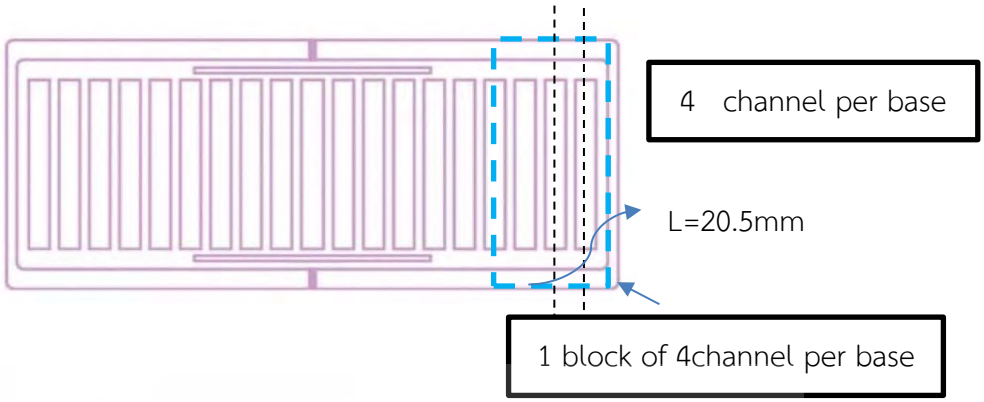

Fig.3.8 Number of Cooling channels = 2*10=20

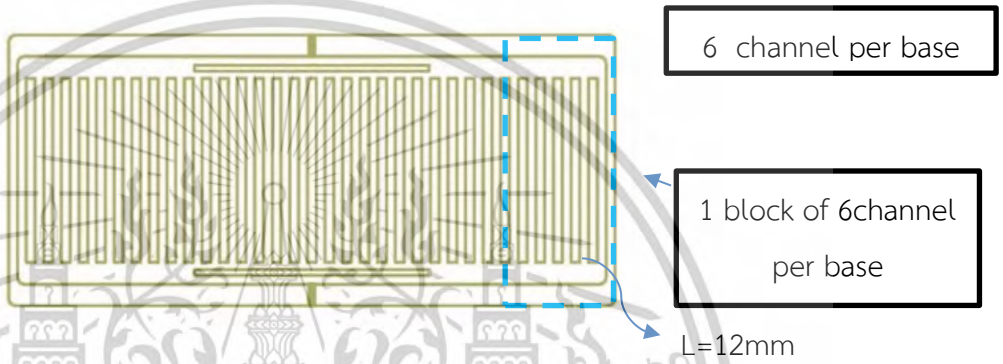

Fig.3.9 Number of Cooling channels = 2*17=34

Fig[3.6-3.9]Design the different numbers of the cooling channel in the Battery Module

3.5 Simulation set up on Cooling system

One of the limitations of assembling battery packs in an electric car is space. Consequently, the liquid cooling system has been chosen because it is more effective than the air-cooling system in terms of space [4]. There are one hundred eighty Li-ion battery cells in the battery pack. Five battery modules are packed within aluminum cooling plates and each battery module has thirty-six cells

Table 3.1 Properties of Material

Material	Phase	Thermal Conductivity [W/(m.K)]	Heat Capacity [J/(kg.K)]	Density [Kg/m^3]	Heat Ratio	Viscosity [Pa.s]
Battery Cell	*Solid*	{1.01,1.01,30.22}	750	2690	-	-
Aluminum	*Solid*	155	893	2730	-	-
Coolant	*Liquid*	0.405	3300	1078	1	0.00429

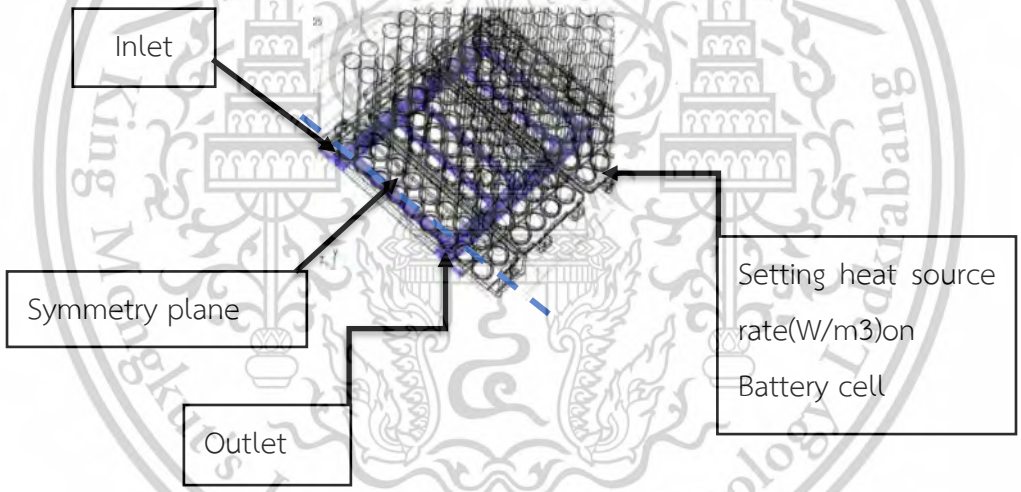

Fig. 3.10 The geometry of the cooling channel design with coolant liquid inside

In the mesh independence test, mesh settling has been used for the fluid area to provide estimation quality. The standard size was 0.20-0.25 mm. Simulation results of the battery module's highest temperature under 0.75 C charging rate using different grid numbers and when the number of grids reaches 100,000, the calculating results become more consistent.

3.6The Parametric Study for Cooling Channel

In this case, the flow rate and coolant inlet temperature are considered under the steady-state model. The flow rate is the first parameter to be adjusted while controlling the inlet temperature to equal the ambient temperature. This is because it is simpler to adjust the flow. However, when the flow rate cannot be further increased due to the limitations of the circulating pump, the inlet temperature will be adjusted as the second parameter.

3.6.1 Consideration of Flow Rate and Coolant Inlet Temperature:

Flow Rate Adjustment: The flow rate is considered as the first parameter to be adjusted. This adjustment is made while controlling the inlet temperature to be equal to the ambient temperature. This initial adjustment likely aims to understand the system's response and performance variations with different flow rates.

Inlet Temperature Control: The inlet temperature was maintained equal to the ambient temperature during the initial adjustment of the flow rate. This provides a controlled baseline condition for assessing the impact of varying flow rates on cooling performance.

Adjustment Sequence: Flow Rate Adjustment Priority: Adjusting the flow rate is chosen as the first parameter due to its simplicity and ease of control. It allows for a systematic variation of the flow conditions to analyze their effects on the cooling system.

Inlet temperature Selection: When the flow rate reaches its limit due to the capacity constraints of the circulating pump, the inlet temperature becomes the second parameter to be adjusted. This suggests a sequential and systematic approach to parameter adjustments.

3.6.2 Analysis Divisions:

This division suggests that each parameter was systematically studied, likely varying one parameter while keeping the others constant to understand their individual effects. The simulation cases for inlet velocity, inlet temperature, and inlet pressure are conducted under the same set of boundary conditions. This approach ensures consistency in the analysis and allows for a more accurate comparison of results.

In summary, the study adopts a systematic approach to analyze the cooling system under different conditions, focusing on variations in flow rate and coolant inlet temperature. The sequential adjustment of parameters and the division of analysis

into distinct parts demonstrate a structured methodology for understanding the system's behavior and performance characteristics.

3.7The cooling strategy in cooling channel simulation

3.7.1Inlet velocity of water selection

Investigating the effect of the flow rate on cooling performance was carried out based on steady-state simulation. The flow speeds were simulated in the sequence of 50 L/h (0.5 m/s), 100 L/h (1.0 m/s), 200 L/h (2.0 m/s), and 300 L/h (3.0 m/s).Moreover, it can be expected that as the flow speed increases, the maximum temperature of the battery module will decline.

3.7.2Inlet temperature of water selection

In this simulation, the battery was assumed to be fully charged under constant current mode [SOC > 0.8] with a constant C-rate [0.75 C]. The coolant temperature also has a significant impact on the amount of heat generated by lithium-ion batteries. The simulation first used low water velocity at 0.5 m/s, and water temperatures started at 25 °C, followed by 30 °C, 35 °C, and 40°C, respectively. After adjusting the coolant temperature and running for a time, the result will show the battery module temperature trend, and it's expected to gradually rise at the same inlet velocity. However, the maximum temperature of the battery module needs to be below 33 °C. (see Fig.1.2).

Table3.2 Boundary conditions properties use for the flow channel Simulation

18650 3350mAh 6.5A Battery Properties	Operating voltage	2.6V - 4.2V	
	Capacity	2.75 Ah	3.3 Ah
Water Coolant	Thermal conductivity (k_w)	0.6 W/m·K	

	Density (ρ_w)	998 kg/m^3
	Heat capacity (C_p)	4128 J/kg·K
	Viscosity (μ)	0.00089 Pa·s
Anodized Aluminum	Thermal conductivity(k_{an})	205 W/m·K
	Density(ρ_{al})	2700 kg/m^3
	Heat capacity (C_p)	910 J/kg·K

3.8Setting Heat generation under various Discharging Conditions

From Kulranut et al. [17], The battery cell's thermal properties while charging and discharging, the battery cell was evaluated in the constant current (CC) and constant voltage (CV) modes. The current stays constant during the initial stages of charging in CC mode at around 80–90% of SOC when the battery is almost fully charged.

Table 3.3 Summary of the result at various discharge rate retrieved for Toriyama brand from Kulranut J al [17]

Event	Charge			Discharge		
Current rate	0.25C	0.5C	0.75C	1st1C	2nd1C	3rd1C
Maximum heat transferred(W)	0.073	0.145	0.307	0.953	1.022	1.041
Maximum temperature (°C)	36.36	41.70	45.813	51.813	52.462	53.012

*****For the current propose of investigation , The maximum Temperature is select at 0.75C during Charging event**

3.9The behavior of the volumetric for heat generation rate

Table3.5 uses Bernardi's equation (eq.4) to show average Heat generation value and Percentage of Variation when use different current discharge rates[0.5C, 1C, and 1.5C].

Table 3.4 Average Heat calculation retrieved from Paccha et al[18]

C-rate at charging Process	Average Heat generation(W/m^3)	Percentage of Variation(%)
0.5C	5761	30.9
1C	23588	5.8
1.5C	52715	0.5

The commercial 18650 lithium-ion cells from the Toriyama brand with NMC (Li-Ni-Mn-Co) cathode are used in this investigation. At a charging rate of 0.75C, the battery was 80% charged and gained the maximum charging current at 2A. After this point, the voltage of the battery will be continuous to decrease in CV mode, as received from Kulranut et al. [17].

Based on experiment results [Table 3.3] that show the maximum temperature at the battery surface under 0.25C, 0.5C, and 0.75C during the charging cycle. The battery surface could reach its highest temperature at 0.75 C, so the heat source value at 0.75 C [0.307 W] will be adopted to find the maximum temperature of the battery.

From Table 3.4,it was necessary to interpolate between 0.5C and 1C to find the average heat generation (w/m3) at 0.75C, and the heat generation rate was 14674.5 w/m3/15000 w/m3. The maximum percentage of variation is 30.9% at 0.5°C and 0.5% at 1.5°C, but the optimum range is between 7 and 14%.

Table3.5 The Steady-state input - Output parameters

Parameter1 Inlet velocity(m/s)	Parameter2 Inlet temperature(°C)	Parameter3 Number of Channels
0.5	25	2
1.0	30	3
2.0	35	4
3.0	40	6

From Table 3.5, all cases of simulation are 4^3 [64 cases]. However, a total of 32 cases were selected using an inlet velocity of 0.5, 1, 2, and 3 m/s with an inlet temperature of 25 and 40 °C [min and max value] for 2,3,4 and 6 channel configurations. Then compared the results to achieve better cooling performance by considering the flow parameters and removal heat rate from the battery module among all designs of cooling channels, such as the maximum temperature at the outlet ($T_{out,max}$) and the amount of pressure drop (ΔP).

3.10 Setting heat generation in steady state model

From Maximum Heat transfer at 0.75C [0.307W] and the entire volume of 18650 Li-ion battery cell is $1.6 * 10^{-5}$ m^3 then the maximum heat generation rate is $\frac{0.307}{1.6*10^{-5}} = 19187.5$ W/m^3 at 0.75C charging rate.

3.11Heat generation in 1 row of battery cell

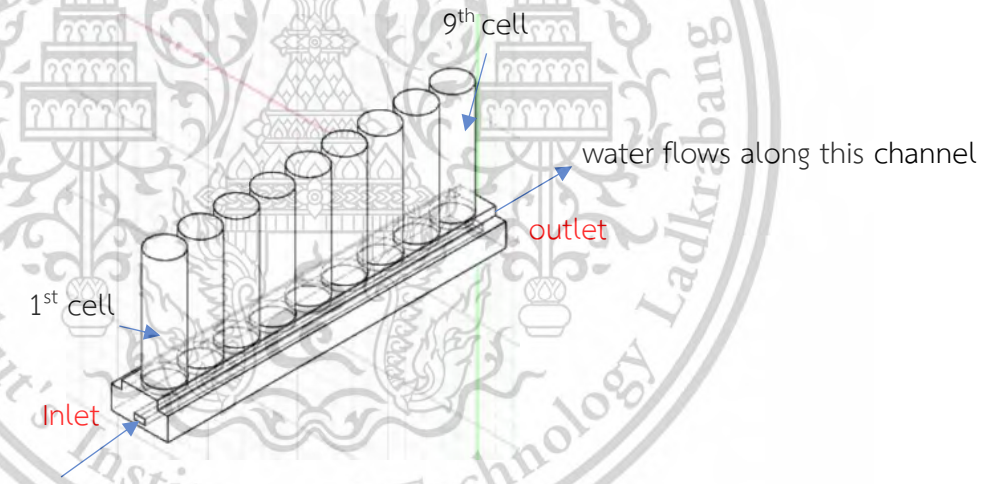

Fig.3.11 The simplified battery module

The simplified battery module see Fig.3.11, was used to reduce the time consumption of parametric studies by considering only flow simulation and the distribution of temperature inside the battery from the 1st cell to 9th cell [imitated only for the 4-channel because the alignment of the flow and the position of the battery's negative side]. In this case, the flow rate and coolant inlet temperature were already considered under this simplified model.

CHAPTER 4

RESULTS AND DISCUSSIONS

4.1Result and Discussions of Steady State Simulation

This chapter show the result of velocity distribution and Temperature distribution of different inlet velocity , temperature. The details of the geometry and the computational set up had already been given in 3.4 and 3.5

4.1.1Flow Visualization in the cooling channel when changing only inlet flowrate

Considering an inlet velocity of 0.5 m/s of 2 channel design, the maximum channel velocity inside the channel was 0.053 m/s, the minimum was 0.046 m/s, and the average velocity was 0.042 m/s. Then the inlet velocity was increased to 3 m/s and at the same temperature inlet. The maximum velocity was found to be 0.234 m/s, and the minimum was 0.165 m/s.

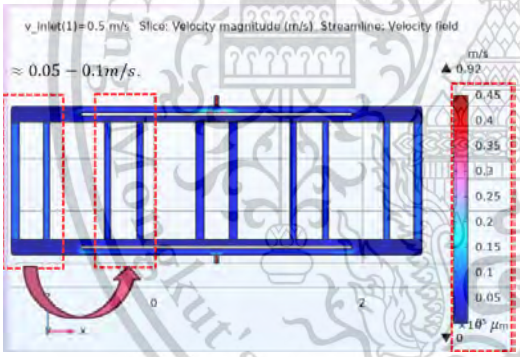

Fig.4.1Contour plot[V_inlet =0.5m/s]

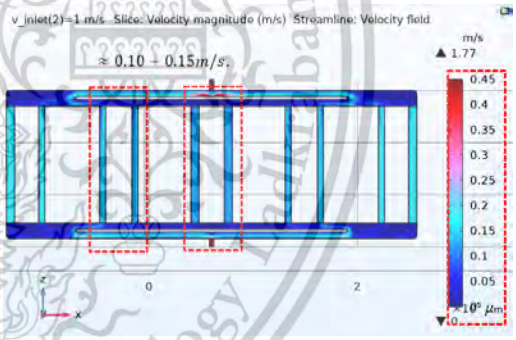

Fig.4.2 Contour plot [V_inlet =1.0m/s]

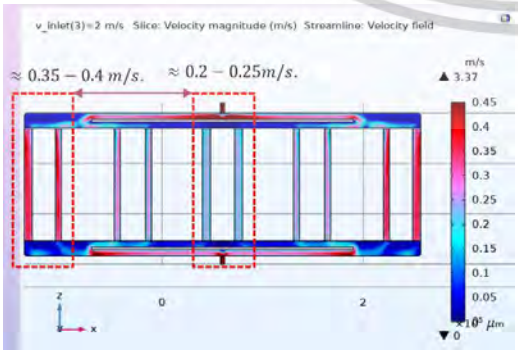

Fig.4.3 Contour plot[V_inlet =2.0m/s]

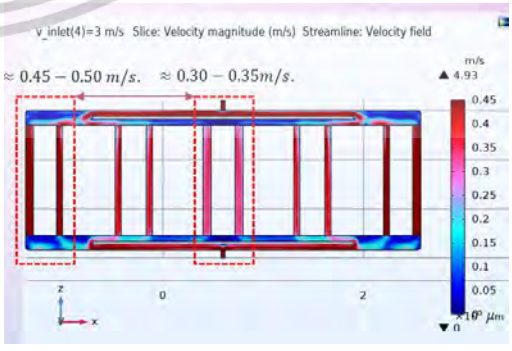

Fig.4.4 Contour plot[V_inlet =3.0m/s]

-Low Inlet Velocities (0.5,1 m/s): Achieve optimal velocity uniformity and water distribution. The flow remains consistent across the channel, minimizing recirculation and ensuring an even distribution of cooling water. This results in a well-distributed temperature profile within the cooling channel, as depicted in Figures 4.1-4.2.

-Higher Inlet Velocities (2,3 m/s): Lead to less uniform velocity distribution and poorer water distribution. Increased velocities cause more pronounced inertia effect, resulting in uneven flow across the channel. For instance, at 2 m/s, the velocity difference within the channel was around 0.25 m/s, indicating poorer distribution compared to lower velocities as depicted in Fig.4.3-4.4

-Setting the manual color range : 0-0.45 to show the velocity magnitude inside the channel, see Figs. 4.1-4.4.

From the above comparison, it was found that the contour plot of the velocity magnitude can merely distinguish the difference in channel flow velocity. For the inlet velocity of 0.5 m/s, the difference in velocity magnitudes among flow channels was not observable. When increasing velocity to 1.0, 2.0, and 3.0 m/s, the difference in channel flow magnitude becomes observable. At 0.5 m/s of inlet velocity, the distribution of water velocity was better than others. It was selected for analyzing battery module temperature distribution.

In summary, increasing the inlet water velocity causes the speed of the water flowing through the cooling channel to increase and a greater difference in channel velocity magnitude regardless of the inlet temperature at the inlet condition.

4.1.2 Result of Velocity contour[Number of channel=2,3,4,6] [Inlet velocity=0.5m/s ,Inlet temperature=40°C]

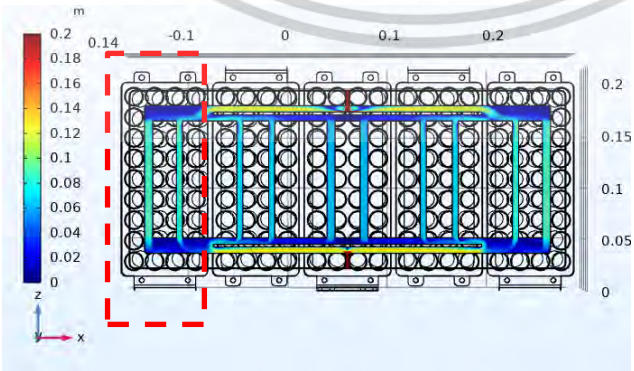

Fig.4.5 Velocity contour plot [Number of channel=2]

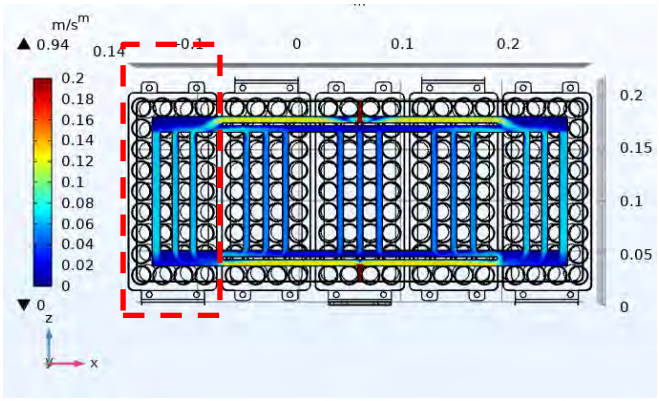

Fig.4.6 Velocity contour plot [Number of channel=3]

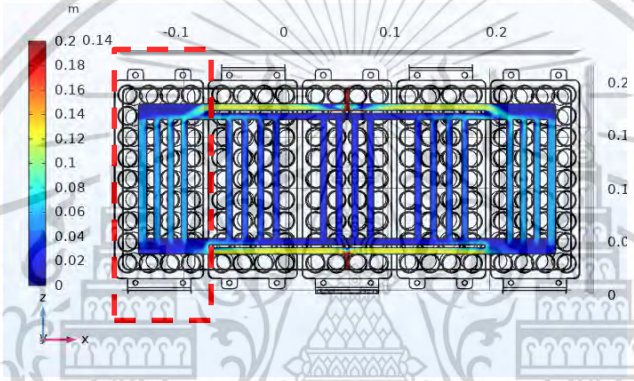

Fig.4.7 Velocity contour plot [Number of channel=4]

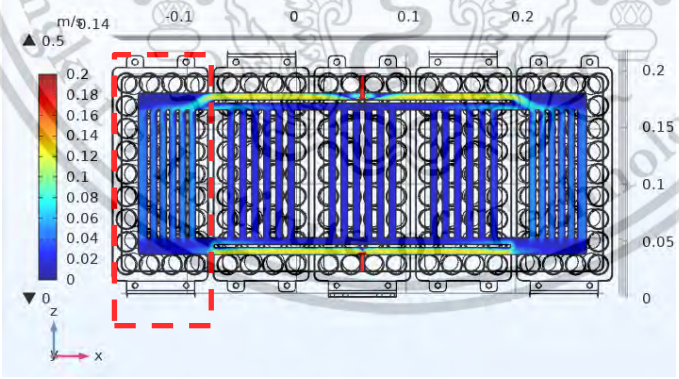

Fig.4.8 Velocity contour plot [Number of channel=6]

Setting the manual color range from 0-0.20 m/s with 10 subclass ranges to show the velocity contour inside the channel, see Figs. 4.5-4.8.

When increasing the number of cooling channels, the 2-channel configuration provides the maximum channel velocity at 0.062 m/s when using an inlet velocity of

0.5 m/s; however, the 6-channel design has the most uniform velocity profile, see Fig. 4.8.

For better comparison, the standard deviation is introduced to quantify flow uniformity, not only the channel velocity that was already mentioned above. The result will be discussed in section 4.1.6

4.1.3 The temperature difference between inlet and outlet with different inlet velocity and different channel design [Inlet Temperature= 40 °C]

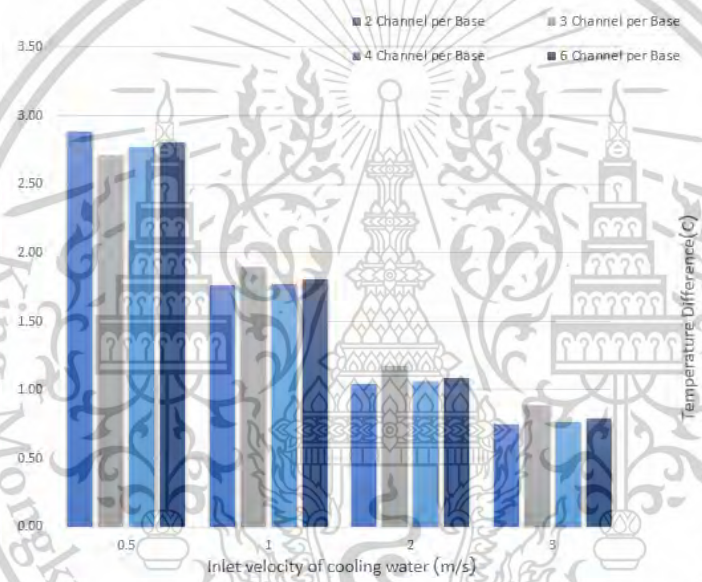

Fig.4.9 Result of Temp difference (ΔT) with inlet velocity using various number of cooling channels[2,3,4,6]

When considering among the inlet velocity of 1, 2, and 3 m/s, the temperature difference was minimum at 2 channels per base with a maximum velocity inlet of 3 m/s. However, the maximum temperature difference was found at 3 channels per base when using an inlet velocity of 1 m/s; moreover, the exception point of 3 channel flow was less than that of 6 channel flow when using a small water inlet velocity [0.5 m/s].

Increasing inlet water velocity caused the water temperature difference between the inlet and outlet sides to be lower. Furthermore, the deviation of the theoretical value of the removal heat rate was found among the different channel designs. A detailed discussion of this error will be given in section 4.1.5. The temperature difference at 0.5

m/s was found to be maximum at nearly 3 °C that had been shown on the 2-channel design.

The cooling water temperatures on the inlet and outlet sides would differ more if the inflow velocity dropped, and the detailed investigation of the temperature distribution inside the channel will be reported in sections 4.2 and 4.3.

4.1.4 The pressure drop between inlet and outlet with different inlet velocity and different channel design

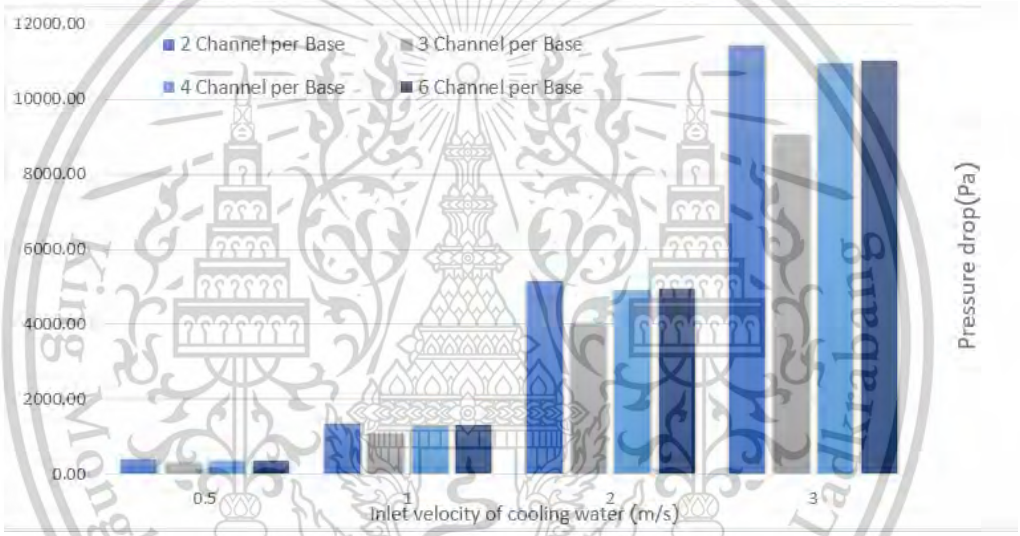

Fig.4.10 Result of Pressure drop(ΔP) with inlet velocity of water using various number of cooling channels[2,3,4,6]

A high amount of water in the inlet caused a significant increase in pressure drop; however, when using a small amount of inlet velocity at 0.5 m/s, The pressure of water inside the cooling channel was observed to be the lowest, with small effect due to change in the Inlet temperatures of cooling water.

At a specified inlet velocity, the maximum amount of pressure drop appeared on the 2-channel designs, followed by 6, 4, and 3 channels per base design, respectively. As appear on the trend, a high amount of water in the velocity inlet caused a large amount of pressure drop to nearly 12000 Pa for 2 channels per base, and the minimum

was 9000 Pa for 3 channels per base when using the maximum inlet water velocity of 3 m/s. When increasing the number of cooling channels, the change in pressure drop do not have an obvious trend. But a large effect appeared when increasing the inlet water velocity from 0.5 to 3 m/s in all cooling channel designs as seen in Fig. 4.10 Finally, the estimation of the removal heat rate will be discussed in 4.1.5

4.1.5 Steady State simulation of heat removal rate(kW) with an Inlet velocity (m/s) compared at different numbers of the channel [2,3,4and6]

Inlet Temperature 25°C

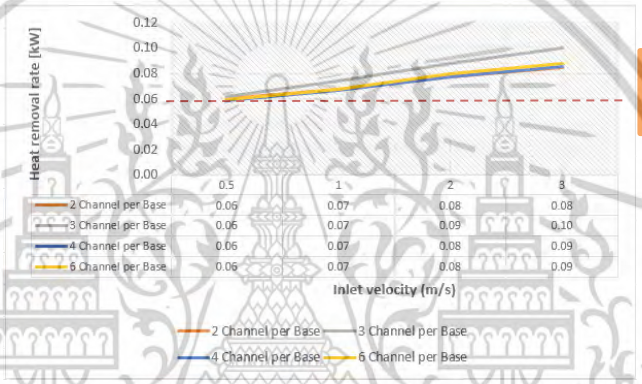

Theoretical value 0.059kW

Inlet Temperature 30°C

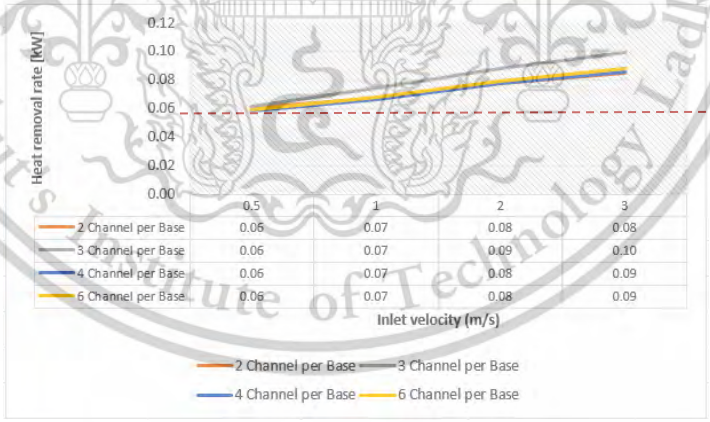

Theoretical value 0.059kW

Inlet Temperature 35°C

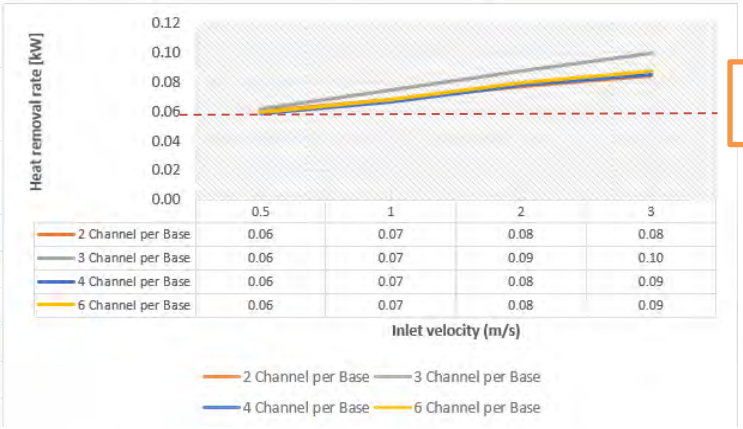

Theoretical value 0.059kW

Inlet Temperature 40°C

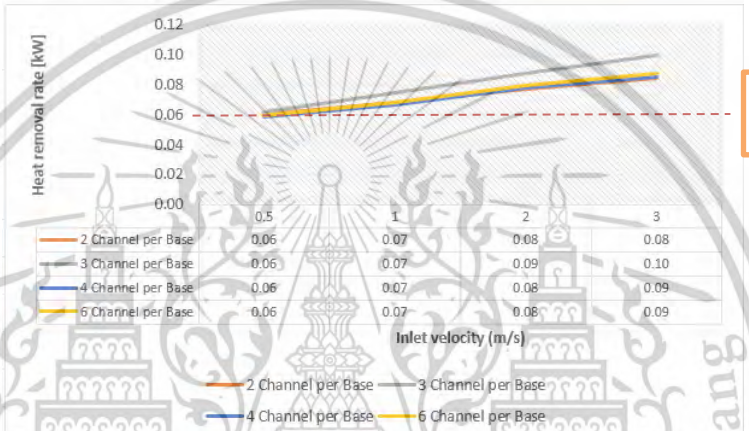

Theoretical value 0.059kW

Fig(4.11)-(4.14)show the heat removal rate(kW) with different Inlet velocity compared using different number of cooling channels[2,3,4and6 channel]

The heat removal rate of the battery cooling module (kW) was shown in Figures 4.11-4.14 for different channel counts (2, 3, 4, and 6 channels per base), inlet water velocity (0.5, 1, 2, and 3 m/s), and inlet temperatures (25, 30, 35, and 40 °C). According to Figs. 4.11, 4.12, and 4.14,

According to the energy conservation law , The heat removal rate of the battery module should be at 0.059 kW, as calculated by $\dot{m}_w C_P (T_i - T_o) = -\dot{Q}_b(t) = \dot{q}_b \forall$

When applying an inlet temperature with an inlet velocity of 0.5 m/s, the heat removal rate was 0.0605 kW, which is nearly the same and has only 5.8% error. But the error was much more over to maximum around 65.8% when using an inlet velocity of 3 m/s with an inlet temperature of 35 °C.

In this investigation, we selected to use the inlet velocity of cooling water of 0.5 m/s and select the value of heat generation of the battery at a charging rate of 0.75 C [19187.5 $\mathbf{W/m^3}$]. to find the maximum temperature at the 9th battery cell, and the result will be explored in sections 4.2 and 4.3.

4.1.6 Standard deviation of the channel velocity [2,3,4and 6 channel configuration]

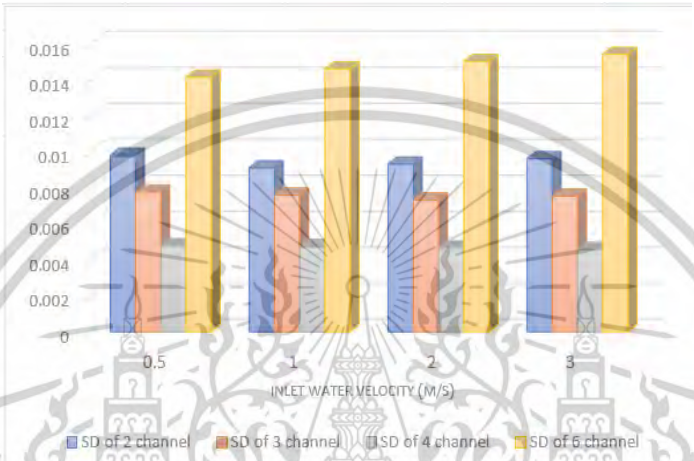

Fig.4.15 The standard deviation with inlet velocity of water (m/s) using different numbers of cooling channels

From Fig. 4.15, The trend line of standard deviation decreased with increasing number of cooling channel for 2, 3, and 4 channels per base. However, due to the limitation of the 6-channel configuration that cannot adjust the channel gap width to be equal, therefore the standard deviation was higher than 2 ,3 and 4 channels at 0.014 when using an inlet velocity of 0.5 m/s and nearly 0.016 when using an inlet velocity of 3 m/s in this case.

This figure demonstrates that a 4-channel design yielded the best uniformity of water velocity since the standard deviation will be more closely observed with the least amount.

For the 6-channel design, the difference between the average channel velocity and the maximum channel velocity was found to be greater when increasing the inlet velocity from a range between 0.016 m/s [inlet velocity 0.5 m/s]-0.10 m/s [inlet velocity 3 m/s]. However, for the 2, 3, and 4 channel designs, the range of the channel velocity

between the average and the maximum value was found to be maximum at around 0.038 m/s when using an inlet velocity of 3 m/s among other conditions.

The 6-channel configuration was also made from anodized aluminum and had a smaller cross-sectional area compared to the 2, 3, and 4 channel designs which brings the standard deviation to be greater than other configurations.

For the 3-channel design, the maximum value of velocity inside was compared to all cases of various channel configurations with less SD value than 2 and 6 channels With an inlet velocity of 0.5 m/s and an inlet temperature of 30 °C, the 2-channel and 6-channel designs have the greatest amount of pressure drop

In summary, the study emphasizes the importance of considering both velocity and the number of cooling channels in optimizing heat transfer within the cooling system for the battery pack. The findings suggest that adjusting these parameters can have effects on the system's performance, highlighting the need for a balanced design that considers both heat dissipation efficiency and flow uniformity.

4.1.7 The comparison between the midpoint velocity in cooling channel [3and 6 number of channels]

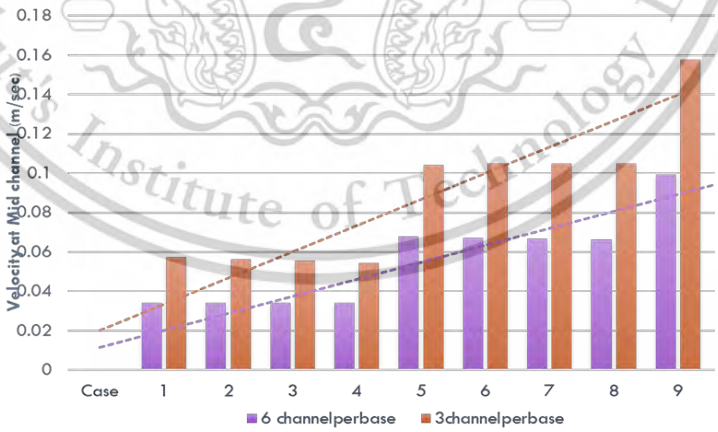

Fig.4.16 The bar chart of velocity at midpoint in cooling channel with number of simulation cases[3and 6 number of channels]

Number of simulation studies: started from inlet velocity = 0.5, 1,2 and 3 m/s with inlet temperature = 25°C, 30°C, 35°C, and 40°C

Case 1: Vin = 0.5 m/s, T =25°C, Case 2: Vin = 0.5 m/s, T = 30°C;

Case 3: Vin = 0.5 m/s, T = 35°C.,Case 4*: Vin = 0.5 m/s, T =40°C;

Case 5: Vin = 1.0 m/s, T =25°C,Case 6: Vin = 1.0 m/s, T =30°C;

Case 7: Vin = 1.0 m/s, T =35°C,Case 8: Vin = 1.0 m/s, T =40 °C; Case 9*: Vin = 2.0 m/s, T =25 °C; and after this case, flows seem to have more turbulence. [Re>4000]

According to Figure 4.16, it was observed that increasing the velocity in the cooling channels had a greater impact on the heat transfer rate compared to the inlet temperature. This implies that manipulating the flow velocity of the cooling medium has a more pronounced effect on the system's heat dissipation capabilities. The average velocity at the midpoint of a 3-channel per base configuration was noted to be greater than 6-channel configuration for all cases used in the simulation. This suggests that the design with fewer channels per base had a higher average velocity at the specified midpoint.

When the inlet water velocity was enhanced to around 2.0 m/s, starting with an inlet water temperature of 25 °C, the flow exhibited more turbulence. This was indicated by a Reynolds number of approximately 6728.72. The study found that when increasing the number of cooling channels, the water velocity inside the channels tended to be lower than in configurations with a smaller number of channels. However, due to the space limit of the 6-channel design , the greater pressure drop and non-uniformity flow was observed.

4.1.8 The Result of channel velocity, Maximum Temperature at outlet and pressure drop

1.) At 6 channel-base at V_{inlet} =0.5 m/s and T_{inlet}=40 °C

The maximum channel velocity was 0.052 m/s and the minimum channel velocity was 0.019 m/s ,the average channel velocity was 0.016 m/s, and the pressure drop was 342.91 Pa. This design yielded T_{out} at 43.81°C (temperature difference = 3.81°C) at the outlet temperature

2.)At 4 channel-base at V_{inlet} =0.5 m/s and T_{inlet}=40 °C

The maximum channel velocity was 0.059 m/s and the minimum channel velocity was only 0.025 m/s, the average channel velocity was 0.042 m/s, and the pressure drop was 335.05 Pa. Finally, this design yielded T_{out} at 42.78℃ (temperature difference = 2.78℃) at the outlet temperature

3.) At 3 channel-base at V_{inlet} =0.5 m/s and T_{inlet}=40 °C

The maximum channel velocity was 0.065 m/s and the minimum channel velocity was only 0.04 m/s, the average channel velocity was 0.054 m/s, and the pressure drop was 283.36 Pa. Finally, this design yielded T_{out} at 43.92℃ (temperature difference = 3.92℃) at the outlet temperature, which was the maximum among all cooling designs.

4.) At 2 channel-base at V_{inlet} =0.5 m/s and T_{inlet}=40 °C

The maximum channel velocity was 0.062 m/s and the minimum channel velocity was only 0.046 m/s, the average channel velocity was 0.058 m/s, and the pressure drop was 362.74 Pa that was highest among all designs Finally, this design yielded T_{out} at 43.82℃ (temperature difference = 3.82℃) at the outlet temperature.

To sum up, the average channel velocity was maximum at 2 channels at 0.058 m/s, followed by 3, 4, and 6 channels, respectively. However, the pressure drop was maximum in this configuration, which brings this case to be not considered.

By comparing 3, 4, and 6 channel designs, the standard deviation in 4 channel was the lowest among all designs. For the 6 channel, it had the least cross-sectional area and the highest surface resistance inside the channel that's flowing along, bringing the flow distribution to be worse than the 4-channel design, and the pressure drop was also highest. Finally, the 4-channel design was selected as the highest uniformity among all cases to find the maximum temperature of the battery in steady and transient, as the result will be explored in sections 4.2 and 4.3.

4.2 Maximum temperature of battery in steady-state model

The heat generation rate was approximately under a charging rate of 0.75 C. Then we used this value as a constant heat source in the single-channel flow simulation. The results of channel velocity for 4 channels design were revealed at V_{avg} [0.037 m/s], V_{max} [0.042 m/s], and V_{min} [0.031 m/s]. Finally, the minimum channel velocity and the inlet temperature of the water at 30°C were selected as inlet conditions

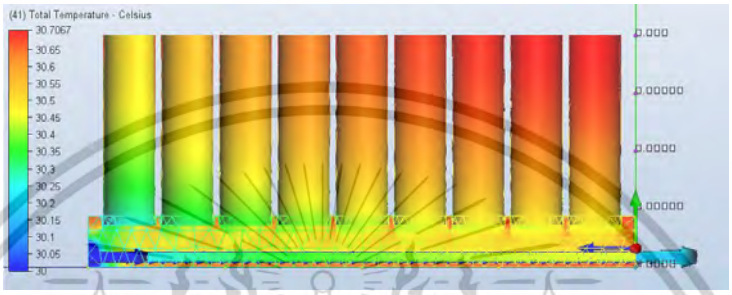

Fig.4.17 The temperature contour of 9 battery cells with Heat source rate 0.307W under 0.75C [steady-state simulation]

The water temperature at the outlet seemed to be higher than at the inlet section when adding a constant heat source, and this figure can be imitated for a four-channel design to see the temperature distribution and water velocity streamline that affected the battery performance during steady-state simulation.

Fig.4.17 shows the simulation of the battery from the 1st cell to the 9th cell: when using the maximum heat generation rate [0.307 W] as a constant heat source term under a 0.75 C discharge rate, the greatest temperature of the battery is almost 30.706 ℃, yielding the highest percentage of battery performance [120%] using the inlet temperature at 30 ℃, and the maximum average temperature difference was around 0.4℃ [less than 5 ℃]. That means the temperature difference between the battery modules was quite small.

4.3 Maximum Temperature of battery in transient model

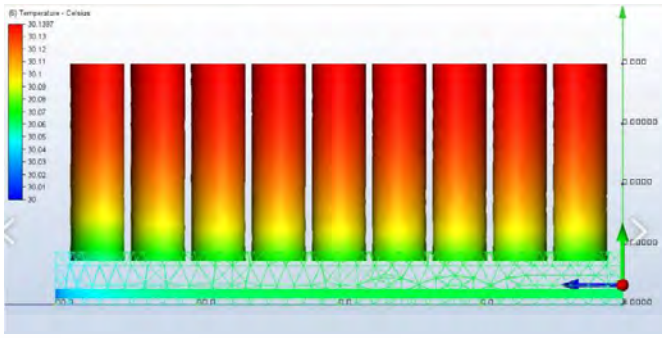

Fig.4.18 The temperature contour of 9 battery cells with heat source rate 0.307W under 0.75C [Transient simulation]

When using heat source Q (t) at a heat source rate of 0.307 W. Then set up a transient model simulation using a time-dependent study from t = 0 to 3600 sec, where the greatest temperature of the battery was 30.14 °C and the maximum average temperature difference was 0.14 °C.

At a charging rate of 0.75C with a maximum heating value of 0.307 W. The highest average temperature at the 9th cell was 30.706°C received from Fig.4.18 which was lower than the maximum allowable battery temperature of 33 °C and yielded the highest percentage of battery performance [120%] when using an inlet temperature of 30 °C for steady state but the highest average temperature at the 9th cell for transient simulation was only 30.14 °C, running from t = 0 to 3600 s. That makes the battery cell temperature in each submodule as close as possible.

4.4 Heat transient Result in half module of battery cooling model

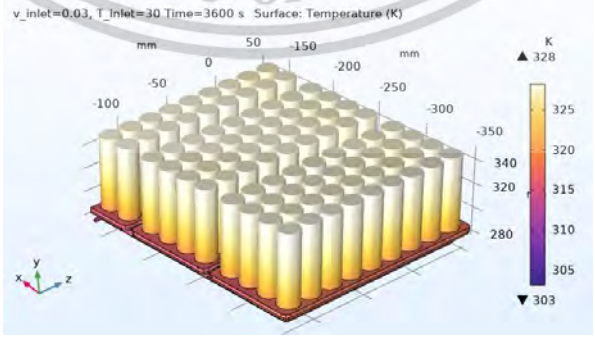

Fig.4.19 The temperature plot of the transient model inside Half Module of Battery using heat source Q =0.307W under 0.75C

All simulation results indicate that adding a heat source to the battery increases the temperature of the battery pack. This is a fundamental observation aligned with the basic principles of thermodynamics and heat transfer. The study developed a three-dimensional thermal model for battery cooling simulations. This model was then used to demonstrate the detailed temperature distribution of the entire battery pack under 0.75C charging rate.

From Fig. 4.19, The temperature of the battery cell near the coolant inlet channel was lower than that of other cells, indicating that the cooling process had been initiated. As the coolant flowed through the inlet channel, it absorbed heat, leading to a rise in temperature along the flow path inside the cooling channel. The temperature of the coolant near the outlet became higher due to heat absorption along the flow path. This resulted in reduced heat exchange capability between the battery and the coolant, contributing to higher coolant temperatures at the outlet zone. The fluid domain used a basic mesh size of 0.2-0.25 mm to ensure computation accuracy in simulating the thermal behavior of the battery module. Proper meshing was crucial for obtaining reliable and accurate simulation results. The greatest temperature observed for the battery module under 0.75C charging rate was 56.85°C.This indicates the maximum temperature reached during the charging process under the specified conditions.

CHAPTER 5

CONCLUSIONS AND RECOMMENDATION

5.1 Conclusion

Firstly, boundary conditions of the water inlet at 0.5, 1.0, 2.0, and 3.0 m/s with inlet temperatures at 25, 30, 35, or 40°C were applied to establish boundary conditions inside the battery and steady states for flows along the channel. The detailed temperature distribution of the whole battery pack was demonstrated under normal operating conditions [0.75 C charging rate].

5.1.1. The summary of the steady-state simulation

- The ability to remove heat from the battery when the inlet velocity increased from 0.5 m/s to 3 m/s was consistent at 0.0585 kW. When applying an inlet temperature with an inlet velocity of 0.5 m/s, the heat removal rate was 0.0605 kW, which is nearly the same and has only 5.8% error. But the error was much more over to maximum around 65.8% when using an inlet velocity of 3 m/s with an inlet temperature of 35 °C.
- Under steady-state conditions, the cooling water temperatures on the inlet and outlet sides would differ more if the inflow velocity dropped, and the pressure drop would be greater if the inlet coolant velocity rose. And finally, no matter how much change in the inlet velocity and the inlet temperature, the heat conservation rate [kW] remains constant.
- From a variety of channel configuration ideas, the two-channel design yielded the highest channel velocity magnitude inside the channel. However, the 4-channel, which had the least amount of standard deviation [the cooling type that had the best velocity uniformity and most water could disperse in this design more than others].

- All cooling designs had very good flow distribution when using low inlet velocities. However, when increasing the inlet velocity, the distribution of water in the channel got worse.

5.1.2. The summary of the heat generation analysis in 1 row of the battery pack [9 cells] [steady-state simulation]

- This result involved developing a three-dimensional thermal model by simulating a battery cooling system. The detailed temperature distribution of the whole battery pack is demonstrated under normal operating conditions at under 0.75 C with a maximum heating value of 0.307 W. The highest average temperature at the 9^{th} cell was 30.706 ℃, which is lower than the maximum allowable battery temperature of 33 ℃.
- When the inlet water velocity was greater than 0.5 m/s, the flow became fully turbulent [Re = 6728.72]. Moreover, discussing the same inlet velocity condition, the minimum channel velocity in a 4-channel [most uniform design] was 0.078 m/s [Re = 292.32], which was in the laminar zone.
- The inlet temperature should be less than or equal to 30℃ to keep the maximum temperature below 33 ℃.

5.1.3.The summary of heat generation analysis in one row of the battery pack [9 cells][transient simulation]

The highest average temperature at the 9^{th} cell for transient simulation was 30.14 ℃, running from t = 0 to 3600s. That brought the battery cell temperature in each submodule as close as possible (0.14℃ from the result of the transient simulation).

5.2 Recommendation for Future Work

- When applying a steady-state scenario for modeling the total amount of water flows, the difference temperatures increase with inlet velocity, with barriers, and without barriers, suggesting that a more adaptable structure type could increase the difference temperature anywhere with inlet velocity. Next, vary the number of cooling channel depths to separate the design . Finally, choosing a design that minimizes the cooling barrier length in the cooling channel configuration can be considered for future investigation.

- For a three-dimensional model, the temperature maximum of the whole pack of battery modules should be evaluated with a heat conjugate equation to find the amount of heat removed from the battery

REFERENCES

[1] A. Greco, X. Jiang, and D. Cao, “An investigation of lithium-ion battery thermal management using paraffin/porous-graphite-matrix composite,” J. Power Sources, vol. 278, pp. 50–68, 2015.

[2] L. H. Saw, Y. Ye, A. A. O. Tay, W. T. Chong, S. H. Kuan, and M. C. Yew, “Computational fluid dynamic and thermal analysis of Lithium-ion battery pack with air cooling,” Appl. Energy, vol. 177, pp. 783–792, 2016

[3] H. Wang, W. Xu, and L. Ma, “Actively controlled thermal management of prismatic. Li-ion cells under elevated temperatures,” Int. J. Heat Mass Transf., vol. 102, pp. 315–322, 2016

[4] Z. Lu, X. Z. Meng, L. C. Wei, W. Y. Hu, L. Y. Zhang, and L. W. Jin, “Thermal Management of Densely packed EV Battery with Forced Air-Cooling Strategies,” Energy Procedia, vol. 88, pp. 682–688, 2016

[5] Z. Qian, Y. Li, and Z. Rao, “Thermal performance of lithium-ion battery thermal management system by using mini-channel cooling,” Energy Convers. Manag., vol.126, pp. 622–631, 2016

[6] C. Lan, J. Xu, Y. Qiao, and Y. Ma, "Thermal management for high power lithium-ion battery by mini channel aluminum tubes," Appl. Therm. Eng., vol. 101, pp. 284–292, 2016

[7] X.-H. Yang, S.-C. Tan, and J. Liu, “Thermal management of Li-ion battery with liquid metal,” Energy Convers. Manag., vol. 117, pp. 577–585, 2016

[8] M. Alipanah and X. Li, “Numerical studies of lithium-ion battery thermal management systems using phase change materials and metal foams,” Int. J. Heat Mass Transf., vol. 102, pp. 1159–1168, 2016

[9] J. Yan, Q. Wang, K. Li, and J. Sun, “Numerical study on the thermal performance of a composite board in battery thermal management system,” Appl. Therm. Eng., vol.106, pp. 131–140, 2016

[10] Y. Azizi and S. M. Sadrameli, "Thermal management of a LiFePO4 battery pack at high-temperature environment using a composite of phase change materials and aluminum wire mesh plates," Energy Convers. Manag., vol. 128, pp. 294–302, 2016

[11] D. Chen, J. Jiang, G.-H. Kim, C. Yang, and A. Pesaran, “Comparison of different cooling methods for lithium-ion battery cells,” Appl. Therm. Eng., vol. 94, pp. 846–854, 2016

[12] Barbir, F., 2005, PEM Fuel Cells, Elsevier Inc., pp. 33-72

[13] Bernardi, D., Pawlikowski, E. and Newman, J., 1984, "General energy balance for battery systems", Journal of the Electrochemical Society, Vol. 84-2, No. 1, pp. 164-165.

[14] Incropera, F.P. and De Witt, D.P., 1990, Introduction to Heat Transfer, 2nd ed., John Wiley & Sons, Inc., PP. 1-9.

[15] Chantheve P., Laoonual Y., Masomtob M., Hirai S., Lailuck V., Rompho S., Sriram P., and Chanurai N., "A Simplified Approach for Heat Generation due to Entropy Change in Cylindrical LCO Battery', 2018 IEEE Transportation Electrification Conference & Expo Asia-Pacific, June 6h - 9th, 2018, Bangkok, Thailand

[16] Y. Huang, P. Mei, Y. Lu, R. Huang, X. Yu, Z. Chen, A.P. Roskilly, A novel approach for Lithium-ion battery thermal management with streamline shape mini channel cooling plates

[17]. Kulranut, J & Depaiwa, N & Yenwichai, Thitiwat & Intano, Watcharakorn & Masomtob, Manop. (2021). IMPROVEMENT OF ESTIMATION METHOD FOR BATTERY CELL HEAT GENERATION. 10.14456/jrame.2021.13].

[18] Paccha-Herrera E, Calderón-Muñoz WR, Orchard M, Jaramillo F, Medjaher K. Thermal Modeling Approaches for a $LiCoO_2$ Lithium-ion Battery—A Comparative Study with Experimental Validation. *Batteries*. 2020; 6(3):40. https://doi.org/10.3390/batteries6030040

[19] Ho V-T, Chang K, Lee SW, Kim SH. Transient Thermal Analysis of a Li-Ion Battery Module for Electric Cars Based on Various Cooling Fan Arrangements. *Energies*. 2020; 13(9):2387. https://doi.org/10.3390/en1309238

[20] H. Liu, Z. Wei, W. He and J. Zhaoa, "Thermal issues about Li-ion batteries and recent progress in battery thermal management systems: A review," *Energy Conversion and Management 150,* pp. 304-330, 2017.

[21] R. Babcock, "EVERYTHING YOU EVER WANTED TO KNOW ABOUT LITHIUM-ION BATTERIES," Vaporauthority, 23 12 2016. [Online].

[22] B. U. Group, "BU-301a: Types of Battery Cells," Battery University, 31 07 2017. [Online].Available:http://batteryuniversity.com/index.php/learn/article/types_of_battery_cells. [Accessed 01 07 2018].

[23] K. Onda, H. Kameyama, T. Hanamoto and Kohei, "Experimental study in heat generation behavour of small Lithium-ion secondary batteries," *Journal of The Electrochemical Society,* pp. A285-A291, 2003.

[24] T. M. Bandager, S. Garimella and T. F.Fuller, "A critical review of thermal issues in Lithium-ion batteries," *Journal of the Electrochemical Society,* 2011.

[25] P. Ramadass, B. Haran, R. White and B. N. Popov, "Capacity fade of Sony 18650 cells cycled at elevated temperatures, Part I. Cycling performance," *Journal of Power Sources 112,* pp. 606-613, 2002.

[26] X. Guodong, C. Lei and B. Guanglong, "A review on battery thermal management in electric vehicle applicaion," *Journal of Power Sources,* pp. 90-105, 2017.

[27] C. Kuan Cheng, C. H. Lin, S. F. Yeh, Y. H. Lin, C. S. Huang and K. C. Chen, "Cycle life analysis of series connected lithium-ion batteries with temperature difference," *Journal of Power Sources,* pp. 75-84, 2014.

[28] X. Feng, M. Fang, X. He, M. Ouyang, L. Lu, H. Wang and M. Zhang, "Thermal runaway features of large format prismatic lithium-ion battery using extended volume accelerating rate calorimetry," *Journal of Power Sources,* pp. 294-301, 2014.

[29] D. Pastrascu, "Toyota Prius' Battery Recycling Plan," 2 July 2009. [Online]. Available: https://www.autoevolution.com/news/toyota-prius-battery-recycling-plan-8360.html. [Accessed 14 09 2018].

[30] T. Wang, K. Tseng, J. Zhao and Z. Wei, "Thermal investigation of lithium-ion battery module with different cell arrangement structures and forced air-cooling strategies," *Applied Energy 134,* pp. 229-238, 2014. 54

[31] C. P. Rajib Mahamud, "Reciprocating air flow for Li-ion battery thermal management to improve temperature uniformity," *Journal of Power Sources 196,* p. 5685–5696, 2011.

[32] Hermann and W. Arthur, "Liquid cooling manifold with multi-function thermal interface". US Patent US20100104938A1, 12 01 2010.

[33] G. Bower and K. Ritter, "Chevy Bolt 200 Mile EV Battery Cooling and Gearbox Details," 18 Jan 2016. [Online]. Available: https://insideevs.com/chevy-bolt-200-mile-ev-battery-cooling-and-gearbox-details- bower/.

[34] 3M, Electronics Markets Materials Division, "3M™ Novec™ 7200 Engineered Fluid," 2009.[Online].Available:https://multimedia.3m.com/mws/media/199819O/3mtm-novectm-7200- engineered-fluid.pdf.

[35] XING Mobility™ Inc, "Xing modular battery system," 2017. [Online]. Available: https://www.xingmobility.com/xing-battery-system.

[36] C. Morris, "XING Mobility's electric supercar uses novel battery cooling system," Chargedevs,01/12/2017.[Online].Available: https://chargedevs.com/newswire/xing-mobilitys-electric-supercar-uses-novel-battery-cooling-system/. [Accessed 27 55 2018].

[37] Rimac, "RIMAC HELPS BRING WORLD'S MOST POWERFUL PRODUCTION CAR TO REALITY," Rimac-automobili, 3 3 2015. [Online]. Available: http://www.rimac-automobili.com/en/press/releases/rimac-helps-bring-world-s-most-powerful-production-car-to-reality/. [Accessed 27 5 2018].

[38] F. Lambert, "Aston Martin's upcoming new hypercar will have a battery pack suppliedbyRimac,"Electrek,1622017.[Online].Available: https://electrek.co/2017/02/16/aston-martin-hypercar-electric-battery-pack-rimac/. [Accessed 27 5 2018].

[39] Selman, S. A. Hallaj and J. Robert, "Thermal management of battery systems". US Patent US6468689B1, 29 02 2000.

[40]AllCell,"Allcelltech,"Allcelltech,[Online].Available: http://www.allcelltech.com/index.php/technology/pcc-thermal-management. [Accessed 27 05 2018].

[41] Y. Ji and C. Y. Wang, "Heating strategies for Li-ion batteries operated from subzero temperatures," *Electrochimica Acta,* vol. 107, pp. 664-674, 2013.

[42] S. Drake, D. Wetz, J. Ostanek, S. Miller, J. Heinzel and A. Jaina, "Measurement of anisotropic thermophysical properties of cylindrical Li-ion cells," *Journal of Power Sources,* pp. 298-304, 2014.

[43] N. S. Spinner, K. M. Hinnant, R. Mazurick, A. Brandon, S. L. Rose-Pehrsson and S. G. Tuttle, "Novel 18650 lithium-ion batterysurrogate cell designwith anisotropic thermophysical properties for studying failure events," *Journal of Power Sources 312,* pp. 1-11, 2016. 55

[44] I. Dinçer, H. S. Hamut and N. Javani, Thermal Management of Electric Vehicle Battery Systems, John Wiley & Sons Ltd, 2017.

[45] "Performance Comparison of Thermal Interface Materials for Power Electronis Applications," in *Applied Power Electronics Conference and Exposition (APEC), 2014 Twenty-Ninth Annual IEEE*, Texas, USA, 2014.

[46] *How does an Electric Car work ? | Tesla Model S.* [Film]. Learn Engineering, 2017.

[47] "Benchmarking the Tesla Model S – A Tour of Ricardo Engineering's Teardown Laboratory," Copper Rotor Induction Motor, 02 11 2014. [Online]. Available: http://www.coppermotor.com/2014/11/benchmarking-the-tesla-model-s-a-tour-of-ricardo-engineerings- teardown-laboratory/?ckattempt=1. [Accessed 30 06 2018].

[48] 3. E. Materials, "3M™ Novec™ 774 Engineered Fluid Product Information," 14 07 2014.[Online].Available: https://multimedia.3m.com/mws/media/815168O/3mtm-novectm-774-engineered-fluid. pdf. [Accessed 30 06 2018].

[49] Resolved Analytics, "A Comparison of CFD Software Packages," Resolved Analytics, 27/04/2017.[Online].Available: https://www.resolvedanalytics.com/theflux/comparing-popular-cfd-software-packages. [Accessed 04 06 2018].

[50] 3. E. M. S. Division, "3M™ Novec™ 774 Engineered Fluid," 07 2014. [Online]. Available: https://multimedia.3m.com/mws/media/815168O/3mtm-novectm-774-engineered-fluid.pdf. [Accessed 14 09 2018].

[51] L. Zhang, C. Lyu, G. Hinds and M. Kehua, "Parameter Sensitivity Analysis of Cylindrical LiFePO4 Battery Performance Using Multi-Physics Modeling," *Journal of The Electrochemical Society,* 2014. [33] H. Schlichting and K. Gersten, Boundary-Layer Theory, Springer, Berlin, Heidelberg, 2017, p. 416– 419.

APPENDIX A

PUBLICATION

Journal of Research and Applications in Mechanical Engineering
ISSN: 2229-2152 (Print); 2697-424x (Online)
Transactions of the TSME (2024) Vol. 12, No. 1.
Paper No. JRAME 24-12-006
[DOI: 10.14456/jrame.2024.6]

Research Article

Parametric Study on Water-Cooling Plates to Improve Cooling Performance on 18650 Li-ion Battery

R. Nanthatanti[1]

J. Charoensuk[1*]
M. Masomtob[2]
S. Hirai[3]

[1] *Department of Mechanical Engineering, School of Engineering, King Mongkut's Institute of Technology Ladkrabang, Bangkok 10520, Thailand*

2. Energy Innovation Research Group (EIRG), National Energy Technology Centre (ENTEC), National Science and Technology Development Agency (NSTDA), Pathum Thani 12120, Thailand

3. Department of Mechanical Engineering, Tokyo Institute of Technology, Tokyo, Japan

Received 27 April 2023
Revised 13 July 2023
Accepted 24 August 2023

ABSTRACT:
With a novel NSTDA design, pressure drop, and standard deviation of cooling water velocity inside the channel of the liquid cooling plate were evaluated under various channel counts [2, 3, 4, and 6 channels per base], inlet temperatures of water [25, 30, 35, and 40 °C], and inlet velocity of water [0.5, 1.0, 2.0, and 3.0 m/s] at steady-state conditions. It was found that the 4-channel design produced the most distributed flow with an inlet water velocity of 0.5 m/s.The average channel velocity was 0.0371 m/s. When increasing the inlet velocity of water, a larger pressure drop was observed.
Simulation of heat transfer on a single row, single cooling channel design of a battery pack was performed with a channel velocity of 0.03 m/s, which imitates the 4-channel design under the heat generation produced at a charging rate of 0.75 C.
An inlet temperature of 30 °C was used to keep the maximum temperature of the battery at 30.706 °C. The temperature difference over the battery pack was approximately 0.4 °C.

Keywords: *Standard deviation, channel counts, liquid-cooling plate*

1. Introduction

At present, Electric vehicles (EVs) tend to be the solution for modern vehicles. EVs require fewer parts compared to Internal combustion engine vehicles (ICEVs) and can use electricity from alternative energy resources such as wind turbines, photovoltaics, water dams, etc. However, battery pack cost, driving range, and thermal management systems are the challenges of EVs. especially the thermal management system, which needs to be developed to prolong the life of the battery pack.

* Corresponding author: J.Jarruwat
E-mail address: jarruwat.ch@kmitl.ac.th

1.1The effect of heat on Battery performance

The battery is one of the most important parts of electric vehicles (EVs). The modern development of EVs requires higher capacity and power densities from battery packs. It is always expected that the number of battery cells can be packed as much as possible to maximize the output capacity and power density. However, high power load usage leads to a serious thermal issue due to heat generation. The temperature is sensitive to the battery performance and lifetime of battery cells. If the battery temperature is higher, the battery performance is higher because the higher temperature can accelerate the chemical reaction over the rated limit as shown in Fig.1.

On the other hand, the battery life is lower when the battery temperature is higher, as shown in Fig. 2, and the last point is that the optimal battery temperature needs to be less than 33°C to protect the battery life span. Therefore, a suitable battery temperature needs to be considered. A. Greco et al. [1] have reported that the battery temperature should be maintained in the range of 20–40 °C, and the maximum temperature difference for entire packs should be less than 5°C.

Fig. 1. The power as a function of the lithium-ion battery temperature

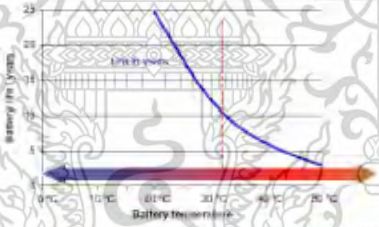

Fig. 2. The battery life/years relative with the Battery temperature

1.2.Battery cooling system

There are different forms of thermal management for battery packs. They are primarily divided into three categories:

Firstly, using coolant in liquid form. Tesla utilized a dual-circuit liquid cooling system in a wavy tube placed between cylindrical cells, using a refrigerant circuit for all connections [10] to cool the liquid inside. Indirect liquid cooling is kept outside the enclosure to avoid leakage of the coolant, as some manufacturers use a cold plate between each prismatic cell that has several microchannels for convective heat removal from batteries. During the operation of the liquid cooling system, the heat would quickly transfer from the coolant to the cold side, as explained by Lyu et al. [20]. Next, [15,16] explained that a U-shaped fluid channel was adopted and water was used as the coolant liquid flowing along the cooling channel attached with an aluminum block on both cold sides of the thermoelectric cooling plate. Compared with other fluids at the same flow rate, liquid cooling systems can be quite good at reducing a

significant quantity of heat from the batteries.[5, 6, 7] explain that in terms of practical design and efficient cooling of Li-ion battery modules, they were primarily used in the cooling system. However, the liquid cooling system needs more attention because of liquid leaks and corrosion.

Secondly, using a phase-change material cooling system that can efficiently lower temperatures in the battery modules and reduce the temperature differences. This type also has limitations in terms of phase changes in volume and encapsulation.

Finally, the air-cooling system is easily available for cooling purposes inside low-density batteries [2]. For the passive cooling system, the Nissan Leaf simply used fresh air to cool the battery pack, and the exhaust air was emitted directly into the ambient air [8, 9], but it also had low capacity and low thermal conductivity when using different configurations of air flow rate and electric vehicles [3, 4]. Despite [13, 18], which used a cooling system inside the HVAC that maximized its efficiency by utilizing the vehicle's climate control system to heat, ventilate, and cool the vehicle, it was found that air cooling had the advantage of being simple to install and lightweight. However, [11] explained that air cooling had the disadvantage of poor cooling effectiveness and was insufficient to sustain temperatures under adverse circumstances. One of the limitations of assembling battery packs in an electric car is space. Consequently, the liquid cooling system has been chosen because it is more effective than the air-cooling system in terms of space [4, 19].

This research focuses on the NSTDA's patent-new design, and it was expected that the design would be better suited for battery heat management systems to use the liquid cooling method and water as the coolant. It has many advantages, as explained before. In this Investigation, There are one hundred eighty Li-ion battery cells in the battery pack. Five battery modules are packed within aluminum cooling plates, and each battery module has thirty-six cells, as shown in Fig. 3.

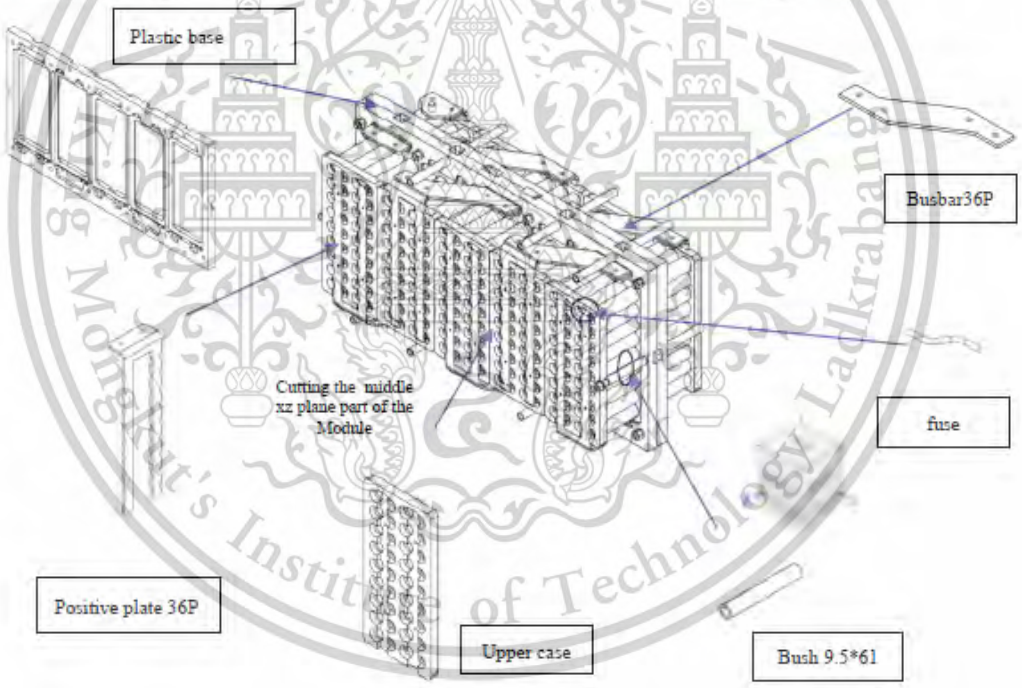

Fig. 3. 10S36P Battery Module Model

1.3 The 10S36P battery module.

For simplicity in problem specification, while keeping the essential components for thermal analysis, the cooling pad and flow channel of a battery module was modeled. Following are the rationales of the problem specification.

1st step: Discard the upper case and positive plate because they are not considered for cooling in the positive terminal.

2nd step: Neglect the ohmic heating on the busbar that conducts the heat to the positive terminal. So, the bus bar will be removed.

3rd step: Discard all of the insulation parts [the bushes and all connectors] that can fasten the battery module.

4th step: Discard the plastic base because it is an insulation part and has lower thermal conductivity.

5th step: Using the x-z plane to show half the cooling module because the cooling system is symmetric. A submodule of the battery cooling system that contains the negative terminal plate, anodized aluminum plate, and nickel plate was found and the liquid cooling plate will be further investigated

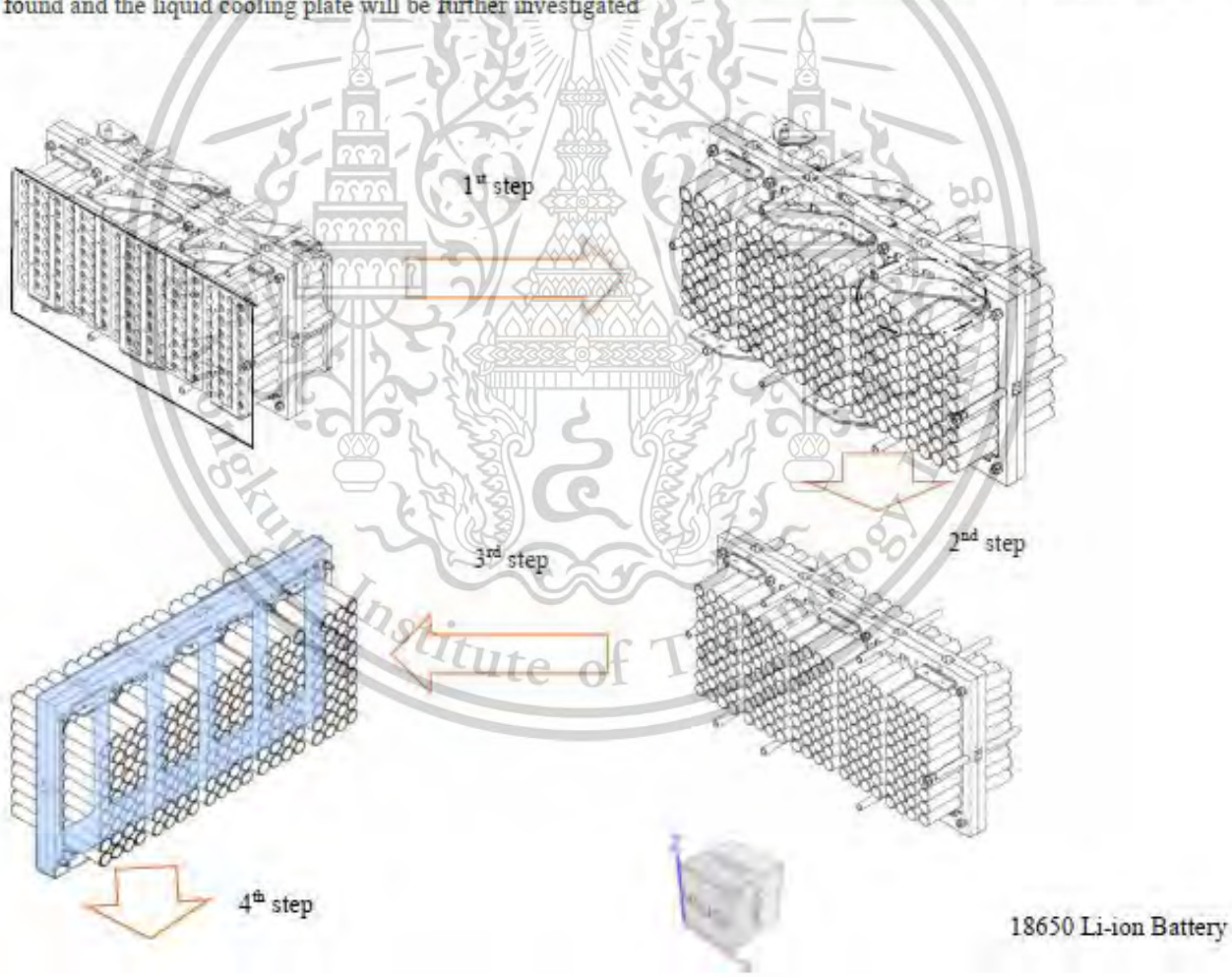

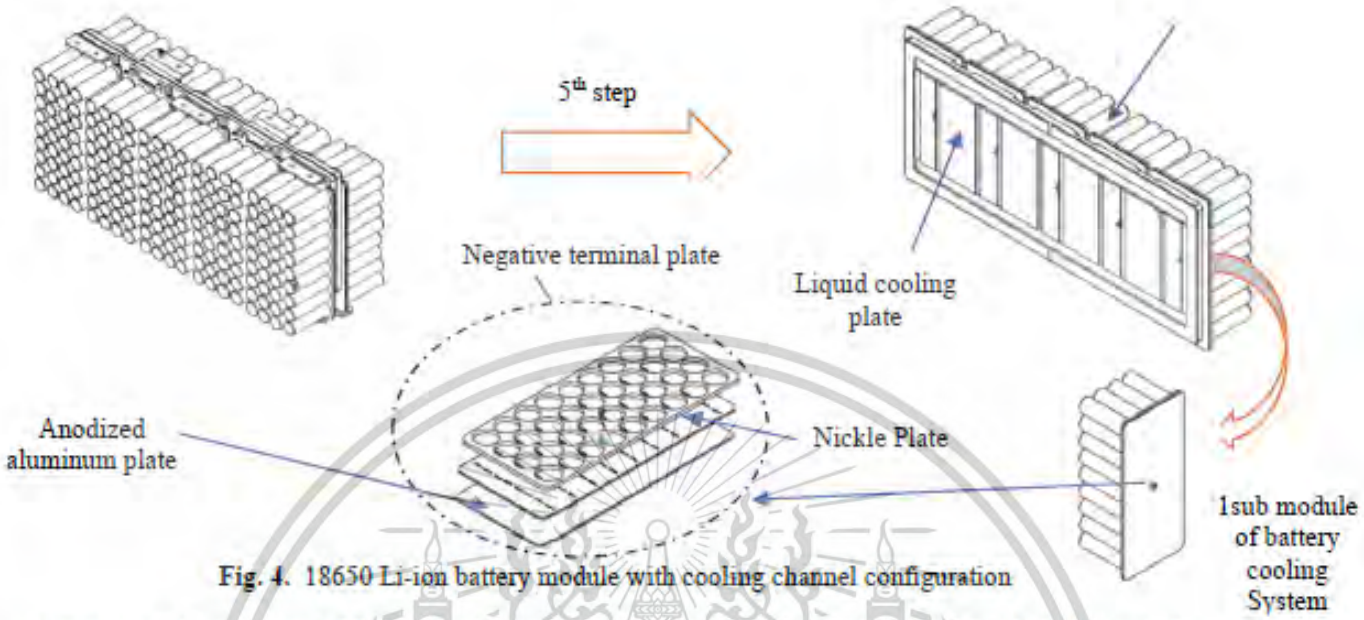

Fig. 4. 18650 Li-ion battery module with cooling channel configuration

Figure 4 displays the novel NSTDA battery module, which has one hundred and eighty 18650 Li-ion battery cells in the battery pack. Each battery module contains 36 cells and is enclosed within aluminum cooling plates. This module is made up of several parts. The first is the busbar, which is a copper strip with connectors for connecting to the battery's negative terminal and is intended to restrict potential negative differences and reduce multiple connections to specific terminals. Then, there is the plastic base, which acts as insulation between the battery pack on both sides. When only each battery module is considered, it has three parts: the nickel coating, which contributes to higher energy density; a larger storage capacity and enhanced electrical conductivity. Anodized aluminum plate can create a stable aluminum oxide layer. This plate is used as a cooling liquid plate because it can protect the dielectric substrates from being damaged while the heat is transferred through the battery module.

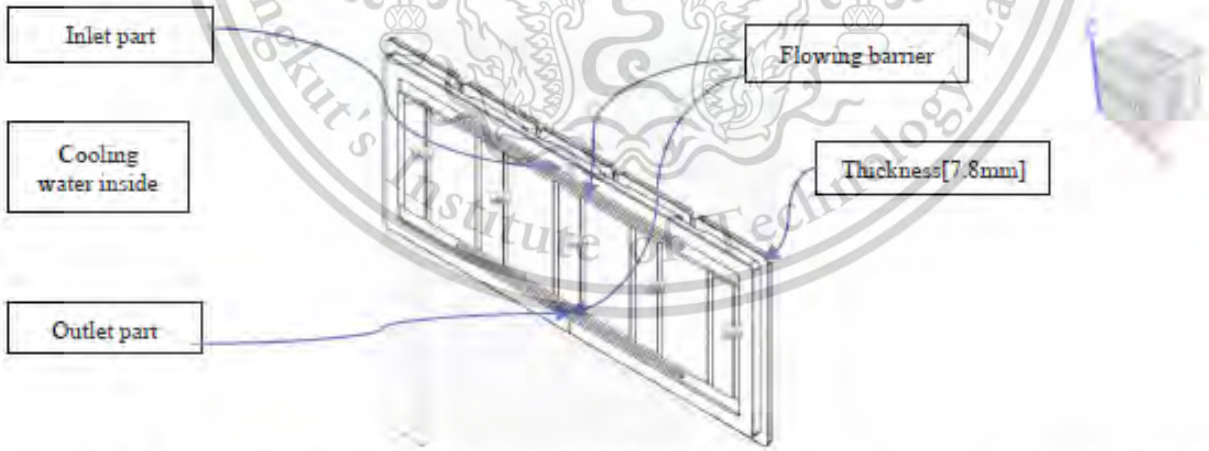

Fig. 5. Previous design of liquid cooling plates with two flow channel per base for the water-cooling system

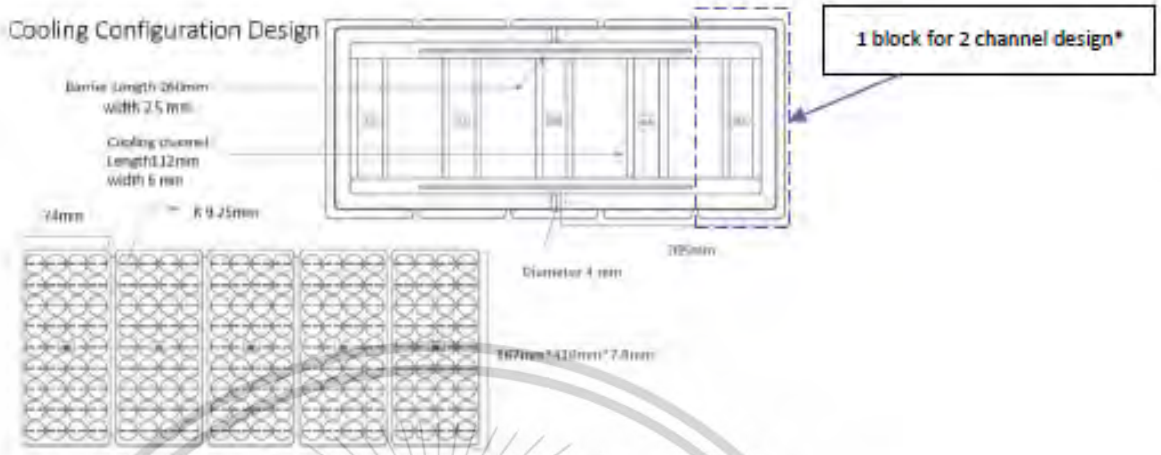

Fig. 6. Specification of previous design of liquid cooling plate

1.4. Cooling channel specification

The bottom plate's output side is where the liquid channel's outflow is located, as indicated in Fig. 5. The liquid path connects the cooling plate to the bottom plate, and The dimensions of the cooling channel are 167*410*7.8 mm in width, span, length, and thickness, respectively. Next, the cooling barrier dimension is 260*2.5mm. Water flows through a water channel 6 mm wide and 112 mm long. Finally, the liquid channel features a circular inlet and outlet of 4 mm in diameter as shown in Fig. 6.

This investigation focuses on factors affecting the performance of the liquid cooling plate, such as the pressure drop and temperature difference between inlet and outlet in the channel, by varying the number of cooling channels, the mass flow rate, and the inlet temperature of cooling water.

1.4.1 Problem Simplification

- Divide the aluminum cooling plate by half along the symmetry plane into 2.5 blocks of channels [length: 96.25 mm]and each block has 2, 3, 4, or 6 channels depending on each channel design. The cooling channel gap was kept constant at 6 mm and 1 mm depth. This model was used for the simulation of flow in the cooling channel. [steady state condition]

1.4.2 The modification of the liquid cooling pad

- Adjusted the distance between cooling channel blocks to be 41,32.5,20.5 and12 mm from center to center for 2,3,4 and 6 numbers of channels per base, respectively, as shown in Figures 7,8,9 and 10

- Decreased cooling barrier length from 260 mm to 160 mm to improve water flow distribution in cooling channel configuration while the cooling gap length was fixed at 6 mm.

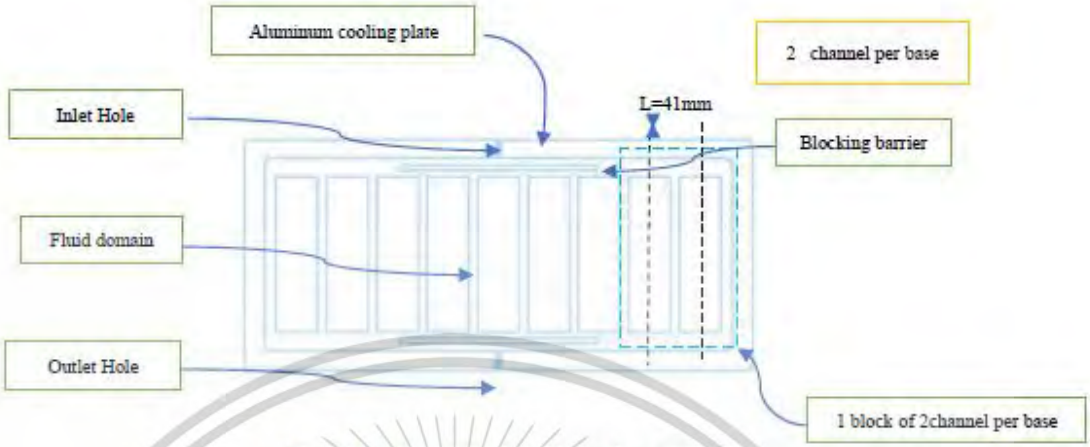

Fig.7 Number of Cooling channels = 2*5=10

Fig.8 Number of Cooling channels = 2*6=12

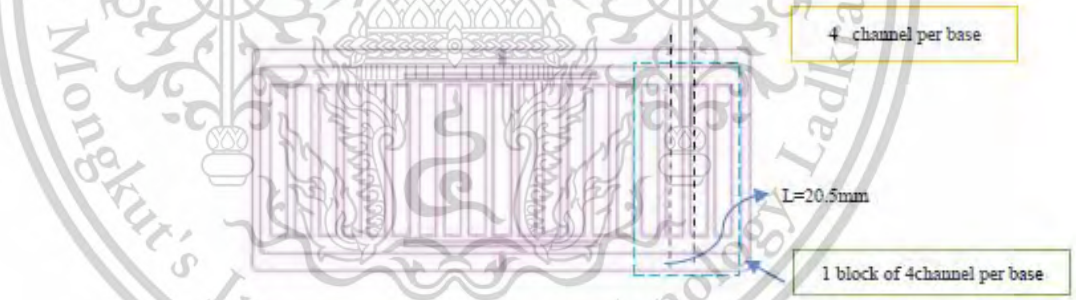

Fig.9 Number of Cooling channels = 2*10=20

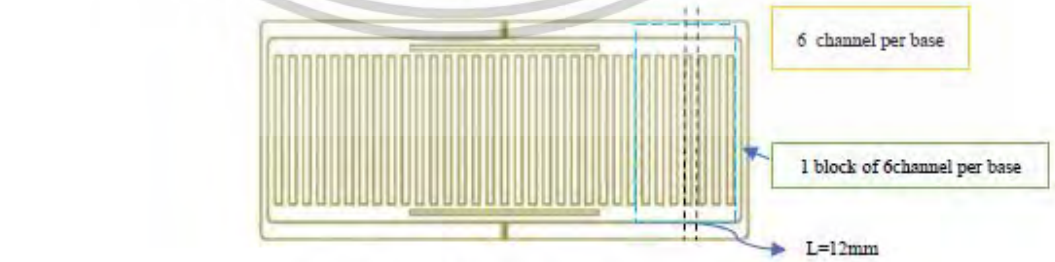

Fig.10 Number of Cooling channels = 2*17=34

Figures 7, 8, 9, and 10 show the new design by varying the number of cooling channels inside the cooling plate that is located in the middle of the 10S36P battery module. The main variables used in this investigation were inlet temperature, inlet water velocity, and the number of cooling channels. The system's total cooling capacity from the cells can be impacted by the aforementioned variables. Moreover, the desirable differential temperature between battery packs should be less than 5°C, which is desirable for maximizing the utilization of the battery pack by considering the cooling plate design.

[21] illustrated more clearly that the temperature field of the unit composed of the liquid cooling plate and battery cell was analyzed under the conditions of an inlet temperature of 25°C at a charging rate of 0.75 C. For the final result, the temperature of the cooling tube of the liquid cooling plate increased gradually from inside to outside; the highest temperature was 31.2 °C, and the temperature difference was 6.21 °C. The target value of the temperature difference for our design should be within 5 °C.

Our simulation was also carried out with the heat generation of the battery at a charging rate of 0.75 C to evaluate the temperature difference, the pressure drop, and the heat removal rate

2. The parametric study of the cooling channel

The battery thermophysical parameters and properties of the material are displayed in **Table.1**

Table 1 Properties of Material

Material	Phase	Thermal Conductivity [W/(m.K)]	Heat Capacity [J/(kg.K)]	Density [kg/m^3]	Heat Ratio	Viscosity [Pa.s]
Battery Cell	*Solid** $[k_x, k_y, k_z]$	{1.01,30.22, 1.01}	750	2690	-	-
Aluminum	*Solid*	155	893	2730	-	-
Coolant	*Liquid*	0.405	3300	1078	1	0.00429

Refer to the global coordinates of the 10S36P battery module model received from Fig. 3.

2.1 Heat generation in the battery cooling system

Although the heat generation rate varies with charging time, its maximum value was adopted as a constant, and the problem was simplified to be a steady state. This ensured that the simulated temperature of the battery would not exceed the instantaneous temperature during the charging period at a rate of 0.75 C.

2.2 The cooling strategy in cooling channel simulation

2.2.1 Mass flow rate selection

An investigation of the effect of the flow rate on cooling performance is carried out based on steady-state simulation. The flow speeds were simulated in the sequence of 50 L/h (0.5 m/s), 100 L/h (1.0 m/s), 200 L/h (2.0 m/s), and 300 L/h (3.0 m/s).The Reynolds number of water in channels and channel velocity would be investigated and compared at various numbers of cooling channels.

2.2.2 Inlet temperature selection

In this simulation, the battery was assumed to be under charging conditions with a constant current mode [SOC > 0.8] at a rate of 0.75 C. The simulation first used low water velocity at 0.5 m/s, and water temperatures started at 25 °C, followed by 30 °C, 35 °C, and 40°C, respectively.

2.3 Governing equation of the water-cooling system

Each battery is assumed to be identical, considering changes in geometry and chemical composition. The basic governing equations of fluid flow and heat transfer for cylindrical battery cells will be discussed below. To solve the 2D steady flow over battery cells, the continuity equation, momentum equation, and energy equations were written as follows:

Continuity equation

$$\nabla(\vec{v}) = 0 \quad (1)$$

Momentum conservation equation

$$\frac{\partial \vec{v}}{\partial t} + (\vec{v}\nabla)\vec{v} = -\frac{\nabla \rho}{\rho} + \frac{\mu}{\rho}\nabla^2\vec{v} \quad (2)$$

Where ∇ = the divergence(the partial derivative) , $\vec{v}$ = the velocity vector of the cooling water

ρ = the cooling water density =998 [kg/m^3] , $\frac{\partial \vec{v}}{\partial t}$ = the partial derivative of velocity vector change with time

μ = the dynamic viscosity coefficient of cooling water (Pa·s)

Energy conservation equation

$$\rho C_P \left(v_x \frac{\partial E}{\partial x} + v_y \frac{\partial E}{\partial y}\right) = k_T \left(\frac{\partial^2 E}{\partial x^2} + \frac{\partial^2 E}{\partial y^2}\right) \quad (3)$$

Where ∇ = the divergence(the partial derivative)

C_P = the specific heat capacity of cooling water= 4.187 [kJ/kg·K]

v_x = the velocity of cooling water in x direction (m/s)

v_y = the velocity of cooling water in y direction (m/s)

$\frac{\partial E}{\partial x}$ = the partial derivative of thermal energy per unit pathlength in x direction

$\frac{\partial E}{\partial y}$ = the partial derivative of thermal energy per unit pathlength in y direction

k_T = the thermal conductivity (W/m·K)

E = the thermal energy (J)

2.3.1 The calculation of heat generation

For the cooling system, the assumption used to calculate the heat generation of the battery cell that the temperature of the entire battery was constant, so the term for the battery's internal conductivity was left out, as was the heat transfer from the battery cell to an electrical wire and the surrounding environment. The equation below can be used to estimate heat generation [12, 13].

$$Q(t)_J + Q(t)_E = Q(t)_b \quad (4)$$

The heat generated inside the battery is denoted by the symbol $Q(t)_b$, which is composed of two sources: Joule heating and entropy change-related heat generation. The two sources of heat creation are specified in Equations (5) and (6) as

$$Q(t)_J = I^2 R_{int} \quad (5)$$

Where Q_J stands for the heat of Ohmic losses, often known as Joule heating (W), I for battery current (A), and R_{int} for internal resistance, which is made up of three terms: diffusion resistance, ion transport resistance, and Ohmic resistance [14].

$$Q(t)_E = -T\Delta S\frac{I}{nF} \quad (6)$$

where Q_E is the heat generation due to entropy change (W), T is the absolute temperature of the battery (°C), ΔS is the entropy change (J/K), n is the number of electrons (mol) and F is Faraday's constant ($9.65 \cdot 10^5$ s·A/mol).

Then, It is also possible to estimate the removal heat rate inside the battery cooling channel

$$Q = \dot{q} = \dot{m}_w C_p (T_o - T_i) ; \quad \dot{m}_w = \rho_\omega \dot{v}_w \; A = \pi(\frac{D}{2})^2 ; \; \dot{v}_w = vA \tag{7}$$

Where Q = the heat removal rate [kW]

$\dot{m}_w$ = the mass flowrate of inlet water [kg/s]

$\dot{v}_w$ = the volumetric flowrate of inlet water [m^3/s]

ρ_ω = the cooling water density=998[kg/m^3]

T_i = Inlet temperature [°C]

T_o = Outlet temperature [°C]

v = Inlet velocity of cooling water [m/s]

A = Cross-sectional area[m^2]

D = Diameter of Inlet cooling Tap (m)

Finally , the battery state of charge (SOC)is estimated by ampere-hour integration

$$SOC = SOC_{t=0} - \frac{1}{C_N} \int I(t) dt \tag{8}$$

where $SOC_{t=0}$=1 (when the battery is 100% charged)and $C_N$is the nominal capacity of the cell

2.4 Heat generation rate under various discharging conditions

Kulranut et al. [17] explained that the battery cell's thermal properties are evaluated during charging and discharging in the constant current (CC) and constant voltage (CV) modes. The current stays constant during the initial stages of charging in CC mode at around 80–90% of SOC when the battery is almost fully charged.

Table 2 Summary of maximum heat transferred rate, maximum temperature at various C-rate retrieved from Kulranut et al. [17]

Event	Charge			Discharge		
Current rate	0.25C	0.5C	0.75C	$1^{st}1C$	$2^{nd}1C$	$3^{rd}1C$
Maximum heat transferred rate(W)	0.073	0.145	0.307	0.953	1.022	1.041
Maximum temperature (°C)	36.361	41.709	45.813	51.813	52.462	53.012

For the current investigation, the maximum temperature is selected at 0.75C during charging event

The commercial 18650 lithium-ion cells from the Toriyama brand with a Li-Ni-Mn-Co (NMC) cathode were used in this investigation. At a charging rate of 0.80 C, the battery is 80% charged and gains the maximum charging current [2A]. After this point, the voltage of the battery would continue to decrease in CV mode, as received from Kulranut et al. [17]. Based on experimental results [Table 2], focusing only on the charging process, the maximum temperature at the battery surface was found at a charging rate of 0.75 C; however, we are not considering the heat value at the discharge rate because it is an intermittent rate and normally takes a short period of time. Finally, the heat generation rate will be decreased to zero at the end of the discharge process.

2.5The behavior of the volumetric for heat generation rate

Table 3 shows the average heat generation and the percentage of variation when using different current charging rates[0.5C, 1C, and 1.5C]

Table 3 Maximum heat generation rate retrieved from Paccha et al[18]

C-rate at charging Process	Volumetric heat generation rate (W/m^3)	Percentage of Variation(%)
0.5C	5761	30.9
1C	23588	5.8
1.5C	52715	0.5

From Table 3, it is necessary to interpolate between 0.5C and 1C to find the maximum heat generation rate(w/m3) at 0.75C, which is between 14674.5 W/m^3 and 15000 W/m^3.The maximum percentage of variation of 30.9% at 0.5 C and 0.5% at 1.5 C, but the ideal range is between 7% and 14% retrieved from Paccha et al[18].

3 The numerical analysis of battery module

The model was made by CAD Software for setting boundary conditions, meshing part, and solver setting. After that, the steady-state model of the cooling channel will be used to find the temperature at outlet, pressure at outlet, and water velocity inside channel by varying parameters [inlet temperature, inlet velocity, and the number of cooling channels]

3.1 Geometry and Materials

The 3D-model CAD file used in this work includes solid and fluid elements. The 36 battery cells in the battery module, 1 nickel plate, 1 insulation layer, and 1 anodized aluminum plate, make up the work's solid components.

3.2 Computational domain

The geometry of the battery module based on the cooling method reduced the complexity of the previous model. It meant that a few parts of the battery module were not considered, such as the insulator between battery cells, small aluminum conducting wires (fuses), the positive and negative busbars, and the plastic housing plate, because a little heat can be transferred to these parts. Secondly, the battery model was performed using steady-state models to investigate the maximum temperature of battery cells. Hence, the fluid flow was taken as laminar with non-isothermal flow. Finally, the simplified geometry of the battery cell with a fluid domain was used to study the thermal characteristics of the battery cell. However, in order to reduce the computational time due to the large number of mesh elements, the half-symmetric cooling model was used, as shown in Fig. 11.

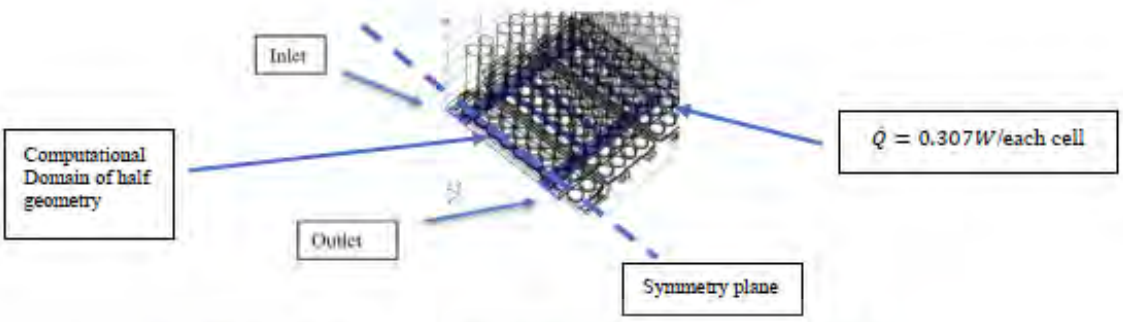

Fig. 11. The geometry of the cooling channel with coolant liquid inside

3.3 Setting Boundary condition in steady state model

Table4 The Steady-state input - output parameters

Parameter1	Parameter2	Parameter3
V_inlet(m/s)	T_inlet of coolant water (°C)	Number of Channels
0.5	25	2
1.0	30	3
2.0	35	4
3.0	40	6

From Table 4, all cases of simulation are 4^3 or 64. Selections of some cases were made that yielded the best cooling parameters, such as the maximum temperature of the battery being the least ($T_{b,min}$) with the minimum pressure drop. For a steady state result, selection was also made for cases with inlet velocity and inlet temperature of two-channel, three-channel, four-channel, and six-channel designs with a constant heat source, then showing the result of flow parameters and the maximum temperature of the battery to see the cooling performance among all designs.

3.4 The mesh generation of cooling channel model

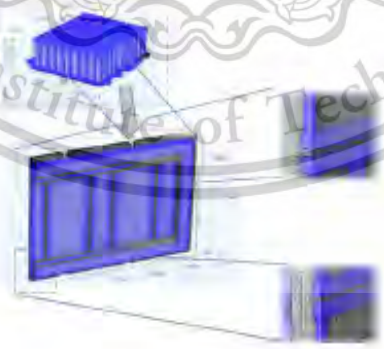

Fig. 12. The mesh generation on the cooling channel with the 18650 Li-ion battery module

The division of multizone in the mesh description was shown in Fig. 12. A meshing part has been set up for the fluid area to provide simulation quality. The standard size was around 0.25 mm. As a general rule, when volume meshing is initiated, the base size refers to the size of the largest elements in the fluid domain. If the base size was large, the mesh would be coarser, whereas if the base size was small, the mesh would be finer. The simulation of the battery was performed with different mesh sizes until insignificance change was observed and after the number of grids reached $8*10^5$, the calculating results did not significantly change with the variation of the meshes. The essential feature of the independence mesh statistics was displayed below in Table 5.

Table 5: The mesh statistics inside mesh model

Description	Value
Average element quality	0.6574
Tetrahedron	670752
Pyramid	514
Prism	21018
Triangle	208732
Quad	2664
Edge element	23704
Vertex element	1107

3.5 Setting heat generation as boundary condition

For 18650 Li-ion battery, the radius of the battery is 9 mm and h = 65 mm.

Under a charging rate of 0.75 C, the maximum heat generation per unit cell was [0.307 W], and the entire volume of 18650 Li-ion battery cell was $1.6 * 10^{-5} m^3$ then the maximum heat generation rate was set at $\frac{0.307}{1.6*10^{-5}} = 19187.5\ W/m3$ (see Fig.13)

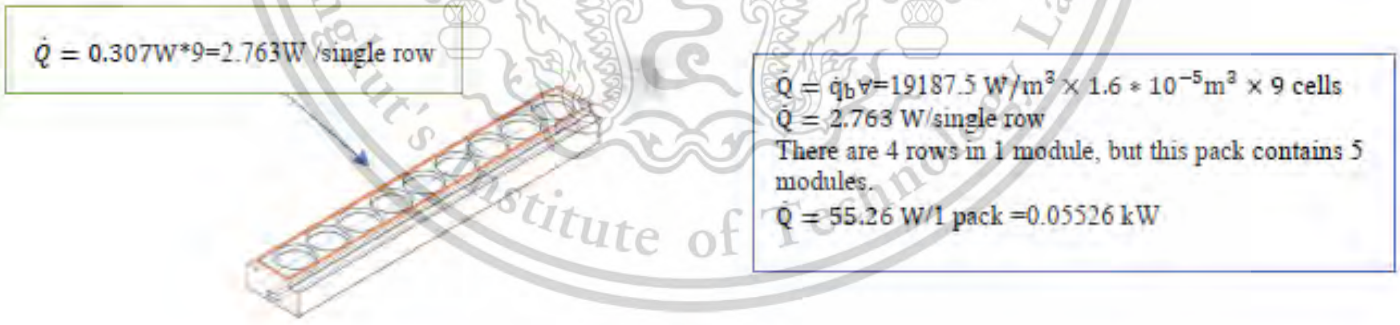

Fig. 13. Setting heat generation inside the simplified battery model

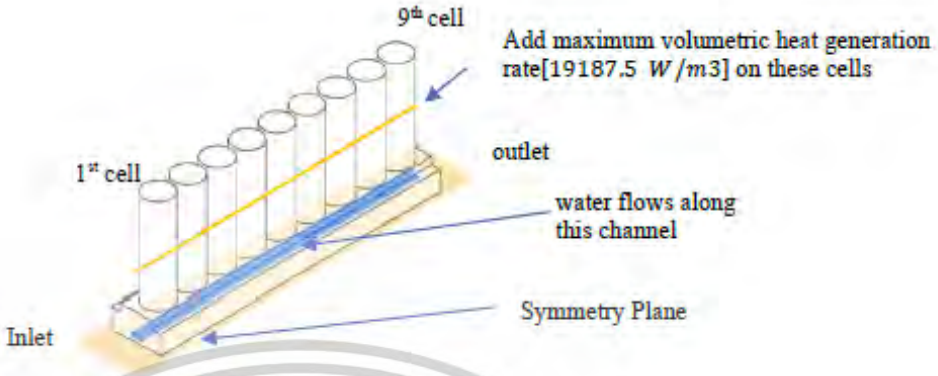

Fig. 14. The simplification battery model assessment

The simplified battery model (see Fig.14) was used to reduce the time consumption of parametric studies by considering the steady flow inside the cooling channel and estimating the maximum temperature of the battery pack from the 1st cell to the 9th cell using steady-state simulation.

4. Results and discussion

4.1 Temperature difference and pressure drop plot with an inlet velocity of cooling water

Fig. 15. Result of temperature difference compared with inlet velocity started with inlet temperature: 25°C to 40°C

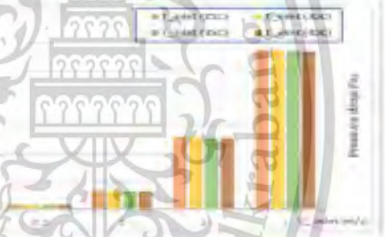

Fig. 16. Result of pressure drop compared with inlet velocity started with inlet temperature: 25 °C to 40 °C

According to Figures 15 and 16, increasing inlet water velocity caused the water temperature difference between the inlet and outlet sides to be lower. A higher amount of water in the inlet caused a significant increase in pressure drop; however, when using a small amount of inlet velocity. The pressure of water inside the cooling channel was observed to be the lowest, with a slight effect at inlet velocity 0.5 m/s due to the inlet temperatures of cooling water. Furthermore, the temperature difference increased to approximately 3°C.

A high-water flow rate creates a high pressure drop, reaching its maximum at 12000 Pa when utilizing the maximum inlet water flow rate of 3 m/s. The water flow rate has a significant impact on the pressure drop and the temperature difference.

Finally, the results of temperature difference and pressure drop have not changed much when increasing the inlet temperatures of water, but these values have been greatly affected when the inlet velocity is increasing, as used in the boundary conditions

4.2 Energy conservation among different numbers of channels [2, 3, 4, and 6 channels per base]

Inlet Temperature 25°C

Fig. 17.

Inlet Temperature 30°C

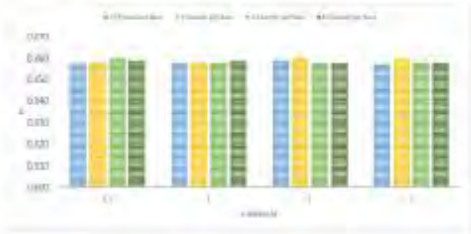

Fig. 18.

Inlet Temperature 35°C

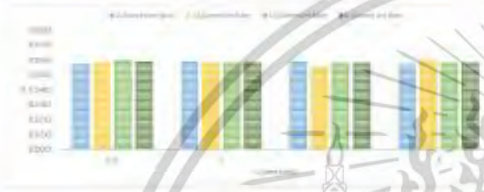

Fig. 19.

Inlet Temperature 40°C

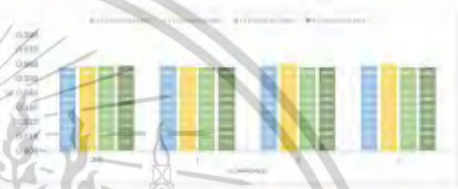

Fig. 20.

Figures 17, 18, 19 and 20 display the steady-state results of the heat removal rate (kW) using various numbers of cooling channels [2, 3, 4, and 6 channels per base] with the starting water velocity [0.5, 1, 2, and 3 m/s] and inlet temperature [25°C, 30°C, 35°C, and 40 °C]. The heat removal rate that occurred inside the battery was consistent at 0.059 kW, as proven by the principal theory of the steady flow energy equation. According to Fig. 18, when applying an inlet temperature of 30°C with an inlet velocity of 2 and 3 m/s, it had a little error of just 5.8% at a heat removal rate of 0.0605 kW.

The precise value of heat removal rate ($\dot{q}$) obtained from eq.(7) was 0.0553 kW, which was very close to the simulation results that had previously been explained.

To sum up, all simulation results express the result as being consistent with a minimal numerical error using various designs of cooling channels, no matter how much inlet velocity and inlet temperature of water were used.

4.3 The comparison of the standard deviation of channel velocity with various numbers of cooling channels

Fig. 21. The Standard deviation with inlet velocity of water (m/s) using different numbers of cooling channels

The cooling barrier length was 260 mm for the previous cooling block version . When using an inlet velocity of 0.5 m/s and an inlet temperature of 30 °C, It was seen that 4-channel designs offer the most uniform flow distribution because the standard deviation was lowest at 0.0046, followed by 3-channel, 2-channel, and 6-channel designs, respectively. as seen in Fig. 21.

With an inlet velocity of 0.5 m/s and an inlet temperature of 30 °C, was setting boundary conditions. The maximum channel velocity in a 4-channel configuration was 0.042 m/s, the lowest channel velocity was around 0.031 m/s, and the average channel velocity was 0.037 m/s. Moreover, In a 3-channel design, the maximum was at 0.065 m/s, which was higher than 4-channels at 0.023 m/s [35.38%] when using the same inlet condition, as shown in Fig. 23.

4.4 The comparison of the standard deviation of channel velocity with various numbers of cooling channels [Reducing cooling barrier length]

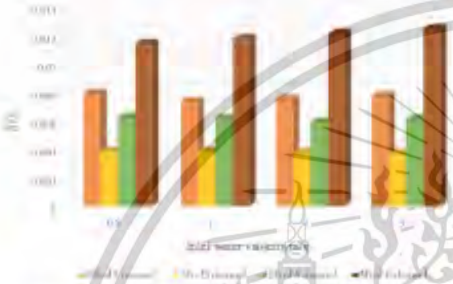

Fig. 22. The Standard deviation with inlet velocity of water (m/s) using different numbers of cooling channels

Fig. 23. The minimum and maximum of channel velocity when inlet velocity was 0.5 m/s compared with 3 and 4 channel designs

In addition to the above findings, the cooling barrier length was reduced from 260 mm to 160 mm to see its effect on water flow distribution in the cooling channel, while the cooling gap length remained constant at 6 mm.

For the modified version of the cooling block, the lowest value of the standard deviations was found in the 3-channel design at 0.0037 when the inlet velocity of cooling water was only 0.5 m/s, followed by the 4-channel, 2-channel, and 6-channel designs, respectively, which are all displayed in Fig. 22 and Fig. 23. After reducing the cooling barrier length, the standard deviation of all channel designs has decreased, which means the shorter length of the cooling barrier has a great effect on the dispersion of flow distribution. When increasing the inlet velocity of cooling water, the standard deviation remains stable, but it seems to increase slightly on a 6-channel design and reached its peak at over 0.012 when the inlet velocity of cooling water was 3 m/s.

Although the 3-channel design had the lowest standard deviation when using the modified version of the cooling block, the flow in the channel was less uniform due to a large velocity difference inside the cooling channel of 0.04 m/s. For the previous version of the cooling block, the 4-channel design reached only 0.026 m/s when using an inlet velocity of 0.5 m/s and had the lowest standard deviation, as stated in 4.3.

From the standard deviation and the channel velocity results that were both already compared, a 4-channel design performed the best uniformity of flow distribution because the least standard deviations brought the greatest velocity distribution, and the minimum channel velocity of this configuration was selected as the boundary condition in the simplified cooling model using steady state simulation.

4.5 The maximum temperature of battery in steady-state simulation

The heat generation rate was approximately under a charging rate of 0.75C. Then this value was used as a constant heat source in the single-channel flow simulation. The results of channel velocity for four channels per base were revealed at V_{avg} [0.037 m/s], V_{max} [0.042 m/s], and V_{min} [0.031 m/s] when use inlet velocity of 0.5 m/s. Finally, V_{min} and the inlet temperature of the water at 30°C were selected as boundary conditions.

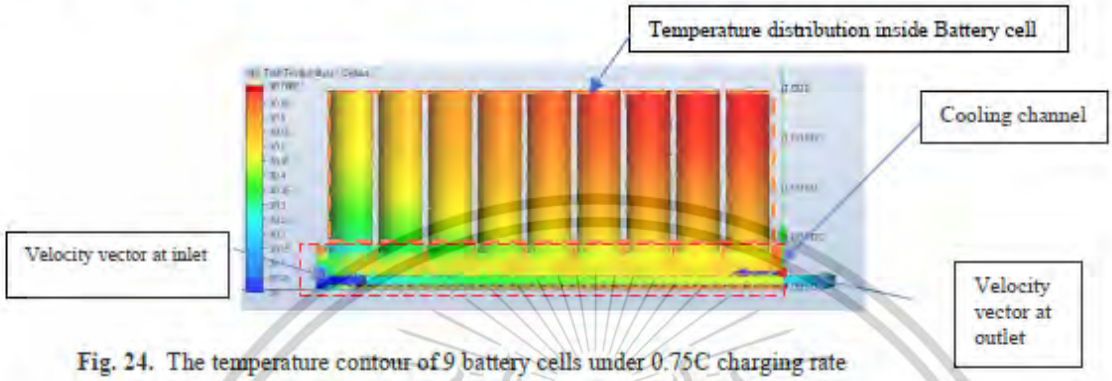

Fig. 24. The temperature contour of 9 battery cells under 0.75C charging rate

When the flow of water in the cooling channel ran through all nine batteries, the channel velocity at the outlet of the cooling channel followed the momentum conservation law. The temperature distribution inside a single row of the cooling channel increased from 30 °C [inlet zone] to nearly 30.5°C [outlet zone]. The result of the single flow simulation from the 1st cell to the 9th cell showed that under a 0.75 C charging rate in steady state, the greatest temperature of the battery was approximately 30.706 °C and yielded the highest percentage of battery performance [120%] from Fig. 1 using the inlet temperature at 30 °C, and the maximum temperature difference of the battery was 0.706°C (see Fig.24).

In summary, after adjusting the coolant temperature, the battery temperature rises irrespective of the value of the inlet velocity. However, it can be stated that as the flow speed increases, the maximum temperature of the battery module will decline. Ohmic loss also caused rises in the battery temperature, while the heat was absorbed by the coolant through heat transfer, which resulted in a temperature difference in the battery.

To find the maximum temperature, the coolant inlet temperature was chosen to be less than 30°C. Battery life is the most important factor that influences battery aging and causes premature battery failure. Higher temperatures mean a faster chemical reaction inside the battery.

5. Conclusion

5.1The summary of steady state simulation

- A 4-channel design offered the highest velocity uniformity of the water flow distribution among all channel configurations.
- The ability to remove heat from the battery when the inlet velocity increased from 0.5 m/s to 3 m/s was consistent at 0.0585 kW. When using an inlet temperature of 30°C with an inlet velocity of 2 and 3 m/s, It had a slight error of only 5.8% at a heat removal rate of 0.0605 kW.
- All cooling designs can produce very good water distribution when using low inlet velocities. However, when increasing the inlet velocity, the distribution of water in the channel got worse, especially for the 6-channel design, which had the highest standard deviation.

5.2The heat generation results in a single channel in the battery pack [9 cells].

- The highest average temperature at the 9th cell was 30.706 °C, which was lower than the maximum allowable battery temperature of 33 °C when using a channel velocity of 0.03 m/s with an inlet temperature of 30 °C as the boundary conditions.
- When the inlet water velocity ≥ 2.0 m/s, the flow became fully turbulent [Re = 6728.72], which was greater than the limited value of the laminar zone [Re<4000].The flow dispersion would be enhanced if the incompressible flow was steady. Moreover, discussing the same inlet velocity condition, the minimum channel velocity in a 4-channel [most uniform design] was 0.078 m/s [Re = 292.32], which was in the laminar zone.
- The inlet temperature should be less than or equal to 30°C to keep the maximum temperature at 33 °C [the maximum allowable battery temperature limit].

Nomenclature

R_{int}	Internal Resistance of battery (Ω)
Q_J	Joule heating (W)
I	Battery current (A)
Q_E	Heat generation due to entropy change (W)
T	Absolute temperature of the battery (°C)
T_{max}	Maximum Surface temperature (°C)
T_{avg}	Average temperature (°C)
T_i	Inlet temperature of cooling water [°C]
T_o	Outlet temperature of cooling water [°C]
Δs	Entropy change [J/°C]
ΔT	Temperature difference [°C]
ΔP	Pressure drop [Pa]
SOC	State of Charge
P_{fluid}	Pressure of fluid in the cooling channel (Pa)
V_{avg}	Average value for channel velocity of cooling water (m/s)
V_{min}	Minimum value for channel velocity of cooling water (m/s)
V_{max}	Maximum value for channel velocity of cooling water (m/s)
C_p	Specific heat capacity of cooling water (J/kg·°C)
k	Thermal conductivity (W/m·°C)
Q	Heat removal rate (KW)
$\dot{m}_w$	The mass flowrate of inlet water [kg/s]
$\dot{v}_w$	The volumetric flowrate of inlet water [m^3/s]
ρ_ω	Density of cooling water [Kg/m^3]
A	Cross-sectional area of Inlet cooling Tap[m^2]
D	Diameter of inlet cooling Tap(m)
ρ_{al}	Density of aluminum[Kg/m^3]
μ	Dynamic viscosity coefficient (Pa·s)

References

[1] Greco A, Jiang X, Cao D. An investigation of lithium-ion battery thermal management using paraffin/porous-graphite-matrix composite. J Power Sources. 2015;278:50-68.
[2] Saw LH, Ye Y, Tay AAO, Chong WT, Kuan SH, Yew MC. Computational fluid dynamic and thermal analysis of Lithium-ion battery pack with air cooling. Appl Energy. 2016;177:783-792.
[3] Wang H, Xu W, Ma L. Actively controlled thermal management of prismatic Li-ion cells under elevated temperatures. Int J Heat Mass Transf. 2016;102:315-322.
[4] Lu Z, Meng XZ, Wei LC, Hu WY, Zhang LY, Jin LW. Thermal Management of densely packed EV battery with forced air-cooling strategies. Energy Procedia. 2016;88:682-688.
[5] Qian Z, Li Y, Rao Z. Thermal performance of lithium-ion battery thermal management system by using mini-channel cooling. Energy Convers Manag. 2016;126:622-631.
[6] Lan C, Xu J, Qiao Y, Ma Y. Thermal management for high power lithium-ion battery by mini channel aluminum tubes. Appl Therm Eng. 2016;101:284-292.
[7] Yang XH, Tan SC, Liu J. Thermal management of Li-ion battery with liquid metal. Energy Convers Manag. 2016;117:577-585.
[8] Alipanah M, Li X. Numerical studies of lithium-ion battery thermal management systems using phase change materials and metal foams. Int J Heat Mass Transf. 2016;102:1159-1168.
[9] Yan J, Wang Q, Li K, Sun J. Numerical study on the thermal performance of a composite board in battery thermal management system. Appl Therm Eng. 2016;106:131-140.
[10] Azizi Y, Sadrameli SM. Thermal management of a LiFePO4 battery pack at high-temperature environment using a composite of phase change materials and aluminum wire mesh plates. Energy Convers Manag. 2016;128:294-302.
[11] Chen D, Jiang J, Kim GH, Yang C, Pesaran A. Comparison of different cooling methods for lithium-ion battery cells. Appl Therm Eng. 2016;94:846-854.
[12] Barbir F. PEM fuel cells. In: Barbir F, editor. PEM Fuel Cells: Theory and Practice. Amsterdam: Elsevier; 2005. p. 33-72.
[13] Bernardi D, Pawlikowski E, Newman J. A general energy balance for battery systems. J Electrochem Soc. 1985;132:5-12.
[14] Incropera FP, DeWitt DP. Introduction to heat transfer. 2nd ed. Hoboken: Wiley; 1990.
[15] Chantheve P, Hirai S, Lailuck V, Laoonual Y, Sriam P, Rompho S, et al. A simplified approach for heat generation due to entropy change in cylindrical LCO Battery. 2018 IEEE Transportation Electrification Conference and Expo, Asia-Pacific; 2018 Jun 6-9; Bangkok, Thailand. USA: IEEE; 2018. p. 1-5.
[16] Huang Y, Mei P, Lu Y, Huang R, Yu X, Chen Z, et al. A novel approach for Lithium-ion battery thermal management with streamline shape mini channel cooling plates. Appl Therm Eng. 2019;157:113623.
[17] Kulranut J, Depaiwa N, Yenwichai T, Intano W, Masomtob M. Improvement of estimation method for battery cell heat generation. J Res Appl Mech Eng. 2021;9(2):1-10.
[18] Paccha-Herrera E, Calderón-Muñoz WR, Orchard M, Jaramillo F, Medjaher K. Thermal modeling approaches for a LiCoO2 lithium-ion battery—a comparative study with experimental validation. Batteries. 2020; 6(3):40.
[19] Ho VT, Chang K, Lee SW, Kim SH. Transient thermal analysis of a Li-ion battery module for electric cars based on various cooling fan arrangements. Energies. 2020;13(9):2387.
[20] Lyu Y, Siddique ARM, Majid SH, Biglarbegian M, Gadsden SA, Mahmud S. Electric vehicle battery thermal management system with thermoelectric cooling. Energy Rep. 2019;5:822-827.
[21] Xu X, Li W, Xu B, Qin J. Numerical study on a water-cooling system for prismatic LiFePO4 batteries at abused operating conditions. Appl Energy. 2019;250:404-412.

APPENDIX B

PROCEEDINGS

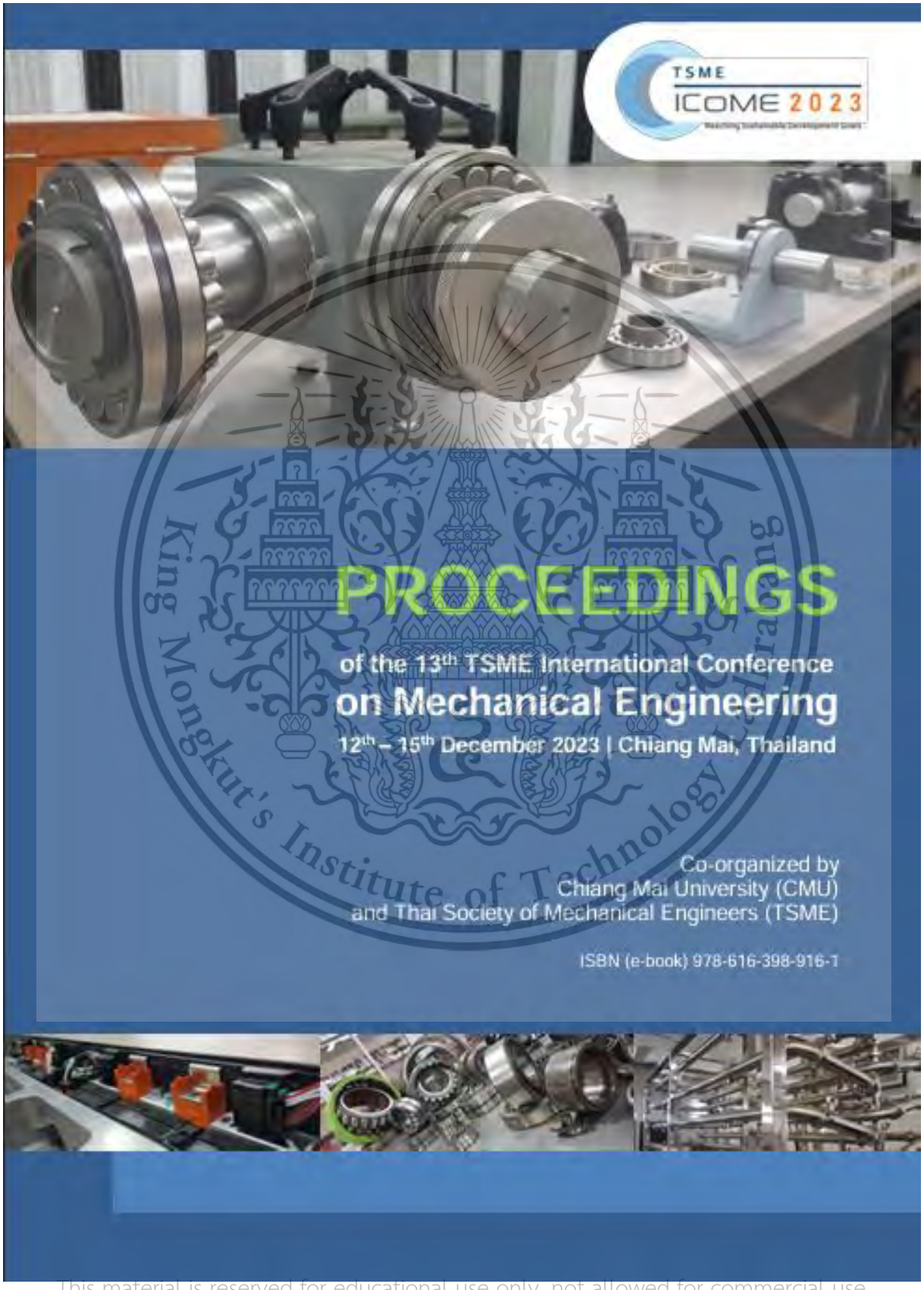

The 13th TSME International Conference on Mechanical Engineering
12th - 15th December 2023
Chiang Mai, Thailand

TSME ICOME 2023

TSF0001

Effect of inlet condition on flow distribution in a Water-Cooling Plates of 18650 Li-ion Battery pack

R. Nanthaiauti[1], J. Charoensuk[1,*], M. Masomtob[2], and S. Hiral[3]

[1]Department of Mechanical Engineering, School of Engineering, King Mongkut's Institute of Technology Ladkrabang, Bangkok 10520, Thailand
[2]Energy Innovation Research Group (EIRG), National Energy Technology Centre (ENTEC), National Science and Technology Development Agency (NSTDA), Pathum Thani 12120, Thailand
[3]Department of Mechanical Engineering, Tokyo Institute of Technology, Tokyo, Japan

* Corresponding Author: jarruwat.ch@kmitl.ac.th

Abstract. The flow distribution inside the liquid-cooling plate located in the middle of lithium-ion battery modules was investigated. Under steady-state circumstances, the most crucial parameters evaluated were the inlet temperature and the inlet velocity of cooling water. The variation in the inlet velocity (0.5, 1.0, 2.0 and 3.0 m/s) and the inlet temperature (25°C, 30°C, 35°C and 40°C) were conducted in a steady-state simulation. As a result, the inlet velocity of cooling water has a great impact on water flow distribution and temperature differences. However, the inlet temperature of cooling water does not have a significant effect on them. The standard deviation of the cooling water velocity when increasing the water speed was lowest at around 0.0098 by using an inlet water velocity of 0.5 m/s with an inlet temperature of 40°C. It was seen that when the inlet temperature increased, the standard deviation would decrease. On the other hand, the result of this value varies with the same trend as the inlet water velocity.

Keywords: Liquid-cooling plate, flow distribution, the standard deviation.

1. Introduction

Now a day,Enhancing the capacity and power density of batteries is required for the current development of electric vehicles. It is commonly considered that the number of battery cells should be packed as densely as possible to maximize output capacity and power density. On the other hand, high-power usage creates a significant thermal problem due to heat generation inside the battery cell. Maximum temperature also has an impact on battery performance and lifetime. Battery performance degrades as temperatures rise because, at higher temperatures, the battery can accelerate the chemical reaction inside beyond the set limit value. According to A. Greco, X. et al. [1], the battery temperature should be kept constant in the range of 20–40°C with a maximum temperature differential of less than 5°C.

1.1. Battery life

As we know that higher temperatures can shorten the battery life, which is the most crucial factor influencing battery aging and causing early battery failure because higher temperatures can accelerate the chemical reaction in the battery and also increase water leakage with corrosion. The temperature of the battery should be less than 33 °C, as indicated by [1], to extend battery life to more than 10 years, as the current projection is that an electric car battery could last between 10 and 20 years before needing to be replaced.

1.2. Battery thermal management system

There are different forms of thermal management for battery packs. They are mainly divided into three categories: Liquid cooling [8–10], phase change materials (PCM) cooling, and air cooling [2-4]. These techniques have advantages and disadvantages. According to D. Chen et al. [11], air cooling is simple to build but has poor cooling effectiveness and is insufficient to maintain temperature under adverse conditions. PCM cooling can efficiently lower temperatures in battery modules and reduce temperature differences, but it was limited by phase changes in volume and encapsulation. Liquid cooling systems can also remove heat from batteries. Compared to other fluids with the same flow rate, this method is quite capable of reducing a significant amount of heat[5]. Due to its practical design and efficient cooling, it is mainly used in the cooling system. However, the liquid cooling system requires more attention because of liquid leakage and corrosion[6]. It is expected that the design would be better suited for battery heat management systems that use the liquid cooling method and water as the coolant.

1.3. The 10S36P battery module

The 10S36P battery module is divided into numerous sections. The first is the busbar, a copper strip with terminals for connecting to the negative terminal of a battery. It is designed to limit possible negative differences and reduce repeat connections to certain terminals. The second one is the plastic housing, which serves as insulation on both sides of the battery pack. If you focus only on one battery module, there are three components inside: the nickel plating, which results in higher energy density, greater storage capacity, and improved electrical conductivity. The anodized aluminium plate provides a durable oxide layer that is fully integrated. This was used as a liquid cooling plate, as shown in Figure 2, that can protect the dielectric substrates from damage during heat transfer of battery cells, and finally, a negative 36P terminal plate that can hold the 18650 li-ion battery to be fixed in the centre[12-15]. It has many advantages, as explained before. There are one hundred eighty Li-ion battery cells in the battery pack. Five battery modules are packed with aluminium cooling plates in the middle, and each battery module has thirty-six cells, as shown in Figure 1.

1.4. Problem simplification of 10S36P battery module

While keeping the essential components for thermal analysis, the cooling pad and flow channel of a battery module was modelled. Following are the rationales of the problem specification.

- 1st step: Discard the upper case and positive plate because they are not considered for cooling in the positive terminal.
- 2nd step: Neglect the ohmic heating on the busbar that conducts the heat to the positive terminal. So, the bus bar will be removed.
- 3rd step: Discard all of the insulation parts [the bushes and all connectors] that can fasten the battery module.
- 4th step: Discard the plastic base because it is an insulation part and has lower thermal conductivity.
- 5th step: Using the x-z plane to show half the cooling module because the cooling system is symmetric. A submodule of the battery cooling system that contains the negative terminal plate, anodized aluminium plate, and nickel plate was found and the liquid cooling plate will be further investigated.

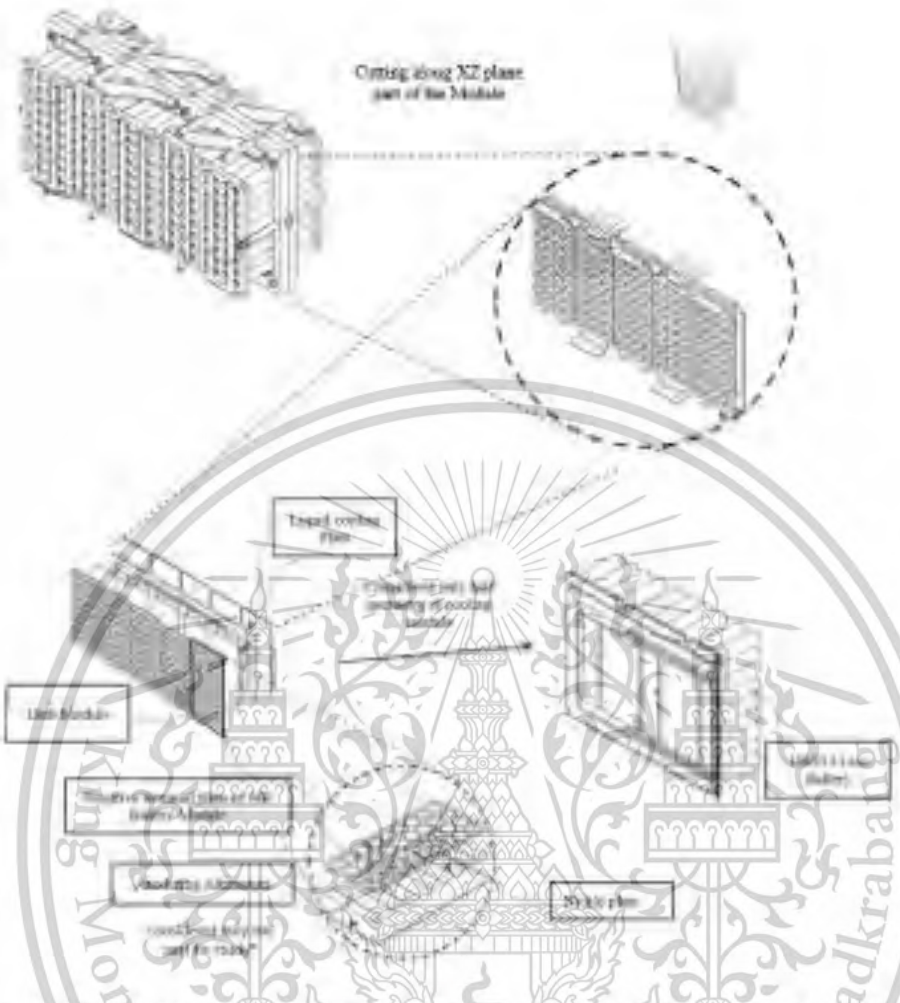

Figure 1. Explode View of 18650 Li-ion battery module with cooling channel configuration

Figure 2. The configuration of liquid cooling plates with two flow channel per base.

2. The effect of flowing parameters and properties of the material

The model was made by using Autodesk Fusion 360 [CAD software] and COMSOL Multiphysics® 6.0 to design 3D modeling of the battery module with cooling channel and explore steady-state simulation to see the uniform flow channel distribution inside the mesh model of the channel inside the liquid cooling plate when using various inlet conditions of cooling inlet temperature and cooling water velocity, respectively. The simulation steps are computational domain, setting boundary conditions in the steady state model, and finally, mesh independence of the cooling channel model for solver setting.

2.1. Geometry and Materials

The 3D-model-CAD file in this work includes solid and fluid elements. 1 submodule contains 36 battery cells; 1 nickel plate, 1 insulation layer, and 1 anodized aluminum plate make up the work's solid components. Because of their poor heat transmission, some solid components, including the battery module housing, the positive common plate, and aluminum wire, are not considered in the model.

Table 1. The battery's thermophysical parameters and properties of the material.

Material	Phase	Thermal Conductivity [W/(m.K)]	Heat Capacity [J/(kg.K)]	Density [kg/m^3]	Heat Ratio	Viscosity [Pa.s]
Battery Cell	Solid	{1.01,30.22, $[k_x, k_y, k_z]$ 1.01}	750	2690	-	-
Aluminum	Solid	155	893	2730	-	-
Coolant	Liquid	0.405	3300	1078	1	0.00429

The geometry influences the average velocity in the cooling channel, which can influence the boundary layers created by the fluid flowing along with the bounding surfaces. This research aims to focus on flowing parameters such as mass flow rate, pressure drop, and temperature differences between the inlet and outlet of the liquid cooling plate that's composed of material and battery cell properties from Table1. As the flow distribution of cooling water increases inside the cooling channel, the heating value that is evacuated from the 18650 Li-ion battery by the aluminum cooling plate will be enhanced, resulting in better cooling performance. The maximum permissible battery temperature is 33 °C, even though the desired difference in temperature between battery packs should be less than 5°C, which might improve the cooling effectiveness of the battery cell [16].

2.2. The Cooling Strategy used in Cooling channel simulation

2.2.1Choosing the inlet velocity of cooling water

The influence of flow rate on cooling performance is investagated using steady-state modelling. Flow rates of 50 L/h (0.5 m/s), 100 L/h (1.0 m/s), 200 L/h (2.0 m/s), and 300 L/h (3.0 m/s) were simulated.

2.2.2 Choosing the inlet temperature of cooling water

As the temperature of the coolant had an influence on the thermal properties of lithium-ion batteries, the simulation started with a small water velocity set at 0.5 m/s, and with the temperature at 25 °C, followed by 30°C, 35°C, and 40°C respectively.

2.3. Governing equation of the water-cooling system

Each battery is assumed to be identical, considering changes in geometry and chemical composition. The basic governing equations of 2D steady flow in the cooling channel of Battery cooling Plate, such as the continuity equation, momentum equation, and energy equations[5-7] will be shown below:

Continuity equation

$$\nabla(\vec{v}) = 0 \quad (1)$$

Momentum conservation equation

$$\frac{\partial \vec{v}}{\partial t} + (\vec{v}\nabla)\vec{v} = -\frac{\nabla \rho}{\rho} + \frac{\mu}{\rho}\nabla^2\vec{v} \quad (2)$$

where ∇ = the divergence
ρ = the cooling water density =998 [kg/m^3]
μ = the dynamic viscosity coefficient of cooling water (Pa·s)
$\frac{\partial \vec{v}}{\partial t}$ = the partial derivative of velocity vector
$\vec{v}$ = the velocity vector of the cooling water

Energy conservation equation

$$\rho C_p \left(v_x \frac{\partial E}{\partial x} + v_y \frac{\partial E}{\partial y}\right) = k_T \left(\frac{\partial^2 E}{\partial x^2} + \frac{\partial^2 E}{\partial y^2}\right) \quad (3)$$

where ∇ = the divergence)the partial derivative(
C_p = the specific heat capacity of cooling water= 4.187 [kJ/kg·K]
v_x = the velocity of cooling water in x direction (m/s)
v_y = the velocity of cooling water in y direction (m/s)
$\frac{\partial E}{\partial x}$ = the partial derivative of thermal energy per unit pathlength in x direction
$\frac{\partial E}{\partial y}$ = the partial derivative of thermal energy per unit pathlength in y direction
k_T = the thermal conductivity (W/m·°C)
E = the thermal energy (J)

The steady flow energy equation has shown below in eq(4)

$mC_p \frac{\partial T_o}{\partial t} = \dot{m}_\omega C_p (T_o - T_i) + \dot{Q}$; $\dot{m}_w = \rho_\omega \dot{v}_w$; $\dot{Q} = \dot{q}_b \forall$ but $\frac{\partial T_o}{\partial t}$ at initial boundary in steady state = 0

then $\dot{m}_w C_p (T_o - T_i) = -\dot{Q}$ and $\dot{m}_\omega C_p (T_i - T_o) = \dot{Q}$ (4)

where $\dot{Q}$ =Heat removal rate to the liquid in the cooling channel [kW]
$\dot{q}_b$ = Volumetric heat generation rate inside battery [W/ m^3]
$\dot{v}_w$ =Volumetric flowrate of inlet water [m^3 /s]
ρ_ω =Density of cooling water [998 kg/m^3]
C_p =Heat capacity of cooling water[4.187 kJ/kg·°C]
T_i = Inlet temperature [°C]
T_o = Outlet temperature [°C]
$\forall$ = The entire volume of 18650 Li-ion Battery[m^3]
m = Fluid mass within the cooling channel [kg]

3. The step for numerical methodology of steady state model

3.1. Computational domain

The geometry of the liquid cooling plate with cooling channels inside focused only on flow parameters, temperature differences between inlet and outlet, and pressure drops across the cooling plate that affect cooling performance. Secondly, the cooling channel model was performed using steady state to investigate the channel velocity and find the standard deviation to perform flow distribution for the result. However, in order to reduce computational time due to the large number of mesh elements, the

half-symmetric cooling channel model was used to reduce the complexity of the previous model, as shown in Figure 3.

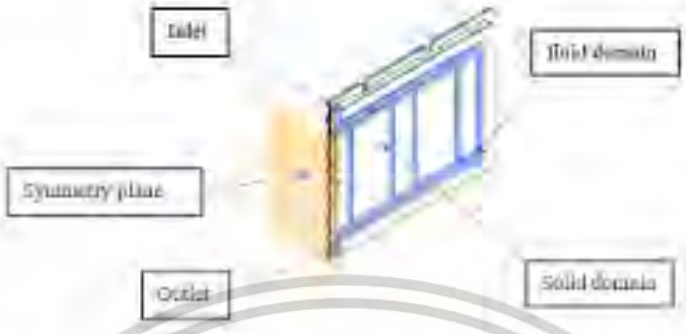

Figure 3. The computational domain of the half geometry for cooling channel configurations.

3.2. Setting boundary condition in steady state model

For the study of the maximum temperature at the outlet ($T_{out,max}$) and the distribution of the water by considering the channel velocity, the flow rate and the coolant inlet temperature are considered boundary conditions within the steady-state model, as shown in Table 2. The flow velocity is the first parameter to be set [0.5, 1, 2, and 3 m/s], and the inlet temperature is set as the second parameter [25, 30, 35, and 40 °C].

Table 2. The boundary inlet parameters of steady state circumstances.

Inlet velocity of water (m/s)	Inlet temperature of water (°C)
0.5	25
1.0	30
2.0	35
3.0	40

3.3. The mesh independence of the cooling channel model

Figure 4 depicts the multizone split. A meshing component has been built up for the fluid region to give the best simulation quality. The typical size was around 0.25 mm. When volume meshing is started, the base size is usually the size of the biggest components in the fluid domain. The mesh would be coarser if the base size was large, whereas the mesh would be finer if the base size was small. The simulations were performed with various mesh sizes until insignificant changed of the temperature difference and pressure drop were noticed.

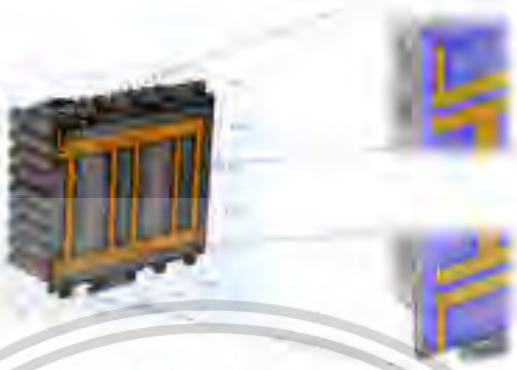

Figure 4. Mesh independence with sizes

The simulation of flow in the water channel was performed with different mesh sizes until insignificance change was observed and after the number of grids reached $8*10^5$, the calculating results did not significantly change with the variation of the meshes. The essential feature of the independence mesh statistics was displayed below in Table 3.

Table 3. The mesh statistics inside mesh model.

Description	Value
Average element quality	0.6574
Tetrahedron	670752
Pyramid	514
Prism	21018
Triangle	208732
Quad	2664
Edge element	23704
Vertex element	1107

4. Steady state Simulation Result

4.1 Temperature difference and pressure drop between inlet and outlet of cooling channel

The pressure drop increased significantly as the amount of water in the inlet rose sharply, however, when using just a bit of inlet velocity, the pressure of water inside the cooling channel appeared to be the smallest, with a slight effect at an inlet velocity of 0.5 m/s due to the inlet temperatures of cooling water. Furthermore, temperature differences climbed to 3°C. When using the maximum incoming water flow rate of 3 m/s, a considerable pressure drop is generated reaching its maximum at 12000 Pa. The pressure drop is considerably influenced by the high flow rate and the temperature difference. Finally, the temperature difference and pressure drop did not vary significantly while raising the inlet temperatures of the fluid, results were significantly influenced when increasing the inlet velocity was utilized for the boundary circumstances.

4.2 Flow Visualization of the cooling channel

Considering an inlet velocity of 0.5 m/s and an inlet temperature of 30 °C, the maximum velocity inside the channel is 0.042 m/s, the minimum is 0.031 m/s, and the average velocity is 0.037 m/s. Then increase

the inlet velocity to 3 m/s and use the same temperature inlet. The maximum velocity will be increased to 0.234 m/s, and the minimum is 0.165 m/s. Then find the relative between the inlet velocity of cooling water and Standard deviation

Figure 5. Inlet Velocity = 0.5m/s

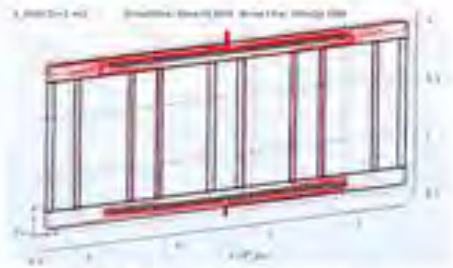

Figure 6. Inlet Velocity = 1.0m/s

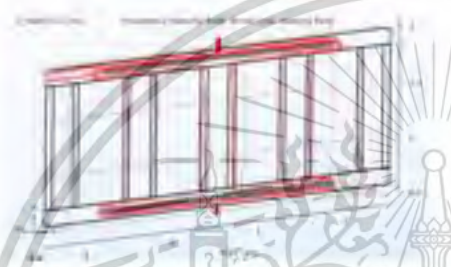

Figure 7. Inlet Velocity = 2.0m/s

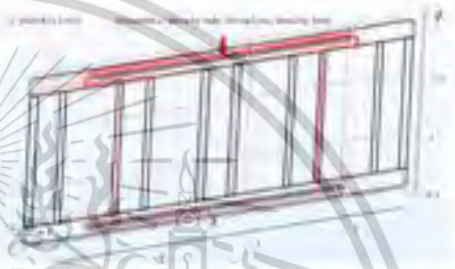

Figure 8. Inlet Velocity = 3.0m/s

Figures 5, 6, 7, and 8 show the velocity streamline inside the cooling channel while varying the water inlet velocity at 0.5, 1, 2, and 3 m/s. This design produced the best velocity uniformity and more water distribution when using the lowest inlet velocity. However, when enhancing the inlet velocity, the distribution of water in the channel is quite bad. This causes the speed of the water flowing through the cooling channel to become more turbulent. Regarding the impact of the inlet temperature of the water.

Figure 9. Result of the standard deviation with the inlet water velocity started from inlet temperature 25 °C to 40 °C.

According to Figure 9, the standard deviation of the cooling water velocity when increasing the water speed was lowest at around 0.0096 by using an inlet water velocity of 0.5 m/s with an inlet temperature of 40 °C, and the least amount of velocity inside the cooling channel was around 0.0309 m/s. It was seen from the chart that when the inlet temperature increased, the Standard deviation would be quite stable when using a low Inlet velocity of water but slighily increase when using an inlet velocity of cooling water> 1 m/s. Moreover, the result of the standard deviation value plot has a more significant effect on the increasing inlet velocity of water that distributes inside the cooling channel than the influence of the inlet temperature parameters.

4.3. Removed heat rate (kW) plot with inlet velocity of cooling water (m/s)

While comparing different inlet temperature values, the capability to remove heat from the battery appeared to be consistent at roughly 0.060 kW as inlet velocity increased. [Error 3.25% from the exact value] According to the chart, increasing the inlet temperature of cooling water within the cooling plate has an insignificant effect on the heat removal rate, regardless of how much the inlet velocity changes. The precise value of heat removal rate obtained from eq(4) is 0.0553 kW, which is very close to the simulation result that was explained before and has an inaccuracy percentage of approximately 16.58% when using inlet velocity at 2 m/s.

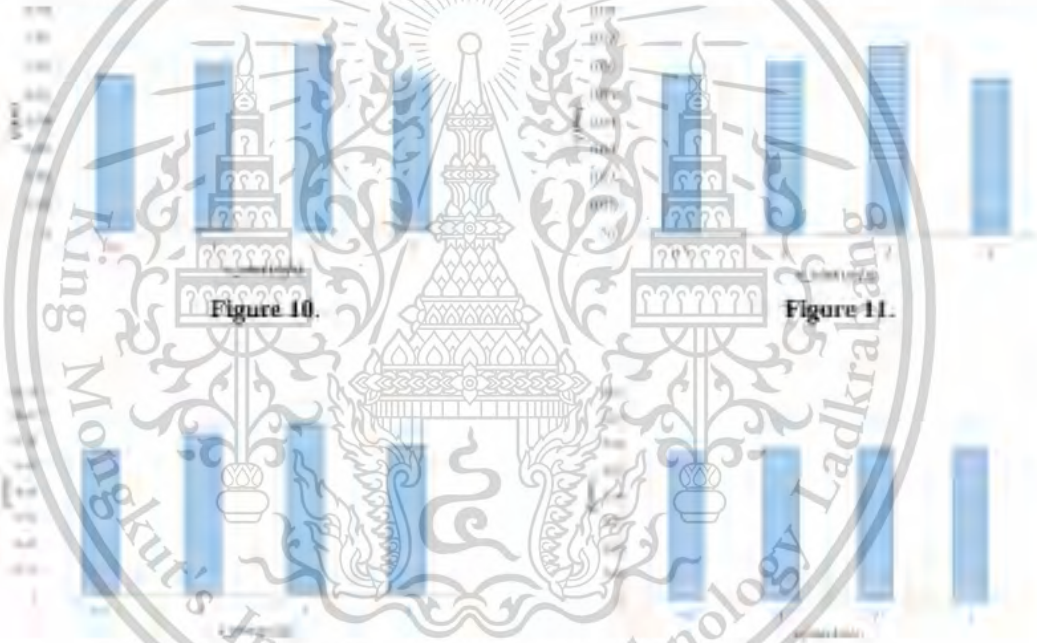

Figure 10.

Figure 11.

Figure 12.

Figure 13.

Figures. 10,11,12 and 13 show the relationship between heat removed rate (kW) and inlet velocity of water (m/s) compared at various inlet temperatures of 25°C, 30°C, 35°C, and 40°C respectively.

5. Conclusion

Employing the lowest inflow velocity can produce the best velocity consistency along with enhanced water dispersion. When inflow velocity increases, water distribution in the channel becomes relatively poor compared to the standard deviation trend, which increases the water flowrate when passing through

the cooling channel. The standard deviation of the cooling water velocity when increasing the water speed was lowest at around 0.0096 by using an inlet water velocity of 0.5 m/s with an inlet temperature of 40 °C, and the least amount of velocity inside the cooling channel was around 0.0309 m/s.The capability to remove heat from the battery appeared to be consistent at roughly 0.060 kW as inlet velocity increased.

6. Acknowledgment

The author would like to thank you for the research facilities from National Science and Technology Development Agency (NSTDA), National Energy Technology Centre (ENTEC), Department of Mechanical Engineering, Faculty of Engineering and King Mongkut's University of Technology Ladkrabang (KMITL)

7. References

[1] A. Greco, X. Jiang, and D. Cao, "An investigation of lithium-ion battery thermal management using paraffin/porous-graphite-matrix composite," J. Power Sources, vol. 278, pp. 50–68, 2015.

[2] L. H. Saw, Y. Ye, A. A. O. Tay, W. T. Chong, S. H. Kuan, and M. C. Yew, "Computational fluid dynamic and thermal analysis of Lithium-ion battery pack with air cooling," Appl. Energy, vol. 177, pp. 783–792, 2016

[3] H. Wang, W. Xu, and L. Ma, "Actively controlled thermal management of prismatic Li-ion cells under elevated temperatures," Int. J. Heat Mass Transf., vol. 102, pp. 315–322, 2016

[4] Z. Lu, X. Z. Meng, L. C. Wei, W. Y. Hu, L. Y. Zhang, and L. W. Jin, "Thermal Management of Densely packed EV Battery with Forced Air-Cooling Strategies," Energy Procedia, vol. 88, pp. 682–688, 2016

[5] Z. Qian, Y. Li, and Z. Rao, "Thermal performance of lithium-ion battery thermal management system by using mini-channel cooling," Energy Convers. Manag., vol.126, pp. 622–631, 2016

[6] C. Lan, J. Xu, Y. Qiao, and Y. Ma, "Thermal management for high power lithium-ion battery by mini channel aluminum tubes," Appl. Therm. Eng., vol. 101, pp. 284–292, 2016

[7] X.-H. Yang, S.-C. Tan, and J. Liu, "Thermal management of Li-ion battery with liquid metal," Energy Convers. Manag., vol. 117, pp. 577–585, 2016

[8] M. Alipanah and X. Li, "Numerical studies of lithium-ion battery thermal management systems using phase change materials and metal foams," Int. J. Heat Mass Transf., vol. 102, pp. 1159–1168, 2016

[9] J. Yan, Q. Wang, K. Li, and J. Sun, "Numerical study on the thermal performance of a composite board in battery thermal management system," Appl. Therm. Eng., vol.106, pp. 131–140, 2016

[10] Y. Azizi and S. M. Sadrameli, "Thermal management of a LiFePO4 battery pack at high-temperature environment using a composite of phase change materials and aluminum wire mesh plates," Energy Convers. Manag., vol. 128, pp. 294–302, 2016

[11] D. Chen, J. Jiang, G.-H. Kim, C. Yang, and A. Pesaran, "Comparison of different cooling methods for lithium-ion battery cells," Appl. Therm. Eng., vol. 94, pp. 846–854, 2016

[12] Barbir, F., 2005, PEM Fuel Cells, Elsevier Inc., pp. 33-72.

[13] Bernardi, D., Pawlikowski, E. and Newman, J., 1984, "General energy balance for battery systems", Journal of the Electrochemical Society, Vol. 84-2, No. 1, pp. 164-165.

[14] Incropera, F.P. and De Witt, D.P., 1990, Introduction to Heat Transfer, 2nd ed., John Wiley & Sons, Inc., pp. 1-9.

[15] Chantheve P., Laoonual Y., Masomtob M., Hirai S., Lailuck V., Rompho S., Sriram P., and Chanurai N., "A Simplified Approach for Heat Generation due to Entropy Change in Cylindrical LCO Battery', 2018 IEEE Transportation Electrification Conference & Expo Asia-Pacific, June 6th - 9th, 2018, Bangkok, Thailand

[16] Y. Huang, P. Mei, Y. Lu, R. Huang, X. Yu, Z. Chen, A.P. Roskilly, A novel approach for Lithium-ion battery thermal management with streamline shape mini channel cooling plates

AUTHOR BIOGRAPHY

Author: Mr. Raksit Nanthatanti

Degree: Master of Engineering

Date of Graduation:

Date of Birth: 25th April 1998

Place of Birth: Thailand

Undergraduate and Graduate Education:

Master's degree in automotive engineering, 2021-2023 founded by National Science and Technology Development Agency (NSTDA, Thailand), Tokyo Institute of Technology (Tokyo-Tech, Japan) and King Mongkut's Institute of Technology Ladkrabang(KMITL), Bangkok, 2021

Bachelor's degree in mechanical engineering
King Mongkut's Institute of Technology Ladkrabang(KMITL), Bangkok, 2016

Scholarship : TAIST-Tokyo Tech scholarship

Publications:

[1]R. Nanthatanti, J.Charoensuk, M. Masomtob and S.Hirai , Parametric Study on Water-Cooling Plates to Improve Cooling Performance on 18650 Li-ion Battery, Journal of Research and Applications in Mechanical Engineering (JRAME)2024 Vol. 12, No. 1. Paper No. JRAME 24-12-006

Proceedings:

[2]R. Nanthatanti, J.Charoensuk, M. Masomtob and S.Hirai "Effect of inlet condition on flow distribution in a Water- Cooling Plates of 18650 Li-ion Battery pack" presented in The 13th TSME-International Conference on Mechanical Engineering (TSME-ICoME 2023)